

CONTEMPORARY MATHEMATICS

283

Advances in Wave Interaction and Turbulence

Proceedings of an AMS-IMS-SIAM
Joint Summer Research Conference
on Dispersive Wave Turbulence
Mount Holyoke College, South Hadley, MA
June 11–15, 2000

Paul A. Milewski
Leslie M. Smith
Fabian Waleffe
Esteban G. Tabak
Editors



Selected Titles in This Series

- 283 **Paul A. Milewski, Leslie M. Smith, Fabian Waleffe, and Esteban G. Tabak, Editors**, *Advances in wave interaction and turbulence*, 2001
- 282 **Arlan Ramsay and Jean Renault, Editors**, *Groupoids in analysis, geometry, and physics*, 2001
- 281 **Vadim Olshevsky, Editor**, *Structured matrices in mathematics, computer science, and engineering II*, 2001
- 280 **Vadim Olshevsky, Editor**, *Structured matrices in mathematics, computer science, and engineering I*, 2001
- 279 **Alejandro Adem, Gunnar Carlsson, and Ralph Cohen, Editors**, *Topology, geometry, and algebra: Interactions and new directions*, 2001
- 278 **Eric Todd Quinto, Leon Ehrenpreis, Adel Faridani, Fulton Gonzalez, and Eric Grinberg, Editors**, *Radon transforms and tomography*, 2001
- 277 **Luca Capogna and Loredana Lanzani, Editors**, *Harmonic analysis and boundary value problems*, 2001
- 276 **Emma Previato, Editor**, *Advances in algebraic geometry motivated by physics*, 2001
- 275 **Alfred G. Noël, Earl Barnes, and Sonya A. F. Stephens, Editors**, *Council for African American researchers in the mathematical sciences: Volume III*, 2001
- 274 **Ken-ichi Maruyama and John W. Rutter, Editors**, *Groups of homotopy self-equivalences and related topics*, 2001
- 273 **A. V. Kelarev, R. Göbel, K. M. Rangaswamy, P. Schultz, and C. Vinsonhaler, Editors**, *Abelian groups, rings and modules*, 2001
- 272 **Eva Bayer-Fluckiger, David Lewis, and Andrew Ranicki, Editors**, *Quadratic forms and their applications*, 2000
- 271 **J. P. C. Greenlees, Robert R. Bruner, and Nicholas Kuhn, Editors**, *Homotopy methods in algebraic topology*, 2001
- 270 **Jan Denef, Leonard Lipschitz, Thanases Pheidas, and Jan Van Geel, Editors**, *Hilbert's tenth problem: Relations with arithmetic and algebraic geometry*, 2000
- 269 **Mikhail Lyubich, John W. Milnor, and Yair N. Minsky, Editors**, *Laminations and foliations in dynamics, geometry and topology*, 2001
- 268 **Robert Gulliver, Walter Littman, and Roberto Triggiani, Editors**, *Differential geometric methods in the control of partial differential equations*, 2000
- 267 **Nicolás Andruskiewitsch, Walter Ricardo Ferrer Santos, and Hans-Jürgen Schneider, Editors**, *New trends in Hopf algebra theory*, 2000
- 266 **Caroline Grant Melles and Ruth I. Michler, Editors**, *Singularities in algebraic and analytic geometry*, 2000
- 265 **Dominique Arlettaz and Kathryn Hess, Editors**, *Une dégustation topologique: Homotopy theory in the Swiss Alps*, 2000
- 264 **Kai Yuen Chan, Alexander A. Mikhalev, Man-Keung Siu, Jie-Tai Yu, and Efim I. Zelmanov, Editors**, *Combinatorial and computational algebra*, 2000
- 263 **Yan Guo, Editor**, *Nonlinear wave equations*, 2000
- 262 **Paul Igodt, Herbert Abels, Yves Félix, and Fritz Grunewald, Editors**, *Crystallographic groups and their generalizations*, 2000
- 261 **Gregory Budzban, Philip Feinsilver, and Arun Mukherjee, Editors**, *Probability on algebraic structures*, 2000
- 260 **Salvador Pérez-Esteva and Carlos Villegas-Blas, Editors**, *First summer school in analysis and mathematical physics: Quantization, the Segal-Bargmann transform and semiclassical analysis*, 2000
- 259 **D. V. Huynh, S. K. Jain, and S. R. López-Permouth, Editors**, *Algebra and its applications*, 2000

(Continued in the back of this publication)

This page intentionally left blank

Advances in Wave Interaction and Turbulence

This page intentionally left blank

CONTEMPORARY MATHEMATICS

283

Advances in Wave Interaction and Turbulence

Proceedings of an AMS-IMS-SIAM
Joint Summer Research Conference
on Dispersive Wave Turbulence
Mount Holyoke College, South Hadley, MA
June 11–15, 2000

Paul A. Milewski
Leslie M. Smith
Fabian Waleffe
Esteban G. Tabak
Editors



American Mathematical Society
Providence, Rhode Island

Editorial Board

Dennis DeTurck, managing editor

Andreas Blass Andy R. Magid Michael Vogelius

This volume contains the proceedings of an AMS-IMS-SIAM Joint Summer Research Conference on Dispersive Wave Turbulence held at Mount Holyoke College, South Hadley, MA on June 11–15, 2000, with support from the National Science Foundation, grant DMS-9973450.

2000 *Mathematics Subject Classification*. Primary 76B15, 35Q53, 37K10, 76B60, 74J20, 74J30, 76F55, 76F65.

Any opinions, findings, and conclusions or recommendations expressed in this material are those of the authors and do not necessarily reflect the views of the National Science Foundation.

Library of Congress Cataloging-in-Publication Data

AMS-IMS-SIAM Joint Summer Research Conference on Dispersive Wave Turbulence (2000 : Mount Holyoke College)

Advances in wave interaction and turbulence : proceedings of an AMS-IMS-SIAM Joint Summer Research Conference on Dispersive Wave Turbulence, Mount Holyoke College, South Hadley, MA, June 11–15, 2000 / Paul A. Milewski . . . [et al.], editors.

p. cm. — (Contemporary mathematics, ISSN 0271-4132 ; 283)

Includes bibliographical references.

ISBN 0-8218-2714-6 (alk. paper)

1. Wave-motion, Theory of—Congresses. 2. Turbulence—Congresses. I. Milewski, Paul A., 1966– II. Title. III. Contemporary mathematics (American Mathematical Society) ; v. 283.

QA927.A48 2000
530.12'4—dc21

2001046252

Copying and reprinting. Material in this book may be reproduced by any means for educational and scientific purposes without fee or permission with the exception of reproduction by services that collect fees for delivery of documents and provided that the customary acknowledgment of the source is given. This consent does not extend to other kinds of copying for general distribution, for advertising or promotional purposes, or for resale. Requests for permission for commercial use of material should be addressed to the Assistant to the Publisher, American Mathematical Society, P. O. Box 6248, Providence, Rhode Island 02940-6248. Requests can also be made by e-mail to reprint-permission@ams.org.

Excluded from these provisions is material in articles for which the author holds copyright. In such cases, requests for permission to use or reprint should be addressed directly to the author(s). (Copyright ownership is indicated in the notice in the lower right-hand corner of the first page of each article.)

© 2001 by the American Mathematical Society. All rights reserved.

The American Mathematical Society retains all rights
except those granted to the United States Government.

Printed in the United States of America.

⊗ The paper used in this book is acid-free and falls within the guidelines
established to ensure permanence and durability.

Visit the AMS home page at URL: <http://www.ams.org/>

10 9 8 7 6 5 4 3 2 1 06 05 04 03 02 01

Contents

Preface	ix
Strongly stratified limit of 3D primitive equations in an infinite layer A. BABIN, A. MAHALOV, AND B. NICOLAENKO	1
Anomalous transport by wave turbulence A. M. BALK	13
Statistical equilibrium theories for the nonlinear Schrödinger equation R. JORDAN AND B. TURKINGTON	27
Is there a 2D cascade in 3D convection? R. M. KERR	41
The forced inviscid Burgers equation as a model for nonlinear interactions among dispersive waves F. MENZAQUE, R. R. ROSALES, E. G. TABAK, AND C. V. TURNER	51
Traveling surface elastic waves in the half-plane P. PANAYOTAROS	83
Numerical study of two-dimensional stratified turbulence L. M. SMITH	91
Turbulence of one-dimensional weakly nonlinear dispersive waves V. E. ZAKHAROV, P. GUYENNE, A. N. PUSHKAREV, AND F. DIAS	107

This page intentionally left blank

Preface

We often think of our natural environment as being composed of very many interacting particles, undergoing individual chaotic motions, of which only very coarse averages are perceptible at scales natural to us. However, we could as well think of the world as being made out of individual waves. This is so not just because the distinction between waves and particles becomes rather blurred at the atomic level, but also because even phenomena at much larger scales are better described in terms of waves rather than of particles: it is rare in both fluids and solids to observe energy being carried from one region of space to another by a given set of material particles; much more often, this transfer occurs through chains of particles, neither of them moving much, but each communicating with the next, and hence creating these immaterial objects we call waves.

Waves occur at many spatial and temporal scales. Many of these waves have small enough amplitude that they can be approximately described by linear theory. However, the joint effect of large sets of waves is governed by nonlinear interactions, which are responsible for huge cascades of energy among very disparate scales. Understanding these energy transfers is crucial in order to determine the response of large systems, such as the atmosphere and the ocean, to external forcings and dissipation mechanisms which act on scales decades apart.

The field of wave turbulence attempts to understand the average behavior of large ensembles of waves, subjected to forcing and dissipation at opposite ends of their spectrum. It does so by studying individual mechanisms for energy transfer, such as resonant triads and quartets, and attempting to draw from them effects that should survive averaging.

The AMS-IMS-SIAM Joint Summer Research Conference on Dispersive Wave Turbulence was held in Mt. Holyoke College, MA, from the 11 to the 15 of June of the year 2000. It drew together a group of researchers from many corners of the world, in the context of a perceived renaissance of the field, driven by heated debate about the fundamental mechanism of energy transfer among large sets of waves, as well as by novel applications – and old ones revisited – to the understanding of the natural world. We hope that these proceedings reflect part of the spirit that permeated the conference, that of friendly scientific disagreement and genuine wonder at the rich phenomenology of waves.

Paul Milewski
Leslie M. Smith
Fabian Waleffe
Esteban G. Tabak

This page intentionally left blank

Strongly Stratified Limit of 3D Primitive Equations in an Infinite Layer

A. Babin, A. Mahalov, and B. Nicolaenko

ABSTRACT. Three-dimensional primitive equations of geophysical fluid dynamics in an infinite rotating layer are analyzed under the Boussinesq approximation in the asymptotic limit of strong stratification. The ‘split’ of the energy transfer of the vortical and the wave components is verified in this geometry. The vertically averaged (barotropic) ageostrophic field is advected by the vertically averaged quasi-geostrophic velocity when both rotation and stratification are dominant.

1. Introduction

In this paper we study initial value problem for the 3D Primitive Equations of geophysical fluid dynamics. The governing flow equations for rotating stably stratified fluids under the Boussinesq approximation are

$$(1.1) \quad \partial_t \mathbf{U} - \nu_1 \Delta \mathbf{U} + \mathbf{U} \cdot \nabla \mathbf{U} + f \mathbf{e}_3 \times \mathbf{U} = -\nabla p + \rho_1 \mathbf{e}_3, \quad \nabla \cdot \mathbf{U} = 0,$$

$$(1.2) \quad \partial_t \rho_1 - \nu_2 \Delta \rho_1 + \mathbf{U} \cdot \nabla \rho_1 = -N^2 U_3,$$

where rotation and mean stratification gradient are aligned parallel to $\mathbf{e}_3 = [0, 0, 1]$. Here $\mathbf{U} = (U_1, U_2, U_3)$ is the velocity field and ρ_1 is the buoyancy variable; N is the Brunt-Väisälä parameter for constant stratification and f is the Coriolis parameter. We focus on inviscid Eqs. (1.1)-(1.2) or with small uniform viscosities. We assume here that the ratio $\eta = f/N$ is fixed and $N \rightarrow \infty$.

We introduce a change of variables $\rho_1 = N\rho$ (Métais and Herring 1989) and combine velocity and buoyancy variable in one variable $\mathbf{U}^\dagger = (\mathbf{U}, \rho)$ after which Eqs. (1.1)-(1.2) written in non-dimensional variables take more symmetric form:

$$(1.3) \quad \partial_t \mathbf{U}^\dagger - \nu \Delta \mathbf{U}^\dagger + \mathbf{U} \cdot \nabla \mathbf{U}^\dagger + f \mathbf{R} \mathbf{U}^\dagger = -\nabla^\dagger p - N \mathbf{S} \mathbf{U}^\dagger, \quad \nabla \cdot \mathbf{U} = 0, \\ \mathbf{U}^\dagger|_{t=0} = \mathbf{U}^\dagger(0)$$

where from now on we take $\nu_1 = \nu_2 = \nu$ and where $\nabla^\dagger p = (\nabla p, 0)$. Here

$$\mathbf{R} = \begin{pmatrix} \mathbf{J} & \mathbf{0} \\ \mathbf{0} & \mathbf{0} \end{pmatrix}, \quad \mathbf{S} = \begin{pmatrix} \mathbf{0} & \mathbf{0} \\ \mathbf{0} & \mathbf{J} \end{pmatrix}, \quad \mathbf{J} = \begin{pmatrix} 0 & -1 \\ 1 & 0 \end{pmatrix},$$

1991 *Mathematics Subject Classification.* Primary 76D05, 76D33; Secondary 35B32, 34C15.

Key words and phrases. Three-dimensional Navier-Stokes equations, waves, geophysical flows.

The work was supported by the AFOSR contracts FG9620-99-1-0300, F49620-99-1-0203 and the Isaac Newton Institute for Mathematical Sciences, Cambridge University.

and \mathbf{R}_n , \mathbf{S}_n will denote the action of \mathbf{R} and \mathbf{S} on n -th Fourier component, $\mathbf{M} = f\mathbf{R} + N\mathbf{S}$. In the next section we write Eqs. (1.1)-(1.2) in the Craya cyclic basis and use this representation to obtain asymptotic limit resonant equations. Fourier series with respect to the vertical variable x_3 and Fourier transform with respect to x_1, x_2 will be used in this paper to represent physical fields in a layer $(-\infty, \infty) \times (-\infty, \infty) \times [-\pi, \pi]$, periodic in x_3 . All results in this paper extend to boundary conditions with zero flux in the vertical direction e_3 on the boundary. One only needs to restrict Fourier series to be even in x_3 for U_1, U_2 and odd in x_3 for U_3 . Such boundary conditions imply zero tangential stress on the vertical boundary (e.g. Drazin and Reid, [24]).

Following Bartello [16], it is useful to distinguish between two sets of wavevectors $k = (k_1, k_2, k_3)$, the barotropic set $\{k : k_3 = 0\}$, and the remaining baroclinic vectors $\{k : k_1^2 + k_2^2 \neq 0, k_3 \neq 0\}$. Then the operation of vertical averaging corresponds to projection on barotropic fields. In this paper as well as in our previous work (see [5], [8], [12], [15]) we emphasize the important role of 3D quasi-geostrophic (3DQG) and barotropic dynamics for rotating and stably stratified flows. We denote by $\bar{\mathbf{U}}$ the vertical average of \mathbf{U} and $\hat{\mathbf{U}} = \mathbf{U} - \bar{\mathbf{U}}$.

There is a big difference between the equations in a finite geometry and an infinite geometry. The case of finite geometry (a periodic box) was considered in detail for the case of 3D rotating Navier-Stokes equations in [5], [8] and [12] and for the 3D Primitive Equations in [6], [10]-[15]; see also [25], [26], [27], [28] and [29]. It was proven in [12] and [13] for 3D rotating Navier-Stokes and the 3D Primitive Equations respectively that solutions of the limit equations are always regular and solutions of the original equations with strong rotation or stratification are regular too.

When the geometry is infinite (the whole space) and the Rossby number tends to zero (that is rotation rate tends to infinity) for solutions of the Navier-Stokes equations with a finite energy it was shown in Chemin, Desjardins, Gallagher and Grenier ([20] and [21]) that the limit dynamics reduces to 2D barotropic Navier-Stokes equations and there is no ageostrophic limit dynamics at the leading order. The reason is that the Coriolis term generates waves which carry away energy to infinity. Therefore oscillating part of solution at every positive time tends to zero as the Rossby number tends to zero. This effect is expressed in the form of Strichartz inequalities ([20] and [21]). Similarly, a finite energy 3D perturbation of 2D periodic initial data generates a solution which tends to a solution of 2D Navier-Stokes equations and the energy of the ageostrophic part is carried away to infinity.

Here we consider the 3D Primitive Equations (1.1)-(1.3) under the Boussinesq approximation in an infinite layer with a finite height, and we derive the limit equations which describe a nontrivial dynamics for both quasigeostrophic and ageostrophic components. The quasigeostrophic component satisfies the quasigeostrophic equation (3DQG). The vertically averaged (barotropic) ageostrophic field is advected by the vertically averaged quasigeostrophic velocity (2D component) in the asymptotic limit equations when both rotation and stratification are dominant.

2. Quasigeostrophic and ageostrophic components in the Craya basis

The inertio-gravity wave propagator is the operator solution $\mathbf{E}(Nt)$ ($\mathbf{E}(0) = \mathbf{Id}$ is the identity) to the linear problem obtained from (1.3):

$$\Phi(t) = \mathbf{E}(Nt)\Phi_0; \quad \Phi(0) = \Phi_0$$

where $\Phi(t) = (\mathbf{U}(t), \rho(t))$ (see [11], [14], [13] for details). The operator $\mathbf{E}(Nt)$ describes propagation of inertio-gravity waves. In the Craya cyclic basis (see [35], [32], [30] and [18]) the linear problem restricted on the subspace of divergence free vector fields reduces to the following 3×3 matrix for the n -th Fourier component:

$$\omega_n \mathbf{M}' = \omega_n \begin{pmatrix} 0 & 0 & 0 \\ 0 & 0 & -1 \\ 0 & 1 & 0 \end{pmatrix}$$

where zero eigenvalue corresponds to the quasi-geostrophic mode (vortical mode). We use the extended notation

$$m = [m_1, m_2, m_3, 0],$$

and similarly for n, k . We introduce the orthonormal basis of the divergence-free subspace for n -th Fourier mode:

$$(2.1) \quad p_{0n} = \left[-\frac{n_2}{|n'|}, \frac{n_1}{|n'|}, 0, 0 \right]; \quad p_{1n} = \left[\frac{n_1 n_3}{|n| |n'|}, \frac{n_2 n_3}{|n| |n'|}, \frac{-n_1^2 - n_2^2}{|n| |n'|}, 0 \right];$$

$$p_{2n} = e_4 = [0, 0, 0, 1].$$

Here $n_1, n_2 \in \mathbb{R}$, $n_3 \in \mathbb{Z}$; $|n|^2 = n_1^2 + n_2^2 + n_3^2$, $|n'|^2 = n_1^2 + n_2^2$. The vectors p_{0k}, p_{0m}, p_{1k} etc. are defined similarly. The vectors p_{0k}, p_{1k}, p_{2k} are orthonormal cyclic vectors for the matrix \mathbf{S} restricted on the divergence free Fourier subspace; let \mathbf{P}_d be the projection on divergence free vectors in the Helmholtz decomposition (for the velocity component):

$$\mathbf{P}_d \mathbf{S}_n p_{0n} = 0; \quad \mathbf{P}_d \mathbf{S}_n p_{1n} = -\phi_n p_{2n}; \quad \mathbf{P}_d \mathbf{S}_n p_{2n} = \phi_n p_{1n}; \quad \phi_n = \frac{|n'|}{|n|}.$$

The p_{jk} are the Craya basis for the purely stratified problem, already used in [35]. In the case $f \neq 0$ we use the following orthonormal basis

$$(2.2) \quad q_{0n} = \frac{1}{\omega_n} (\phi_n p_{0n} + \eta \xi_n p_{2n}), \quad q_{1n} = p_{1n}, \quad q_{2n} = \frac{1}{\omega_n} (\phi_n p_{2n} - \eta \xi_n p_{0n})$$

where

$$(2.3) \quad \xi_n = \frac{n_3}{|n|}, \quad \omega_n^2 = \phi_n^2 + \eta^2 \xi_n^2, \quad \eta = f/N$$

(see for details [15], [10]); the algebra is the same for periodic box and infinite layer, one has to use Fourier transform with respect to horizontal variables. For the matrix of linear problem in (1.3)

$$\mathbf{M}_n = N\mathbf{S}_n + f\mathbf{R}_n$$

the vectors (2.2) form a cyclic basis since, after projection on divergence-free vector fields via Helmholtz decomposition:

$$\mathbf{P}_d \mathbf{M} q_{0n} = 0, \quad \mathbf{P}_d \mathbf{M} q_{1n} = -\omega_n q_{2n}, \quad \mathbf{P}_d \mathbf{M} q_{2n} = \omega_n q_{1n}.$$

Any arbitrary divergence-free vector field \mathbf{U}_n^\dagger can be written as

$$\mathbf{U}_n^\dagger = V_n^0 q_{0n} + V_n^1 q_{1n} + V_n^2 q_{2n}.$$

We shall use the variables V to denote vector of coefficients corresponding to \mathbf{U}_n^\dagger : $\mathbf{V}_n = [V_n^0, V_n^1, V_n^2] = [V_n^0, \mathbf{V}'_n]$, $\mathbf{V}'_n = [V_n^1, V_n^2]$. We denote by Π_n^{QG} the projection onto q_{0n} (quasi-geostrophic mode):

$$\mathbf{U}^{QG}(x, t) = \Pi^{QG} \mathbf{U}^\dagger(x) = \sum_{n_3} \frac{1}{(2\pi)^2} \int \int V_n^0 q_{0n} e^{in \cdot x} dn_1 dn_2, \quad \Pi_n^{QG} \mathbf{U}_n^\dagger = V_n^0 q_{0n}.$$

Similarly, we define the projection Π^{AG} onto ageostrophic component $\Pi_n^{AG} \mathbf{U}_n^\dagger = V_n^1 q_{1n} + V_n^2 q_{2n}$:

$$\mathbf{U}^{AG}(x, t) = \Pi^{AG} \mathbf{U}^\dagger(x) = \sum_{n_3} \frac{1}{(2\pi)^2} \int \int (V_n^1 q_{1n} + V_n^2 q_{2n}) e^{in \cdot x} dn_1 dn_2.$$

The action of the linear propagator $\mathbf{E}(Nt)$ on the Fourier components can be written in V -variables

$$(2.4) \quad \mathbf{E}(Nt)[V^0, \mathbf{V}']_n = \exp(N\omega_n t \mathbf{M}'_n)[V^0, \mathbf{V}']_n = [V^0, \exp(N\omega_n t \mathbf{J}) \mathbf{V}'].$$

Here \mathbf{J} , \mathbf{M}'_n are given by

$$(2.5) \quad \mathbf{M}'_n = \begin{pmatrix} 0 & 0 & 0 \\ 0 & 0 & -1 \\ 0 & 1 & 0 \end{pmatrix}, \quad \mathbf{J} = \begin{pmatrix} 0 & -1 \\ 1 & 0 \end{pmatrix}.$$

Then Eqs. (1.3) in Fourier representation in V variables can be written in the cyclic basis (2.2) as

$$(2.6) \quad \partial_t V_n^{i_3} = -i \sum_{k+m=n, i_1, i_2} Q_{kmn}^{i_1 i_2 i_3} V_k^{i_1} V_m^{i_2} - N\omega_n (M'_n V_n)^{i_3} - \nu |n|^2 V_n^{i_3}$$

where $i_1, i_2, i_3 = 0, 1, 2$, M' is the matrix M in V -variables. The coefficients $Q_{kmn}^{i_1 i_2 i_3}$ are determined in the Craya basis as follows

$$Q_{kmn}^{i_1 i_2 i_3} = (q_{i_1 k} \cdot m)(q_{i_2 m} \cdot q_{i_3 n}).$$

The coefficients $Q_{kmn}^{i_1 i_2 i_3}$, $k+m=n$, are obtained by a straightforward computation using (2.2), they are given explicitly in [15]. For the coefficient describing interaction of 0-modes (quasi-geostrophic = vortical) we obtain ($n' \wedge m' \equiv n_1 m_2 - n_2 m_1$).

$$Q_{kmn}^{000} = \frac{n' \wedge m'}{\omega_k \omega_m \omega_n |k| |m| |n|} (n' \cdot m' + \eta^2 n_3 m_3).$$

Since skew-symmetric in k, m component of Q_{kmn}^{000} makes no contribution to Eq. (2.6), we can use the following Q_{kmn}^{000} in Eq. (2.6):

$$Q_{kmn}^{000} = \frac{k' \wedge m'}{\omega_k \omega_m \omega_n |k| |m| |n|} (|m'|^2 + \eta^2 m_3^2) = \frac{\omega_m |m| k' \wedge m'}{\omega_k \omega_n |k| |n|}$$

where we have used $|m|^2 \omega_n^2 = |m'|^2 + \eta^2 m_3^2$. The coefficient Q_{kmn}^{000} is the familiar coefficient in 3DQG equations written in cyclic basis.

3. The limit resonant equations for an infinite layer

In this section we derive the limit resonant equations for an infinite layer and prove the corresponding convergence theorems. Eqs. (2.6) have the form

$$(3.1) \quad \partial_t \mathbf{V}_n + N\omega_n \mathbf{M}'_n \mathbf{V}_n = (\mathbf{B}(\mathbf{V}, \mathbf{V}))_n - \nu |n|^2 \mathbf{V}_n.$$

Here \mathbf{M}' is the linear propagator operator corresponding to inertio-gravity waves given in cyclic V -variables. We introduce the linear propagator directly into non-linearity using the change of variables

$$(3.2) \quad \mathbf{V}(t) = \mathbf{E}(-Nt)\mathbf{v}(t), \mathbf{V}_n = \exp(-N\omega_n\mathbf{M}'_nt)\mathbf{v}_n$$

where $\mathbf{v} = [v^0, v^1, v^2]$ and \mathbf{M}' is defined by Eq. (2.5). Eqs. (3.1) written in slow ‘‘Poincare’’ \mathbf{v} variables ([34]) have the form

$$(3.3) \quad \partial_t\mathbf{v} = \mathbf{B}_p(Nt, \mathbf{v}, \mathbf{v}) + \nu\Delta\mathbf{v},$$

$$(3.4) \quad \mathbf{B}_p(Nt, \mathbf{v}, \mathbf{v}) = \mathbf{E}(Nt)\mathbf{B}(\mathbf{E}(-Nt)\mathbf{v}, \mathbf{E}(-Nt)\mathbf{v}).$$

Eqs. (3.3) are explicitly time-dependent with rapidly varying coefficients.

The following equations describing the asymptotic limit dynamics are associated with Eqs. (3.4) (see [6], [10]-[15]):

$$(3.5) \quad \partial_t\mathbf{w} = \tilde{\mathbf{B}}(\mathbf{w}, \mathbf{w}) + \nu\Delta\mathbf{w}, \tilde{\mathbf{B}}(\mathbf{w}, \mathbf{w}) = \lim_{N \rightarrow +\infty} \frac{1}{T} \int_0^T \mathbf{B}_p(Ns, \mathbf{w}, \mathbf{w}) ds$$

where the arguments \mathbf{w} are s -independent (that is frozen in ‘‘slow’’ time). Recall that we take the limit $\eta = f/N$ fixed, $N \rightarrow +\infty$. The limit resonant equations (3.5) are obtained by annihilating all terms in the averaging of \mathbf{B}_p which contain fast oscillating factors.

The bilinear form $\tilde{\mathbf{B}}(\mathbf{w}, \mathbf{w})$ in Eqs. (3.5) can be conveniently represented in the cyclic basis (2.2). We explicit the resonant (limit) equation for $\mathbf{w} = w^0q_0 + w^1q_1 + w^2q_2$ in the Craya basis where w^0 is simply projection of \mathbf{w} on QG mode. Then w^0 satisfies the quasi-geostrophic equation; the proof of operator splitting in [6], [15] [10], [13], [25] and [26] is easily extended to an infinite layer domain, see details in Section 2.2. The ageostrophic component $\mathbf{w}' = (w^1, w^2)$ is found from inertio-gravity wave limit equation. The quasi-geostrophic equation is given by

$$(3.6) \quad \partial_t w_n^0 = \mathbf{B}_0(w^0, w^0)_n - \nu|n|^2 w_n^0,$$

$$(3.7) \quad \mathbf{B}_0(w^0, w^0)_n = -i \sum_{k+m=n} Q_{kmn}^{000} w_k^0 w_m^0, \quad Q_{kmn}^{000} = \frac{\omega_m |m| k' \wedge m'}{\omega_k \omega_n |k| |n|}.$$

See for details [11]-[15]. We introduce variables \tilde{q} , \mathbf{U}^{QG} (quasi-geostrophic potential and velocity, not to be confused with the cyclic basis vectors q_{0n} , q_{1n} and q_{2n}):

$$(3.8) \quad \tilde{q}_m = \omega_m |\tilde{m}| w_m^0, \quad \mathbf{U}_k^{QG} = [-k_2/a_2, k_1, 0, 0] \tilde{\Psi}_k^0, \quad \tilde{\Psi}_k^0 = \tilde{q}_k / (\omega_k^2 |\tilde{k}|^2).$$

Recalling that $\omega_k^2 |\tilde{k}|^2 = |\tilde{k}'|^2 + \eta^2 \tilde{k}_3^2$, $\eta = f/N$, we have the familiar formula which relates $\tilde{\Psi}^0$ and \tilde{q} in physical space

$$(3.9) \quad -(\nabla_h^2 + \eta^2 \partial_3^2) \tilde{\Psi}^0 = \tilde{q}.$$

Using (3.8), Eq. (3.6) is written in the form:

$$\partial_t \tilde{q}_n = -i \sum_{k+m=n} (\mathbf{U}_k^{QG} \cdot m) \tilde{q}_m - \nu|n|^2 \tilde{q}_n,$$

where in the inviscid case $\tilde{q}(t, x)$ obeys in physical space the 3D quasi-geostrophic equations (Bourgeois and Beale, [17])

$$\frac{\tilde{D}}{\tilde{D}t} \tilde{q} = 0$$

where $\frac{\hat{D}}{Dt}$ is the advective derivative, based on the quasi-geostrophic velocity and \tilde{q} is the quasi-geostrophic potential.

3.1. Estimates for the baroclinic ageostrophic component. In this section we show that for every fixed $x = (x_1, x_2, x_3)$ and $t > 0$, $0 < t \leq t_1$ the baroclinic part of the ageostrophic component with zero vertical average tends to zero; first define the barotropic ageostrophic component

$$(3.10) \quad \bar{\mathbf{U}}^{AG}(x_1, x_2, t) = \frac{1}{2\pi} \int_{-\pi}^{\pi} \mathbf{U}^{AG}(x_1, x_2, x_3, t) dx_3$$

and

$$(3.11) \quad \hat{\mathbf{U}}^{AG}(x_1, x_2, x_3, t) = \mathbf{U}^{AG}(x, t) - \bar{\mathbf{U}}^{AG}(x_1, x_2, t)$$

which is the baroclinic ageostrophic component. Then $\hat{\mathbf{U}}^{AG}(x, t) \rightarrow 0$ as $N \rightarrow \infty$. We repeat the proof of [20]-[21] for the situation of $\hat{\mathbf{U}}^{AG}$ satisfying 3D rotating Boussinesq equations in a finite width layer.

We denote by H_s the standard Sobolev space with the norm

$$(3.12) \quad \|u\|_s^2 = \sum_{n_3} \int \int (1 + |n|^2)^s |u(n)|^2 dn_1 dn_2$$

where $u(n)$ are the Fourier coefficients of $u(x)$, where Fourier transform is taken in x_1, x_2 and Fourier series in x_3 . First we give a standard small time regularity theorem for Eqs. (1.1)-(1.3).

THEOREM 3.1. *Let $\mathbf{U}^\dagger(0) \in H_s$, $s > 1/2$. Then there exists a unique solution $\mathbf{U}^\dagger(t) \in H_s$, $0 \leq t \leq t_1$ and $\|\mathbf{U}^\dagger(t)\|_s \leq C$ where t_1, C depend only on the norm of $\mathbf{U}^\dagger(0)$.*

The proof is the same as in [11]-[14], unboundedness in horizontal directions does not make any essential difference. Using Sobolev embedding theorems we get:

THEOREM 3.2. *Let $\mathbf{U}^\dagger(0) \in H_s$, $s > 3/2$. Then $\mathbf{B}(\mathbf{U}^\dagger, \mathbf{U}^\dagger)$ is bounded in $L_\infty([0, t_1], L_2)$, where*

$$(3.13) \quad \mathbf{B}(\mathbf{U}^\dagger, \mathbf{U}^\dagger) = (-\mathbf{P}_d(\mathbf{U} \cdot \nabla \mathbf{U}), -\mathbf{U} \cdot \nabla U_4), \quad \mathbf{U}^\dagger = (\mathbf{U}, U_4) = (\mathbf{U}, \rho).$$

Here \mathbf{P}_d is the Leray projection on divergence free vector fields.

Now we apply the method of [20]-[21].

THEOREM 3.3. *Let $\mathbf{U}^\dagger(0) \in H_s$, $s > 3/2$. Then for every $R > 0$, $t_0 > 0$, $t \leq t_1$ and $\epsilon > 0$ we have $\hat{\mathbf{U}}^{AG}(t) \rightarrow 0$ as $N \rightarrow \infty$ in $L_{loc}^2([t_0, t_1], H_{s-\epsilon}(B_R))$, where B_R is a ball of radius R .*

PROOF. In Fourier representation we expand $\mathbf{U}^\dagger(k) = \mathbf{U}^{QG}(k) + \mathbf{U}^{AG}(k)$ (see [11], [14] and [13] for details). Note that now $k = (k_1, k_2, k_3)$ where k_1, k_2 are continuous and $k_3 = 0, \pm 1, \pm 2, \dots$. The equation for two components of $\hat{\mathbf{U}}^{AG}$ is

$$\partial_t \hat{\mathbf{U}}^{AG}(k) = -N\omega(k) \mathbf{J} \hat{\mathbf{U}}^{AG} - \nu |k|^2 \hat{\mathbf{U}}^{AG} + \mathbf{D}(\mathbf{U}^\dagger)(k),$$

where $\mathbf{D}(\mathbf{U}^\dagger)$ contains nonlinear terms and righthand sides; it is considered as a given forcing term of a linear equation. We use boundedness of $\mathbf{D}(\mathbf{U}^\dagger)$ in $L_\infty([0, t_1]L_2)$ for small t_1 (see [11], [14] and [13] for details).

Here the eigenvalues $\omega(k)$ satisfy the dispersion relation

$$(3.14) \quad \omega(k) = \sqrt{1 + b \frac{k_3^2}{|k|^2}},$$

with $b = \eta^2 - 1$. The equations for $\hat{\mathbf{U}}^{AG}$ are of the kind considered in [20] and [21], with a slightly different dispersion relation; this dispersion relation is also invariant with respect to rotation around k_3 axis. Note that in [20] and [21] only continuity of k_2, k_1 is used. In our case we have

$$(3.15) \quad \partial_1 \omega(n) = -\frac{bn_1 n_3^2}{\omega(n)(n_1^2 + n_2^2 + n_3^2)^2}, |\partial_1 \omega(n)| \geq cn_1 n_3^2,$$

with $c > 0$. The above holds when $n_3^2 \geq 1, |n| \leq R$. The estimates (3.15) are similar to $\alpha(k)$ in [21], for the pure rotating Navier-Stokes case:

$$(3.16) \quad \alpha(k) = -\partial_2 \omega(k) = \frac{k_2 k_3}{|k|^3}, \partial_2 \alpha(k) = -\frac{3k_2^2 k_3}{|k|^5} + \frac{k_3}{|k|^3},$$

where $\omega(k) = \frac{k_3}{|k|}$ in the pure rotation case.

With the use of Strichartz-type estimates, this implies, following closely the methods in [21], $\hat{\mathbf{U}}^{AG}(k) \rightarrow 0$ as $N \rightarrow \infty$ when $n_3 \neq 0$ in $L^2_{loc}([t_0, t_1], L_4)$ when $t_0 > 0$. Using Theorem 3.1 we obtain that $\|\hat{\mathbf{U}}^{AG}\|_{L^2_{loc}([t_0, t_1], H_{s-\epsilon}(B_R))} \rightarrow 0$ as $N \rightarrow \infty$, in $H'_s(B_R)$, $s' < s$ where B_R is a ball of radius R . Theorem 3.3 is proven. \square

3.2. The split of the energy transfer for the vortical and the wave components in an infinite layer. In this section we establish the split of the energy transfer for the vortical component (3DQG) and the wave components (AG fields) for the asymptotic limit equations in a layer. The structure of the asymptotic limit equations is given by Eqs. (3.19)-(3.20).

THEOREM 3.4. *Under the conditions of Theorem 3.3, \mathbf{U}^{QG} and $\bar{\mathbf{U}}^{AG}$ (vertical averaging of \mathbf{U}^{AG}) tend to a solution of the 3DQG equation (3.19) and an advected system (3.20) for a barotropic ageostrophic component respectively.*

PROOF. Applying the projection Π^{QG} to Eq. (1.3), the equation for QG component is

$$(3.17) \quad \partial_t \mathbf{U}^{QG} = \nu \Delta \mathbf{U}^{QG} + \mathbf{B}^{QG}(\mathbf{U}^{QG} + \bar{\mathbf{U}}^{AG} + \hat{\mathbf{U}}^{AG}, \mathbf{U}^{QG} + \bar{\mathbf{U}}^{AG} + \hat{\mathbf{U}}^{AG})$$

where $\mathbf{B}^{QG} = \Pi^{QG} \mathbf{B}$ and $\mathbf{B}^{AG} = \Pi^{AG} \mathbf{B}$. Eq. (3.17) does not include explicit dependence on N ; therefore one obtains using Theorem 3.1 the estimate of $\partial_t \mathbf{U}^{QG}$ uniform in N , and we can choose a convergent subsequence of $\partial_t \bar{\mathbf{U}}^{QG}$.

For the component $\bar{\mathbf{U}}^{AG}$ we use the same ‘‘Poincare’’ variables substitution as in Eq. (3.2): $\bar{\mathbf{U}}_{AG} = \mathbf{E}(-Nt) \bar{\mathbf{u}}^{AG}$ where $\mathbf{E}(-Nt)$ is the linear wave propagator. The frequencies for $\bar{\mathbf{U}}^{AG}$ are not dispersive in k_1, k_2 for $k_3 = 0$, since $\omega(k) = 1$ for $k_3 = 0$ (see eq. (2.3)). We have

$$(3.18) \quad \begin{aligned} \partial_t \bar{\mathbf{u}}^{AG} &= \nu \Delta \bar{\mathbf{u}}^{AG} \\ &+ \bar{\mathbf{E}}(Nt) \bar{\mathbf{B}}^{AG}(\mathbf{U}^{QG} + \mathbf{E}(-Nt) \bar{\mathbf{u}}^{AG} + \hat{\mathbf{U}}^{AG}, \mathbf{U}^{QG} + \mathbf{E}(-Nt) \bar{\mathbf{u}}^{AG} + \hat{\mathbf{U}}^{AG}). \end{aligned}$$

Using Theorem 3.1 we get the estimate of $\partial_t \bar{\mathbf{u}}^{AG}$ uniform in N , and we can choose a convergent subsequence of $\partial_t \bar{\mathbf{u}}^{AG}$. Integrating (3.17) in time we get exactly like in [6], [14], [15] and [10] that

$$\lim_{N \rightarrow +\infty} \frac{1}{T} \int_0^T \mathbf{B}^{QG}(\mathbf{E}(-Ns) \bar{\mathbf{u}}^{AG}, \mathbf{E}(-Ns) \bar{\mathbf{u}}^{AG}) ds = 0$$

where averaging is done in the sense of Eq. (3.5) (the algebra which is used here to show that the above resonant operator is zero is the same as in [6], [14], [15] and [10]). We also have obviously non-resonant terms

$$\lim_{N \rightarrow +\infty} \frac{1}{T} \int_0^T \mathbf{B}^{QG}(\mathbf{U}^{QG}, \mathbf{E}(-Ns) \bar{\mathbf{u}}^{AG}) ds = 0,$$

$$\lim_{N \rightarrow +\infty} \frac{1}{T} \int_0^T \mathbf{B}^{QG}(\mathbf{E}(-Ns) \bar{\mathbf{u}}^{AG}, \mathbf{U}^{QG}) ds = 0.$$

Since three-wave interaction resonance condition takes the form $\pm 1 \pm 1 \pm 1 = 0$ for $k_3 = m_3 = n_3 = 0$ (recall that $\omega_k = 1$ for $k_3 = 0$ and similarly for m, n) we do not have resonant terms for

$$\lim_{N \rightarrow +\infty} \frac{1}{T} \int_0^T \mathbf{E}(Ns) \mathbf{B}^{AG}(\mathbf{E}(-Ns) \bar{\mathbf{u}}^{AG}, \mathbf{E}(-Ns) \bar{\mathbf{u}}^{AG}) ds = 0.$$

Note that the continuity of k_1, k_2 does not create a difficulty since $|\pm 1 \pm 1 \pm 1| \geq 1$. Passing to the limit in integrated equations (3.17), (3.18) and using that $\hat{\mathbf{U}}^{AG} \rightarrow 0$ we get the limit equations

$$(3.19) \quad \partial_t \mathbf{U}^{QG} = \nu \Delta \mathbf{U}^{QG} + \mathbf{B}^{QG}(\mathbf{U}^{QG}, \mathbf{U}^{QG})$$

$$(3.20) \quad \partial_t \bar{\mathbf{u}}^{AG} = \nu \Delta \bar{\mathbf{u}}^{AG} + \bar{\mathbf{B}}_{res}^{AG}(\bar{\mathbf{u}}_{AG}, \mathbf{U}_{QG}) + \bar{\mathbf{B}}_{res}^{AG}(\mathbf{U}_{QG}, \bar{\mathbf{u}}_{AG}),$$

where $\bar{\mathbf{B}}_{res}^{AG}$ is the limit resonant operator to be calculated explicitly in the next section. Eq. (3.19) is the 3D quasigeostrophic equation ([17]). Eq. (3.20) is the asymptotic limit equation for barotropic ageostrophic field with time and space dependent coefficients corresponding to 3DQG field. \square

3.3. Explicit computation of the limit barotropic ageostrophic equations. Recall that from Eqs. (2.25)-(2.27) of [15] we have for $n_3 = k_3 = m_3 = 0$

$$(3.21) \quad Q_{kmn}^{012} = Q_{kmn}^{102} = Q_{kmn}^{021} = Q_{kmn}^{201} = Q_{kmn}^{101} = Q_{kmn}^{202} = 0.$$

Two nonzero coefficients are

$$(3.22) \quad Q_{kmn}^{011} = \frac{(k' \wedge m') |m'|^2 |n'|^2}{\omega_k |m'| |n'| |k'| |m'| |n'|} = \frac{(k' \wedge m')}{\omega_k |k'|}, \omega_k = \sqrt{\frac{|k'|^2}{|k'|^2}} = 1.$$

Therefore,

$$(3.23) \quad Q_{kmn}^{011} = \frac{(k' \wedge m')}{|k'|}.$$

In physical space it is the advection operator by the vertically averaged quasigeostrophic velocity field \mathbf{U}^{QG} defined in (3.8). Similarly,

$$(3.24) \quad Q_{kmn}^{022} = \frac{(k' \wedge m')}{|k'|}.$$

This implies the AG advection equation for the barotropic AG component

$$(3.25) \quad \partial_t \bar{\mathbf{u}}_n^{AG} = -\frac{(ik' \wedge im')}{|k'|} \bar{\mathbf{u}}_m^{AG} \bar{\mathbf{U}}_k^{QG}.$$

When viscosity is present we get

$$(3.26) \quad \partial_t \bar{\mathbf{u}}_n^{AG} = -\frac{(ik' \wedge im')}{|k'|} \bar{\mathbf{u}}_m^{AG} \bar{\mathbf{U}}_k^{QG} - \nu |n'|^2 \bar{\mathbf{u}}_n^{AG}.$$

Note that QG component is determined from the 3DQG equation and the solution is subsequently vertically averaged.

The leading term ageostrophic dynamics is non-trivial only for the barotropic ageostrophic component which is determined from the above advection equation. In spatial representation it is written

$$(3.27) \quad \partial_t \bar{\mathbf{u}}^{AG}(x_1, x_2, t) = -\bar{\mathbf{U}}^{QG} \cdot \nabla' \bar{\mathbf{u}}^{AG}(x_1, x_2, t) + \nu \Delta \bar{\mathbf{u}}^{AG}$$

where ∇' is the horizontal gradient operator. Here

$$(3.28) \quad \bar{\mathbf{u}}^{AG} = \bar{\mathbf{u}}^{AG}(x_1, x_2, t), \bar{\mathbf{U}}^{QG} = \bar{\mathbf{U}}^{QG}(x_1, x_2, t),$$

where $\bar{\mathbf{U}}^{QG}$ is the vertical average of the QG component velocity \mathbf{U}^{QG} defined in Eqs. (3.8). Note that Eq. (3.27) is given in terms of slow ‘‘Poincare’’ variable $\bar{\mathbf{u}}^{AG}$. To obtain the corresponding original physical field $\bar{\mathbf{U}}^{AG}$, simply use in the Craya basis the identity $\bar{\mathbf{u}}^{AG} = \exp(Nt\mathbf{J}) \bar{\mathbf{U}}^{AG}$, since $\omega(n) = 1$ for $n_3 = 0$ in Eq. (2.4). Eq. (3.27) is an advection equation for $\bar{\mathbf{u}}^{AG}$ by the barotropic 3DQG velocity field $\bar{\mathbf{U}}^{QG}$. For 3D primitive equations under the Boussinesq approximation in a triply periodic cell similar results on advection of barotropic ageostrophic fields were obtained in [15] (see Section 3, p. 238) for the catalytic equations in the asymptotic limit $N \rightarrow +\infty$, $f \rightarrow +\infty$, $\eta = f/N = O(1)$. Clearly, barotropic projection corresponds to vertical averaging. The importance of horizontal averaging and the corresponding dynamics of vertically sheared modes in the asymptotic limit $N \rightarrow +\infty$, $\eta = f/N \rightarrow 0$ is emphasized in [26] and [10].

REMARK 3.5. The background decomposition 3DQG-AG has much in common with the ones presented by Bartello, Cambon and Smith during the conference, but the results do not involve additional assumptions or numerics. With respect to ‘‘classical’’ wave-turbulence theory, there is no need for assuming Gaussian random phases. The vertically averaged 3DQG (2D modes) are particularly relevant when rotation is dominant. Concentration of energy towards these modes was demonstrated in the talks by Cambon (reporting on generalized EDQNM and LES) and Smith (reporting on forced DNS simulations). See [18], [30] for more details on EDQNM approach.

REMARK 3.6. Through a simple computation in [10], [15], [26] of 2-wave resonances in the Craya basis the effective differential spectral molecular viscosities ν_{QG} and ν_{AG} are given by

$$\nu_{QG}(n) = \nu_2 + (\nu_1 - \nu_2) \frac{|n'|^2}{|n'|^2 + \mu^2 n_3^2}, \quad \nu_{AG}(n) = \nu_1 + (\nu_2 - \nu_1) \frac{|n'|^2}{|n'|^2 + \mu^2 n_3^2}$$

where $\mu = f/N$, $|n'|^2 = n_1^2 + n_2^2/a_2^2$. It shows that dissipation affects QG and AG fields differently. This impacts on direct numerical simulations of QG and AG

fields in the context of numerical simulations of atmospheric flows (see [15] and [26] where the above formulas for ν_{QG} and ν_{AG} are given and physical effects of varying Prandtl number on the limiting dynamics are discussed). When $n_3 = 0$ we get

$$\nu_{QG}(n) = \nu_2 + (\nu_1 - \nu_2) = \nu_1, \quad \nu_{AG}(n) = \nu_1 + (\nu_2 - \nu_1) = \nu_2.$$

We note that the derivation of the effective viscosity coefficients for QG and AG dynamics does not require any additional assumptions such as used in other approaches (e.g. renormalization group approach).

Acknowledgments:

We would like to thank an anonymous referee for carefully reading our manuscript and for the very useful suggestions.

References

- [1] V.I. Arnold (1965), Small denominators. I. Mappings of the circumference onto itself, *Amer. Math. Soc. Transl. Ser. 2*, **46**, 213-284.
- [2] V.I. Arnold and B.A. Khesin (1997), *Topological Methods in Hydrodynamics*, Applied Mathematical Sciences, **125**, Springer.
- [3] J. Avrin, A. Babin, A. Mahalov and B. Nicolaenko (1999), On regularity of solutions of 3D Navier-Stokes equations, *Applicable Analysis*, **71**, p. 197-214.
- [4] A. Babin, A. Mahalov, and B. Nicolaenko (1995), Long-time averaged Euler and Navier-Stokes equations for rotating fluids, In “*Structure and Dynamics of Nonlinear Waves in Fluids*”, 1994 IUTAM Conference, K. Kirchgässner and A. Mielke (eds), World Scientific, 145–157.
- [5] A. Babin, A. Mahalov, and B. Nicolaenko (1996), Global splitting, integrability and regularity of 3D Euler and Navier-Stokes equations for uniformly rotating fluids, *Europ. J. of Mech., B/Fluids*, **15**, No. 3, 291–300.
- [6] A. Babin, A. Mahalov, and B. Nicolaenko (1996), Resonances and regularity for Boussinesq equations, *Russian J. Math. Phys.*, **4**, No. 4, 417–428.
- [7] A. Babin, A. Mahalov, and B. Nicolaenko (1997), Regularity and integrability of rotating shallow-water equations, *Proc. Acad. Sci. Paris*, **324**, Ser. 1, 593–598.
- [8] A. Babin, A. Mahalov, and B. Nicolaenko (1997), Global regularity and integrability of 3D Euler and Navier-Stokes equations for uniformly rotating fluids, *Asymptotic Analysis*, **15**, 103–150.
- [9] A. Babin, A. Mahalov, and B. Nicolaenko (1997), Global splitting and regularity of rotating shallow-water equations, *Eur. J. Mech., B/Fluids*, **16**, no. 1, 725–754.
- [10] A. Babin, A. Mahalov, and B. Nicolaenko (1998), On the nonlinear baroclinic waves and adjustment of pancake dynamics, *Theor. and Comp. Fluid Dynamics*, **11**, 215-235.
- [11] A. Babin, A. Mahalov and B. Nicolaenko (1999), On the regularity of three-dimensional rotating Euler-Boussinesq equations, *Mathematical Models and Methods in Applied Sciences*, **9**, No. 7, p. 1089-1121.
- [12] A. Babin, A. Mahalov and B. Nicolaenko (1999), Global Regularity of 3D Rotating Navier-Stokes Equations for Resonant Domains, *Indiana University Mathematics Journal*, **48**, No. 3, p. 1133-1176.
- [13] A. Babin, A. Mahalov and B. Nicolaenko (2000), Fast Singular Oscillating Limits and Global Regularity for the 3D Primitive Equations of Geophysics, *Mathematical Modelling and Numerical Analysis*, **34**, No.2, p.201-222.
- [14] A. Babin, A. Mahalov and B. Nicolaenko (2000), Fast singular oscillating limits of stably stratified three-dimensional Euler-Boussinesq equations and ageostrophic wave fronts, to appear in *Mathematics of Atmosphere and Ocean Dynamics*, Cambridge University Press.
- [15] A. Babin, A. Mahalov, B. Nicolaenko and Y. Zhou (1997), On the asymptotic regimes and the strongly stratified limit of rotating Boussinesq equations, *Theor. and Comp. Fluid Dyn.*, **9**, 223–251.
- [16] P. Bartello (1995), Geostrophic adjustment and inverse cascades in rotating stratified turbulence, *J. Atm. Sci.*, **52**, No. 24, 4410–4428.

- [17] A.J. Bourgeois and J.T. Beale (1994), Validity of the quasigeostrophic model for large-scale flow in the atmosphere and the ocean, *SIAM J. Math. Anal.*, **25**, No. 4, 1023–1068.
- [18] C. Cambon and L. Jacquin (1989), Spectral approach to non-isotropic turbulence subject to rotation, *J. Fluid Mech.*, **202**, p. 295-310.
- [19] J.-Y. Chemin (1995), A propos d'un probleme de pénalisation de type antisymétrique, *Proc. Paris Acad. Sci.*, **321**, 861–864.
- [20] J.-Y. Chemin, B. Desjardins, I. Gallagher and E. Grenier (2000), Fluids with anisotropic viscosity, *Mathematical Modelling and Numerical Analysis*, **34**, No.2, p. 315-335.
- [21] J.-Y. Chemin, B. Desjardins, I. Gallagher and E. Grenier (2000), Anisotropy and dispersion in rotating fluids, preprint, Université de Paris-Sud.
- [22] P. Constantin and C. Foias (1988), *Navier-Stokes Equations*, The University of Chicago Press.
- [23] A. Craya (1958), Contribution à l'analyse de la turbulence associée à des vitesses moyennes, *P.S.T. Ministère de l'Air*, **345**.
- [24] P.G. Drazin and W.H. Reid (1981), *Hydrodynamic Stability*, Cambridge University Press.
- [25] P.F. Embid and A.J. Majda (1996), Averaging over fast gravity waves for geophysical flows with arbitrary potential vorticity, *Comm. Partial Diff. Eqs.*, **21**, 619-658.
- [26] P.F. Embid and A.J. Majda, Low Froude number limiting dynamics for stably stratified flow with small or finite Rossby numbers. *Geophys. Astrophys. Fluid Dynam.* 87 (1998), no. 1-2, 1–50.
- [27] I. Gallagher (1997), Un résultat de stabilité pour les équations des fluides tournants, *C.R. Acad. Sci. Paris*, Série I, 183–186.
- [28] I. Gallagher (1998), Asymptotics of the solutions of hyperbolic equations with a skew-symmetric perturbation, *J. of Diff. Equations*, **150**, p. 363-384.
- [29] I. Gallagher (1998), Applications of Schochet's methods to parabolic equations, *J. Math. Pures Appl.* **77**, p. 989-1054.
- [30] F.S. Godeferd and C. Cambon (1994), Detailed investigation of energy transfer in homogeneous stratified turbulence, *Phys. of Fluids*, **6**, No. 6, 2084-2100.
- [31] D.A. Jones, A. Mahalov and B. Nicolaenko (1998), A numerical study of an operator splitting method for rotating flows with large ageostrophic initial data, *Theor. and Comp. Fluid Dyn.*, **13**, No. 2, p. 143-159.
- [32] O. Métais and J.R. Herring (1989), Numerical experiments of freely evolving turbulence in stably stratified fluids, *J. Fluid Mech.*, **202**, 117.
- [33] J. Pedlosky, *Geophysical Fluid Dynamics*, 2nd edition, Springer-Verlag, (1987).
- [34] H. Poincaré (1910), Sur la précession des corps déformables, *Bull. Astronomique*, **27**, 321.
- [35] J.J. Riley, R.W. Metcalfe and M.A. Weisman (1981), Direct numerical simulations of homogeneous turbulence in density-stratified fluids, *Proc. AIP Conf. Nonl. Prop. of Internal Waves*, B.J. West (ed.), 79.
- [36] S. Schochet (1994), Fast singular limits of hyperbolic PDE's, *J. Diff. Eq.*, **114**, 476–512.
- [37] R. Temam (1983), *Navier-Stokes Equations and Nonlinear Functional Analysis*, SIAM, Philadelphia.

DEPARTMENT OF MATHEMATICS, UNIVERSITY OF CALIFORNIA AT IRVINE, IRVINE, CA 92697
E-mail address: ababine@math.uci.edu

DEPARTMENT OF MATHEMATICS, ARIZONA STATE UNIVERSITY, TEMPE, AZ 85287
E-mail address: mahalov@asu.edu

DEPARTMENT OF MATHEMATICS, ARIZONA STATE UNIVERSITY, TEMPE, AZ 85287
E-mail address: byn@stokes.la.asu.edu

This page intentionally left blank

Anomalous Transport by Wave Turbulence

Alexander M. Balk

ABSTRACT. We consider the advection of a passive tracer when the velocity field is a superposition of random waves. Besides the anomalous diffusion, we find the *anomalous drift*, when the mean displacement $\langle x \rangle$ grows like t^μ with $\mu > 1$. The effects of the boundaries of the inertial range (cut-off parameters) are considered, and the corrections resulted from these effects are calculated. The results are confirmed by numerical simulations.

1. Introduction

This conference is devoted to a particular case of the general Turbulence Problem, namely to the Turbulence of Waves. The Wave Turbulence seems to be simpler since it contains a certain small parameter: The wave amplitudes are assumed to be small enough. Besides a number of physical applications, the theory of Wave Turbulence promised to give some insights into the general Turbulence Problem.

Thanks to the small parameter, the Wave Turbulence can be approached by perturbation methods. This was started in the 60s [1, 2, 3, 4, 5, 6, 7]. And it still continues. And the reason for that is not just because people want to have a rigorous derivation, but because the theory does not always work, and people would like to understand when it should work and when it should not.

Recently several attempts have been made to analyze the Wave Turbulence, to see how theoretical predictions compare with numerical experiments. For example, see [8, 9, 10, 11, 12, 13]. At this conference, the talk by Professor Newell considers some aspects of applicability of the Wave Turbulence. The talk by Professor Zakharov describes several unsolved problems of Wave Turbulence; many of them are about the validation of the Weak Turbulence theory.

In the present talk I consider an even simpler problem, simpler than the Wave Turbulence Problem. I believe that it is the simplest possible turbulence problem. However, this problem contains almost all the essential elements of the general Wave Turbulence Problem. In this situation the computations are relatively simple, and the theoretical predictions can be readily compared with numerical experiments.

2000 *Mathematics Subject Classification.* Primary 76F55 Secondary 76F25.

I wish to thank the organizers of the Conference on Dispersive Wave Turbulence for the great conference and for the support. I am also thankful to D. Cai and A. Majda for valuable discussions during the Conference. The author was supported by NSF Grant DMS-9971640.

2. The Problem

We consider the problem of turbulent transport, which is described by the passive scalar equation

$$(2.1) \quad \frac{\partial \phi}{\partial t} + \frac{\partial}{\partial x} [v(x, t)\phi] = 0.$$

Here $v(x, t)$ is a given velocity field, and $\phi(x, t)$ is the unknown function. We assume that the velocity field is the superposition of random waves:

$$(2.2) \quad v(x, t) = \int c_k e^{i(kx - \Omega_k t)} dk;$$

Ω_k is the dispersion law, and c_k are (time-independent) random wave amplitudes.

In this talk we consider the one-dimensional situation, when x, k , and v are scalars. The derivation can be modified for any dimension, but the formulas become less transparent (since one needs to introduce the polarization vector). We should note also that the expression (2.2) is not the most general representation of a wave field: For the velocity field (2.2) to be real we need to require that the dispersion law is odd, $\Omega_{-k} = -\Omega_k$ (besides $c_{-k} = c_k^*$). However, in this talk we assume this symmetry in order to focus on the simplest possible case. No essential differences appear in the general situation, but the formulas become longer; the same final formulas result in the general situation, when the assumption $\Omega_{-k} = -\Omega_k$ is not made.

We assume that the wave amplitudes have Gaussian statistics with zero mean $\langle c_k \rangle = 0$ and variance

$$\langle c_k^* c_{k_1} \rangle = E_k \delta(k - k_1).$$

So the ensemble of the velocity fields is completely defined by two functions: the dispersion law Ω_k and the energy spectrum E_k . In this talk we assume that these two functions have power-law form:

$$(2.3) \quad \Omega_k = Bk^\alpha \quad \text{with a positive exponent } \alpha \quad (k > 0),$$

$$(2.4) \quad E_k = Ck^{-\nu} \quad \text{in some inertial range } k_a \ll k \ll k_b \quad (k_a \ll k_b)$$

(the exponent ν is not necessarily positive).

The problem is to find the evolution of the ensemble average

$$\Phi(x, t) = \langle \phi(x, t) \rangle.$$

The equation (2.1) is linear, but it still has the ‘‘closure problem’’: The evolution of $\langle \phi \rangle$ depends on $\langle v\phi \rangle$, in its turn the evolution of $\langle v\phi \rangle$ depends on $\langle v^2\phi \rangle$, and so on.

Our equation is so simple that it is equivalent to a single (one-dimensional) ordinary differential equation

$$\dot{x} = v(x, t);$$

$\phi(x, t)$ is the concentration of the particles moving according to this ordinary differential equation. We can also interpret the function $\phi(x, t)$ as the probability to find a particle at point x at instant t . The possibility to reduce our equation to an ordinary differential equation enables us to perform computations relatively easy.

Our model equation actually has several physical applications. For example, imagine that somewhere in the ocean we have put a little piece of wood, and we

would like to know the probability to find this piece of wood at some point x at some instant t .

A molecular diffusion could be also included, but it is often very small, and we neglect it. As well, we neglect some other effects, e.g. surface tension in the ocean example.

The problem of turbulent transport was considered by several people, often under the assumption of well separated scales: One considers the large-scale, long-time behavior of the passive scalar field $\phi(x, t)$, while the velocity field $v(x, t)$ is *short range correlated* (see e.g. [14, 15, 16, 17] and the references cited therein). In this situation the homogenized advection-diffusion equation was derived

$$(2.5) \quad \frac{\partial \Phi}{\partial t} + u \frac{\partial \Phi}{\partial x} = m \frac{\partial^2 \Phi}{\partial x^2}.$$

Here u is the drift velocity, and m is the coefficient of turbulent diffusion.

According to this equation, the variance grows linearly in time:

$$(2.6) \quad D \equiv \langle (x - \langle x \rangle)^2 \rangle = K_1 t + K_0,$$

like in the Brownian motion. Here $K_1 = 2m$, and the constant K_0 appears because equation (2.5) is not valid during some initial time.

For example, when the velocity field is delta-correlated in time:

$$\langle v(x_1, t_1) v(x_2, t_2) \rangle = F(x_1 - x_2) \delta(t_1 - t_2),$$

then the coefficient of turbulent diffusion is $m = F(0)/2$.

The situation of well separated scales was considered also in the case of waves (when the velocity field is a superposition of waves) [18, 19, 20]. To be specific, let us assume that the dispersion law has a power-law form (2.3), and the energy spectrum has a bell-shaped form around some characteristic wave number k_0 . In this situation the velocity field is characterized by characteristic length-scale $L_0 = \pi/k_0$ and time-scale $T_0 = \pi/\omega(k_0)$. We can also consider a small parameter

$$(2.7) \quad \epsilon = \frac{\text{characteristic speed of the fluid particles } v}{\text{characteristic group velocity of the waves } \omega'(k_0)},$$

and we can approach this problem by the perturbation methods.

For observation time $t \gg T_0$, we can derive the diffusion equation (2.5). However, it turns out that in the case of waves the diffusion coefficient is proportional to the fourth power of the velocity, not to the second power as in the case of delta-correlated velocity field. In other words, the diffusion coefficient vanishes at the order ϵ^2 ; the non-zero diffusion coefficient arises only at the order ϵ^4 .

3. The Main Physical Results

In this talk we consider the situation when the velocity field is characterized by a wide interval of time and length scales; the energy spectrum has a wide inertial range, see (2.4). So, the velocity field $v(x, t)$ contains a range of time scales from $T_b = \pi/Bk_b^\alpha$ to $T_a = \pi/Bk_a^\alpha$. We consider the observation time t inside this range: $T_b \ll t \ll T_a$.

If we observed our system at instants $t \gg T_a$, then we would find that the variance $D(t) = \langle (x - \langle x \rangle)^2 \rangle$ grows linearly in time, see (2.6). Since we consider the wave case, at the order ϵ^2 we would find that $D(t)$ approaches a certain constant value (non-zero effective diffusivity arises only at the order ϵ^4). Similar we would find that the mean displacement $R(t) = \langle x \rangle$ grows linearly in time.

During time $t \ll T_b$, the tracer “feels” as if it moves in a constant (but random) velocity field (without spatial and temporal variations), and so, $D \propto t^2, R \propto t^3$.

During intermediate time $T_b \ll t \ll T_a$ we can expect to observe a more complicated dependence when $D(t)$ is “in between the constant and the t^2 -dependence”, while $R(t)$ is “in between the t and the t^3 -dependence”. In particular, one could expect to see the *anomalous* transport, when

$$(3.1) \quad D = K t^\lambda \quad (0 \leq \lambda < 2) \quad \text{and} \quad R = L t^\mu \quad (1 \leq \mu < 3).$$

The anomalous diffusion (the anomalous dependence $D(t)$) was reported in [21]. Here we show that the anomalous drift (the anomalous dependence $R(t)$) can occur along with the anomalous diffusion. In particular we find

$$(3.2) \quad \lambda = 2 + \frac{\nu - d}{\alpha} \quad \text{and} \quad \mu = 2 + \frac{\nu - d - 1}{\alpha} = \lambda - \frac{1}{\alpha}.$$

More precisely,

$$\lambda = \max(0, 2 + \frac{\nu - d}{\alpha}) \quad \text{and} \quad \mu = \max(1, 2 + \frac{\nu - d - 1}{\alpha}) = \max(1, \lambda - \frac{1}{\alpha}),$$

so that the exponent λ cannot be less than 0, and the exponent μ cannot be less than 1.

When $0 < \lambda < 1$, we have *sub-diffusion*; when $1 < \lambda < 2$, we have *super-diffusion* (see [21]). The anomalous drift is realized when $\mu > 1$; we can only have super-drift (since $\mu \geq 1$, we cannot have the *sub-drift* or *slow drift*). Since $\alpha > 0$, we have $\mu < \lambda < 2$. The anomalous drift can occur only if $\alpha > 1$ and only when a super-diffusion takes place, $\lambda > 1$.

We calculate the factors K and L , as well as the exponents λ and μ . Then we compare these theoretical predictions with numerical experiments and find a good agreement. For the numerical simulation we consider the case with $\alpha = 3$ and $\nu = 1/4$. Then $\lambda = 7/4$ and $\mu = 17/12$, so that we should observe super-diffusion and super-drift.

We also consider the effects of the *cut-off* parameters k_a and k_b in (2.4). Actually, in this talk we consider the energy spectrum of the following form

$$(3.3) \quad E_k = \begin{cases} C k^{-\nu} & \text{if } k_a < k < k_b, \\ 0 & \text{if } k < k_a \text{ or } k > k_b. \end{cases}$$

The cut-off parameters k_a and k_b lead to certain corrections of the power-law form (3.1):

$$(3.4) \quad D(t) = K t^\lambda - K_1 t^2 - K_2,$$

$$(3.5) \quad R(t) = L t^\mu - L_1 t^3 - L_2 t.$$

The power law regimes (3.1) are similar to the *Kolmogorov-type power-law spectra* inside the inertial range (see [22, 23]).

Let us note that anomalous diffusion was investigated by Avellaneda and Majda [24, 25], but the nature of their velocity fields (random shear flows) is quite different from the wave fields, considered here.

Finally, let us make the following remark. In order to present the ideas clearly, in this talk we focus on 1-D. In this situation the flow is necessarily compressible, but in higher dimensions it can be incompressible. The theory works equally well for compressible or incompressible flow, as well as for any dimension d . However, in

higher dimensions ($d > 1$) the formulas become heavier since one needs to introduce the polarization vector (see [21]).

4. Statistical Near-Identity Transformation.

Using the Fourier transform

$$\phi(x, t) = \int f_k(t) e^{ik \cdot x} dk$$

we re-write the passive advection equation (2.1) in the Fourier representation

$$(4.1) \quad \dot{f}_1 + \int ik_1 e^{-i\Omega_3 t} \delta(-k_1 + k_2 + k_3) f_2 c_3 d_{23} = 0$$

Here and below we use notations of the following type: for any function h we write h_j instead of $h(k_j)$ or h_{k_j} , ($j = 1, 2, \dots$), e.g. $f_1 = f_{k_1}$, $f_2 = f_{k_2}$, $c_3 = c_{k_3}$, $\Omega_3 = \Omega_{k_3}$; and d_{23} stands for $dk_2 dk_3$.

The solution of the equation (4.1) can be represented by the Wiener-Hermite expansion

$$f_1 = f_1^0 + \int \hat{X}_{-123} f_2^0 H_3 d_{23} + \frac{1}{2} \int \hat{Y}_{-1234} f_2^0 H_{34} d_{234} + \frac{1}{3!} \int \hat{Z}_{-12345} f_2^0 H_{345} d_{2345} + \dots$$

where H denotes the sequence of the Wiener-Hermite polynomials (see e.g. [28, 29]) with respect to the Gaussian random field c_k :

$$H_3 = c_3, \quad H_{34} = c_3 c_4 - E_3 \delta(k_3 + k_4),$$

$$H_{345} = c_3 c_4 c_5 - c_3 E_4 \delta(k_4 + k_5) - c_4 E_5 \delta(k_5 + k_3) - c_5 E_3 \delta(k_3 + k_4), \dots$$

The function f_k^0 denotes the initial condition: $f_k(0) = f_k^0$, and the hat symbol denotes the multiplication by the corresponding δ -function:

$$\hat{X}_{-123} = X(-k_1, k_2, k_3) \delta(-k_1 + k_2 + k_3),$$

$$\hat{Y}_{-1234} = Y(-k_1, k_2, k_3, k_4) \delta(-k_1 + k_2 + k_3 + k_4), \dots$$

The kernels \hat{X}_{-123} , \hat{Y}_{-1234} , ... can depend on time t .

Assuming that the characteristic wave velocity is of the order 1, we suppose that $c = O(\epsilon)$, $H_{34} = O(\epsilon^2)$, $H_{345} = O(\epsilon^3)$, ...

Instead of studying the infinite Wiener-Hermite expansion, we consider the truncated expansion (up to the second order) and change the initial condition f_k^0 to a new variable $g_k(t)$:

$$(4.2) \quad f_1 = g_1 + \int \hat{X}_{-123} g_2 c_3 d_{23} + \frac{1}{2} \int \hat{Y}_{-1234} g_2 [c_3 c_4 - E_3 \delta(k_3 + k_4)] d_{234}.$$

Now we consider this equation as a change of variables from the old variable $f_k(t)$ to the new variable $g_k(t)$. Substituting (4.2) into the equation (4.1) for $f_k(t)$, we

find the equation for $g_k(t)$:

$$\begin{aligned} & \dot{g}_1 + \int \dot{X}_{-123} g_2 c_3 d_{23} + \frac{1}{2} \int \dot{Y}_{-1234} g_2 [c_3 c_4 - E_3 \delta(k_3 + k_4)] d_{234} + \\ & + \int \hat{X}_{-123} \dot{g}_2 c_3 d_{23} + \frac{1}{2} \int \hat{Y}_{-1234} \dot{g}_2 [c_3 c_4 - E_3 \delta(k_3 + k_4)] d_{234} + \\ & + \int i k_1 e^{-i\Omega_3 t} \delta(-k_1 + k_2 + k_3) \times \\ & \times \left\{ g_2 + \int \hat{X}_{-256} g_5 A_6 d_{56} + \frac{1}{2} \int \hat{Y}_{-2567} g_5 [c_6 c_7 - E_6 \delta(k_6 + k_7)] d_{567} \right\} c_3 d_{23} \end{aligned}$$

In accordance with the general idea of the Near-identity transformation [26, 27], we choose the kernel X_{-123} so that the terms linear in the field c_k disappear from the new equation. This is possible if

$$\dot{X}_{-123} = -i k_1 e^{-i\Omega_3 t} \quad \text{provided} \quad -k_1 + k_2 + k_3 = 0.$$

Then \dot{g}_1 has the order ϵ^2 , and the integrals with time derivative \dot{g} have the order ϵ^3 . So, we obtain the following equation

$$(4.3) \quad \begin{aligned} \dot{g}_1 + \frac{1}{2} \int \dot{Y}_{-1234} g_2 [c_3 c_4 - E_3 \delta(k_3 + k_4)] d_{234} + \\ + \int i k_1 e^{-i\Omega_3 t} \hat{X}_{-256} g_5 c_6 c_3 d_{2356} + \epsilon^3 \{ \dots \} = 0. \end{aligned}$$

We want to make the second integral look similar to the first integral. So, we rename the integration variables in the last integral:

$$5 \rightarrow 2, 3 \rightarrow 3, 6 \rightarrow 4, 2 \rightarrow 5 \quad \Rightarrow \quad \int i k_1 e^{-i\Omega_3 t} \hat{X}_{-524} g_2 c_4 c_3 d_{2345};$$

then we symmetrize this integral with respect to transposition $3 \leftrightarrow 4$

$$\frac{1}{2} \int i k_1 \left(e^{-i\Omega_3 t} \hat{X}_{-524} + e^{-i\Omega_4 t} \hat{X}_{-523} \right) g_2 c_3 c_4 d_{2345}$$

and write $c_3 c_4$ in the later integral as $c_3 c_4 - E_3 \delta(k_3 + k_4) + E_3 \delta(k_3 + k_4)$. In the result we re-write the equation (4.3) in the form

$$\begin{aligned} \dot{g}_1 + \frac{1}{2} \int \dot{Y}_{-1234} g_2 [c_3 c_4 - E_3 \delta(k_3 + k_4)] d_{234} + \\ + \frac{1}{2} \int i k_1 \left(e^{-i\Omega_3 t} \hat{X}_{-524} + e^{-i\Omega_4 t} \hat{X}_{-523} \right) g_2 [c_3 c_4 - E_3 \delta(k_3 + k_4)] + \\ + \frac{1}{2} \int i k_1 e^{-i\Omega_3 t} X_{-51-3} g_2 E_3 \delta(-k_1 + k_5 + k_3) d_{35} + \epsilon^3 \{ \dots \} = 0. \end{aligned}$$

Now we choose the kernel Y_{-1234} to “kill” the second-order Wiener-Hermite polynomial $H_{34} = c_3 c_4 - E_3 \delta(k_3 + k_4)$:

$$\dot{Y}_{-1234} = -i k_1 e^{-i\Omega_3 t} X_{-524} \Big|_{k_5=k_1-k_3=k_2+k_4} - i k_1 e^{-i\Omega_4 t} X_{-523} \Big|_{k_5=k_1-k_4=k_2+k_3}.$$

Then

$$(4.4) \quad \dot{g}_1 + i g_1 \int k_1 e^{-i\Omega_3 t} X_{-21-3} E_3 \delta(-k_1 + k_2 + k_3) d_{23} + \epsilon^3 \{ \dots \} = 0.$$

Since only the time derivatives of the kernels X and Y have been determined, we choose the constants of time integration so that the initial condition for the new

variable $g_k(t)$ would be the same as for the old variable $f_k(t)$ (see the near-identity transformation (4.2)). Hence

$$\begin{aligned} X_{-123} &= k_1 \frac{e^{-i\Omega_3 t} - 1}{\Omega_3}; \\ Y_{-1234} &= k_1 k_5 \left\{ \frac{e^{-i(\Omega_3 + \Omega_4)t} - 1}{(\Omega_3 + \Omega_4)\Omega_4} - \frac{e^{-i\Omega_3 t} - 1}{\Omega_3 \Omega_4} \right\}_{k_5 = k_1 - k_3 = k_2 + k_4} \\ &\quad + k_1 k_5 \left\{ \frac{e^{-i(\Omega_3 + \Omega_4)t} - 1}{(\Omega_3 + \Omega_4)\Omega_3} - \frac{e^{-i\Omega_4 t} - 1}{\Omega_4 \Omega_3} \right\}_{k_5 = k_1 - k_4 = k_2 + k_3}. \end{aligned}$$

The kernel Y_{-1234} does not affect the approximation (4.4). This is usual for a near identity transformations that the highest order term in such transformation does not affect the corresponding equation. Thus the equation (4.4) takes the form

$$(4.5) \quad \dot{g}_1 = ig_1 \int k_1 k_2 \frac{1 - e^{-i\Omega_3 t}}{\Omega_3} E_3 \delta(-k_1 + k_2 + k_3) d_{23}$$

(ϵ^3 -terms are neglected). Here we have taken into account that the dispersion law is odd, $\Omega_{-3} = -\Omega_3$. If from the very beginning we considered the general dispersion law, we would obtain a similar equation, but the derivation would be slightly longer.

5. The Averaged Evolution

In the equation (4.5) we can easily integrate with respect to k_2 :

$$(5.1) \quad \dot{g}_1 = ig_1 \int k_1 (k_1 - k_3) \frac{1 - e^{-i\Omega_3 t}}{\Omega_3} E_3 d_3$$

This equation has the form

$$(5.2) \quad \dot{g}_1 = -g_1 [k_1^2 Q(t) + ik_1 P(t)]$$

where

$$Q = \int \frac{1 - e^{-i\Omega_k t}}{i\Omega_k} E_k dk, \quad P = \int k \frac{1 - e^{-i\Omega_k t}}{\Omega_k} E_k dk.$$

Since $\Omega_k = -\Omega_{-k}$, $E_k = E_{-k}$, we can symmetrize these integrals with respect to $k \leftrightarrow -k$

$$(5.3) \quad Q = \int \frac{\sin \Omega_k t}{\Omega_k} E_k dk, \quad P = \int k \frac{1 - \cos \Omega_k t}{\Omega_k} E_k dk.$$

The equation (5.2) defines $g_k(t)$ in terms of the initial value of this function. Due to our choice of the kernels X and Y , the initial condition for the variable $g_k(t)$ is the same as for the original variable $f_k(t)$: $g_k(0) = f_k(0) = f_k^0$. Thus,

$$(5.4) \quad g_k(t) = f_k^0 e^{-[\frac{1}{2} D(t)k^2 + iR(t)k]}$$

where $\frac{1}{2}D$ and R are the time integrals of the functions (5.3) respectively:

$$(5.5) \quad \frac{D}{2} = \int \frac{1 - \cos \Omega_k t}{\Omega_k^2} E_k dk, \quad R = \int k \frac{\Omega_k t - \sin \Omega_k t}{\Omega_k^2} E_k dk.$$

In order to find the original field $f_k(t)$, we need to substitute (5.4) into the near-identity transformation (4.2). Since (5.4) is not a random function, and the average of each Wiener-Hermite polynomial is zero, we have $\langle f_k \rangle = g_k$, and

$$\Phi(x, t) = \langle \phi(x, t) \rangle = \int \langle f_k \rangle e^{ikx} dk = \int g_k e^{ikx} dk.$$

So,

$$\langle x \rangle = \int x \Phi(x, t) dx = 2\pi i \left. \frac{dg_k}{dk} \right|_{k=0}, \quad \langle x^2 \rangle = \int x^2 \Phi(x, t) dx = -2\pi \left. \frac{d^2 g_k}{dk^2} \right|_{k=0}.$$

The quantities R and D , that determine $g_k(t)$ according to (5.4), have direct physical meaning. They are respectively the mean displacement and the variance of a particle that was at the origin $x = 0$ at instant $t = 0$. Indeed, when we consider the transport of such particle, we assume $\Phi(x, 0) = \delta(x)$, i.e. $f_k^0 \equiv 1/2\pi$. Then

$$\langle x \rangle = R(t), \quad \langle x^2 \rangle = D(t) + R^2(t) \Rightarrow \langle (x - \langle x \rangle)^2 \rangle = \langle x^2 \rangle - \langle x \rangle^2 = D(t).$$

6. Anomalous Transport

Now let us find the functions $R(t)$ and $D(t)$ for the power-law dispersion and energy spectrum (2.3), (3.3). According to (5.5) we have

$$R(t) = 2 \int_{k_a}^{k_b} k \frac{Bk^\alpha - \sin Bk^\alpha t}{(Bk^\alpha)^2} Ck^{-\nu} dk$$

(the factor 2 in front of this integral appears because here we integrate only over the positive k whereas in (5.5) we integrated over the whole line from $-\infty$ to $+\infty$). We write this integral as the integral from 0 to ∞ minus the integrals from 0 to k_a and from k_b to ∞ :

$$\begin{aligned} R(t) &= 2 \int_0^\infty k \frac{Bk^\alpha - \sin Bk^\alpha t}{(Bk^\alpha)^2} Ck^{-\nu} dk - 2 \int_0^{k_a} k \frac{Bk^\alpha - \sin Bk^\alpha t}{(Bk^\alpha)^2} Ck^{-\nu} dk \\ &\quad - 2 \int_{k_b}^\infty k \frac{Bk^\alpha - \sin Bk^\alpha t}{(Bk^\alpha)^2} Ck^{-\nu} dk. \end{aligned}$$

In the first integral we change the integration variable to $y = Bk^\alpha t$, $\frac{dy}{y} = \alpha \frac{dk}{k}$. Since we consider the time t in the intermediate range, in between the shortest and the longest characteristic times

$$\frac{\pi}{Bk_b^\alpha} \ll t \ll \frac{\pi}{Bk_a^\alpha},$$

we can simplify the second and the third integral in the following way: In the second integral, the argument of sin is small, $Bk_a^\alpha t \ll \pi$, and we expand the sin by Taylor's formula. In the third integral, the argument of sin is large, $Bk_b^\alpha t \gg \pi$, and we neglect this oscillating term. Thus

$$\begin{aligned} R(t) &= t^\mu \frac{2C}{\alpha B^{\frac{2-\nu}{\alpha}}} \int_0^\infty \frac{y - \sin y}{y^\mu} \frac{dy}{y} - t^3 \frac{BC}{3} \int_0^{k_a} k^{(1+\alpha-\nu)} dk \\ &\quad - t \frac{2C}{B} \int_{k_b}^\infty k^{(1-\alpha-\nu)} dk \end{aligned}$$

where

$$\mu = 2 + \frac{\nu - 2}{\alpha}.$$

This is the expression for the anomalous drift exponent in Section 3 when dimension $d = 1$.

The conditions for the convergence of those integrals are as follows: for the first integral $1 < \mu < 3$; for the second — $\alpha - \nu + 2 > 0 \Leftrightarrow \mu < 3$; for the third —

$\alpha + \nu - 2 > 0 \Leftrightarrow \mu > 1$. Thus, if $1 < \mu < 3$, we have the expression (3.5) for the *anomalous drift* with

$$L = \frac{2C}{\alpha B^{\frac{2-\nu}{\alpha}}} \int_0^\infty \frac{y - \sin y}{y^{\mu+1}} dy, \quad L_1 = \frac{BC}{3} \frac{k_a^{\alpha-\nu+2}}{\alpha - \nu + 2}, \quad L_2 = \frac{2C}{B} \frac{k_b^{\alpha+\nu-2}}{\alpha + \nu - 2}.$$

Similarly we derive the expression (3.4) for the *anomalous diffusion*. According to (5.5) we have

$$\begin{aligned} D(t) &= 4 \int_{k_a}^{k_b} \frac{1 - \cos Bk^\alpha t}{(Bk^\alpha)^2} Ck^{-\nu} dk = \\ &= 4 \int_0^\infty \frac{1 - \cos Bk^\alpha t}{(Bk^\alpha)^2} Ck^{-\nu} dk - 4 \int_0^{k_a} \frac{1 - \cos Bk^\alpha t}{(Bk^\alpha)^2} Ck^{-\nu} dk \\ &\quad - 4 \int_{k_b}^\infty k \frac{1 - \cos Bk^\alpha t}{(Bk^\alpha)^2} Ck^{-\nu} dk. \end{aligned}$$

In the first integral we change the integration variable to $y = Bk^\alpha t$. In the second integral we expand \cos by Taylor's formula since $Bk_a^\alpha t \ll \pi$. In the second integral we neglect \cos -term since $Bk_b^\alpha t \gg \pi$. Thus

$$\begin{aligned} D(t) &= t^\lambda \frac{4C}{\alpha B^{\frac{1-\nu}{\alpha}}} \int_0^\infty \frac{1 - \cos y}{y^\lambda} \frac{dy}{y} - t^2 2C \int_0^{k_a} k^{-\nu} dk \\ &\quad - t \frac{4C}{B^2} \int_{k_b}^\infty k^{-\nu-2\alpha} dk \end{aligned}$$

where

$$\lambda = 2 + \frac{\nu - 2}{\alpha}.$$

This is the expression for the anomalous diffusion exponent in Section 3 when dimension $d = 1$. The conditions for the convergence of those integrals are as follows: for the first integral $0 < \lambda < 2$; for the second $-\nu < 1 \Leftrightarrow \lambda < 2$; for the third $-2\alpha + \nu > 1 \Leftrightarrow \lambda > 0$. Thus, if $0 < \lambda < 2$, we have the expression (3.4) for the *anomalous diffusion* with

$$K = \frac{4C}{\alpha B^{\frac{1-\nu}{\alpha}}} \int_0^\infty \frac{1 - \cos y}{y^{\lambda+1}} dy, \quad K_1 = 2C \frac{k_a^{1-\nu}}{1 - \nu}, \quad K_2 = \frac{2C}{B^2} \frac{k_b^{-2\alpha-\nu+1}}{-2\alpha - \nu + 1}.$$

7. Numerical Simulations

We have tested the predictions (3.4) and (3.5) in numerical experiments and found a good agreement not only in the exponents (3.2), but also in the factors K, K_1, K_2 and L, L_1, L_2 . We have considered a wave field with exponents $\alpha = 3$ and $\nu = 1/4$ (see the expressions (2.3), (2.4) for the dispersion law and the energy spectrum). In this situation we have the super-diffusion, $\lambda = 7/4 > 1$, as well as the super-drift, $\mu = 17/12 > 1$. The factors in (2.3) and (3.3) are $B = 1$ and $C = 0.001$. In the simulation cut-off parameters are $k_a = 0.1$ and $k_b = 10$ (see (3.3)). So, we should observe the anomalous transport during intermediate time $T_b \ll t \ll T_a$, where $T_b = \pi/k_b^\alpha \approx 3 \times 10^{-3}$ and $T_a = \pi/k_a^\alpha \approx 3 \times 10^3$. The results are represented in figures 1 and 2 in log-log scale; the dashed line — theory, the solid line — numerics. Figure 1 shows the variance and Figure 2 shows the mean displacement as functions of time. To generate the realizations of the random velocity field, we fixed the spectrum $E_{\mathbf{k}}$ and chose random phases of the amplitudes $c_{\mathbf{k}}$ (uniformly

distributed over interval $(0, 2\pi)$. To obtain the numerical curves, we have averaged over 1000 realizations.

References

- [1] M. M. Litvak, *A transport equation for magneto-hydrodynamic waves*. Avco Everett Res. Rep. No 92, 1960.
- [2] K. Hasselmann, *On the nonlinear energy transfer in a gravity wave spectrum*, **12** (1962), 481-500.
- [3] A. A. Galeev and V. I. Karpman, *Turbulence theory of a weakly non-equilibrium low-density plasma and structure of shock waves*, Sov. Phys.-JETP, **17** (1963), 403-409.
- [4] D. J. Benney and P. G. Saffman, *Nonlinear interactions of random waves in a dispersive medium*, Proc. Roy. Soc. A **289** (1966), 301-320.
- [5] A. C. Newell, *The closure problem in a system of random gravity waves*, Rev. Geophys. **6** (1968), 1-31.
- [6] R. C. Davidson, "General weak turbulence theory of resonant four-wave processes," Phys. Fluids **12** (1969), 149-161.
- [7] A. A. Galeev and R. Z. Sagdeev, *Nonlinear Plasma Theory* (Benjamin, New York, 1969).
- [8] A. N. Puchkarev and V. E. Zakharov, *Turbulence of capillary waves*, Phys. Rev. Lett. **76** (1996), 3320-3323.
- [9] A. J. Majda, D. W. McLaughlin, and E. G. Tabak, *A one dimensional model for dispersive wave turbulence*, J. Nonlinear Sci. **6** (1997),
- [10] D. Cai, A. J. Majda, D. W. McLaughlin, and E. G. Tabak, *Spectral Bifurcations in Dispersive Wave Turbulence*, Proc. Nat. Acad. of Sci. (USA) **96** (1999), 14216-14221.
- [11] P. Guyenne, V. E. Zakharov, A. N. Puchkarev, and F. Dias, *Turbulence d'ones dans des modèles unidimensionnels*, C. R. Acad. Sci. Paris **328 II** (2000), 757-762.
- [12] V. E. Zakharov, P. Guyenne, A. N. Puchkarev, and F. Dias, *Wave turbulence in one-dimensional models*, Physica D **152-153** (2001), 573-576.
- [13] V. E. Zakharov, P. Guyenne, A. N. Puchkarev, and F. Dias, *Turbulence of one-dimensional weakly nonlinear dispersive waves*, These proceedings.
- [14] A. J. Majda and P. R. Kramer, *Simplified models for turbulent diffusion: Theory, numerical modeling, and physical phenomena*, Phys. Reports **314** (1999), 237-574.
- [15] T. Komorovski and G. Papanicolaou, *Motion in a Gaussian incompressible flow*, Ann. Appl. Probab. **7** (1997), 229-264.
- [16] R. Carmona and L. Xu, *Homogenization for time-dependent two-dimensional incompressible Gaussian flows*, Ann. Appl. Probab. **7** (1997), 265-279.
- [17] L. I. Piterbarg, *Short-correlation approximation in models of turbulent diffusion*, in *Stochastic Models in Geosystems*, ed. by S. A. Molchanov and W. A. Wojczinski (Springer, New York, 1997).
- [18] K. Herterich and K. Hasselmann, *The horizontal diffusion of tracers by surface waves*, Phys. Oceanography **12** (1982), 704-711.
- [19] P. B. Weichman and R. E. Glazman, *Passive scalar transport by traveling wave fields*, J. Fluid Mech. **420** (2000), 147-200.
- [20] A. M. Balk and R. M. McLaughlin, *Passive scalar in a random wave field: the weak turbulence approach*, Phys. Lett. A **256** (1999), 299-306.
- [21] A. M. Balk, *Anomalous Diffusion of a Tracer Advected by Wave Turbulence* Phys. Lett. A **279** (2001), 370-378.
- [22] V. E. Zakharov, *Kolmogorov spectra in weak turbulence problems*, in: *Basic Plasma Physics, Vol. 2*, edited by A. A. Galeev and R. N. Sudan (Elsevier, North-Holland, 1985), pp. 3-36.
- [23] V. E. Zakharov, V. S. L'vov, G. Fal'kovich, *Kolmogorov Spectra of Turbulence* (Springer-Verlag, Berlin - New York, 1992).
- [24] M. Avellaneda and A. J. Majda, *Mathematical models with exact renormalization for turbulent transport*, Comm. Pure Appl. Math. **131** (1990), 381-429.
- [25] M. Avellaneda and A. J. Majda, *Mathematical models with exact renormalization for turbulent transport, II: fractal interfaces, non-Gaussian statistics and the sweeping effect*, Comm. Pure Appl. Math. **146** (1992), 139-204.
- [26] N. N. Bogoliubov and Y. A. Mitropolsky, *Asymptotic Methods in the Theory of Nonlinear Oscillations* (Gordon and Breach, New York, 1961).

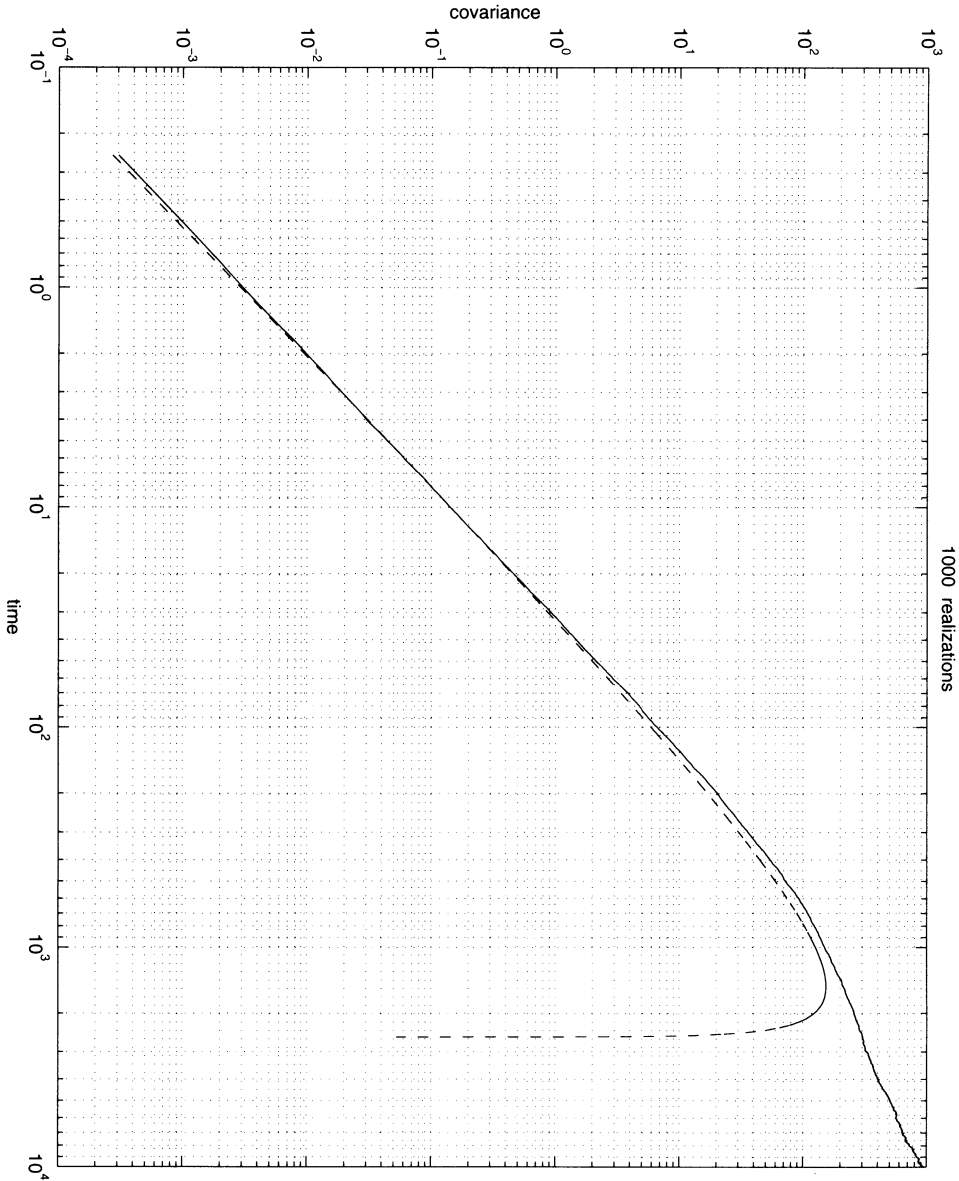


FIGURE 1. The covariance $D(t) = \langle (x - R)^2 \rangle$ of a tracer particle, shown in the log – log scale. The solid line shows the numerical simulation, and the dashed line shows the theoretical prediction. In the intermediate range $T_b \ll t \ll T_a$ the theoretical curve represents a straight line corresponding to the dependence $R = Lt^\mu$ with $\lambda = 7/4$. Large deviation for $t \gg T_a$ should not be considered since the theoretical prediction is only valid in the intermediate range $T_b \ll t \ll T_a$. However, the theoretical prediction “catches” the real behavior at the end of the inertial range: both, the theoretical and the numerical, curves deviate down from the straight line $R = Lt^\mu$ as t approaches T_a .

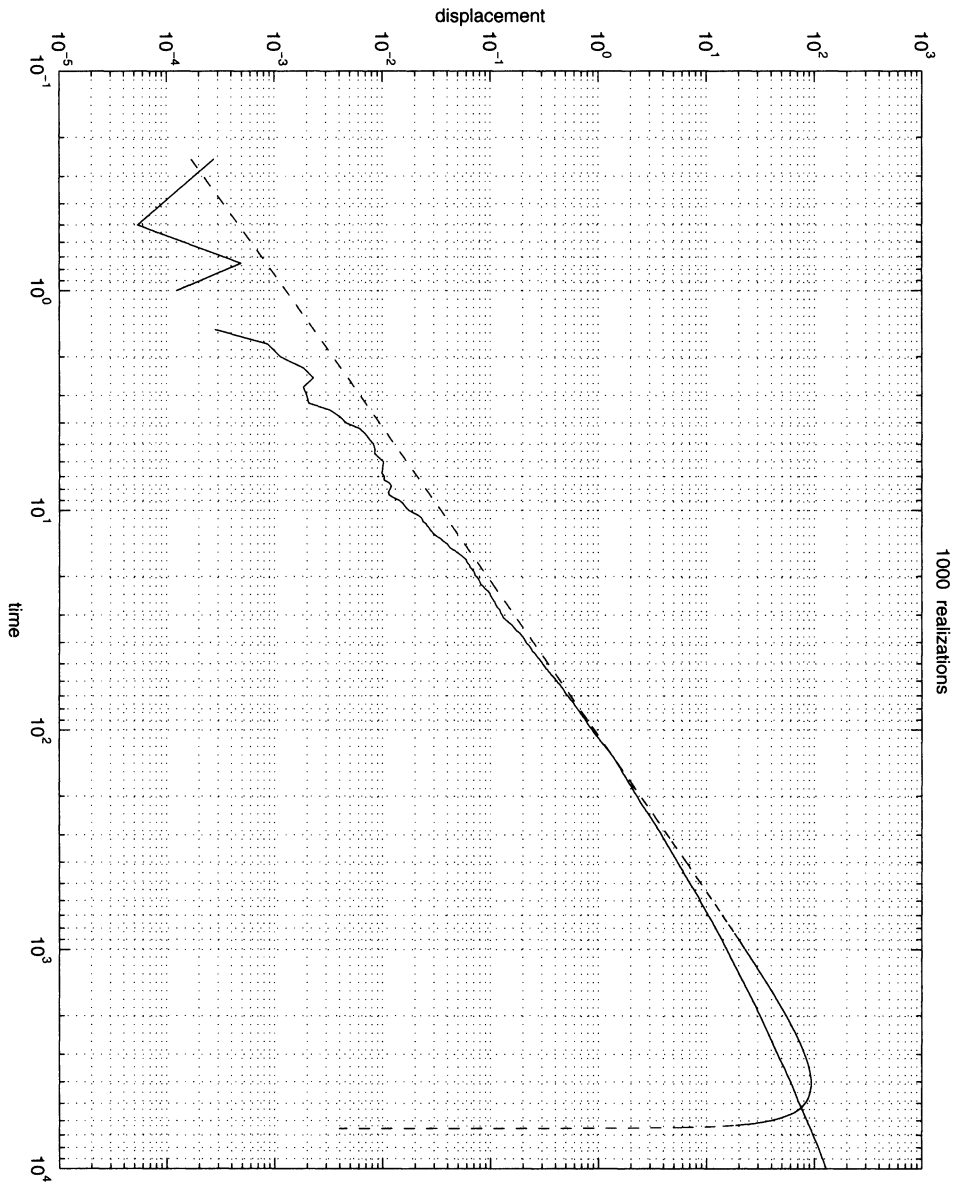


FIGURE 2. The mean displacement $R(t) = \langle x \rangle$ of a tracer particle, shown in the log – log scale. The dashed line shows the theoretical prediction. In the intermediate range $T_b \ll t \ll T_a$ the theoretical curve represents a straight line corresponding to the dependence $R = Lt^\mu$ with $\mu = 17/12$. Large deviation for $t \gg T_a$ should not be considered since the theoretical prediction is only valid in the intermediate range $T_b \ll t \ll T_a$. The solid line shows the numerical simulation. The discontinuity of the solid line (at small time) is not physical, but software-related: in that region $R(t) < 0$, and MATLAB does not plot $\log R(t)$.

- [27] J. A. Sanders and F. Verhulst, *Averaging Methods in Nonlinear Dynamical Systems* (Springer-Verlag, 1985).
- [28] N. Wiener, *Nonlinear Problems in Random Theory* (MIT press, 1958).
- [29] C. Eftimiu, *Wave propagation in random media: Wiener-Hermite expansion approach* J. Electromagn. Waves Applications **4** (1990), 847-864.

DEPARTMENT OF MATHEMATICS, UNIVERSITY OF UTAH, 155 SOUTH 1400 EAST, ROOM 233,
SALT LAKE CITY, UT 84112

E-mail address: `balk@math.utah.edu`

This page intentionally left blank

Statistical Equilibrium Theories for the Nonlinear Schrödinger Equation

Richard Jordan and Bruce Turkington

Introduction

Turbulence in nonlinear media is often accompanied by the formation of large-scale coherent structures that persist against a background of small-scale turbulent fluctuations [11]. A familiar example is the emergence of quasi-steady vortices in a two-dimensional fluid flow at large Reynolds number [19, 22]. Such coherent structures also occur in various dispersive wave systems, where they typically take the form of solitary waves, or quasi-solitons [6, 25, 4, 13].

In this note we formulate and analyze statistical equilibrium models of coherent structures for a particular class of dispersive wave systems. Specifically, we consider the dynamics of a complex field $\psi(x, t)$ governed by a one-dimensional nonlinear Schrödinger (NLS) equation of the form

$$(1) \quad i\psi_t + \psi_{xx} + f(|\psi|^2)\psi = 0$$

We restrict our attention to nonlinearities f that are focusing (attractive) and saturated (bounded); that is, $f(0) = 0$, $f'(a) > 0$ for $a \geq 0$, and $f(a) = O(1)$, $af'(a) = O(1)$ as $a \rightarrow \infty$. Nonlinearities with these properties, such as $f(|\psi|^2) = |\psi|^2/(1 + |\psi|^2)$, arise in physical applications as corrections to the cubic NLS equation for large wave amplitudes [21, 20]. As our goal is to model the long-time behavior of solutions, especially the phenomenon of self-organization into coherent structures, NLS systems of this kind furnish a natural class of prototypes because their dynamics are nonintegrable and free of wave collapse, and they support stable solitary waves.

In constructing an equilibrium model of a turbulent dynamical system such as (1) we follow the classical approach of Gibbs – that is, we use a statistical ensemble based on the conserved quantities for the dynamics. This construction

1991 *Mathematics Subject Classification*. Primary 76F55; 35Q55, 76M35, 76X05, 82B05.

Key words and phrases. Nonlinear wave turbulence, statistical equilibrium, large deviations.

The first author was supported in part by an NSF Mathematical Sciences Postdoctoral Research Fellowship, DMS-9705918.

The second author was supported in part by NSF grant DMS-9971204 and DOE grant DE-FG02-99ER25376.

rests fundamentally on the Hamiltonian structure of the system. For the NLS equation (1) the Hamiltonian, or energy functional, is

$$(2) \quad H(\psi) = \frac{1}{2} \int [|\psi_x|^2 - F(|\psi|^2)] dx,$$

where the potential F is related to the nonlinearity f by $F(a) = \int_0^a f(s) ds$. In addition to the Hamiltonian, the dynamics (1) conserves the particle number, or L^2 norm squared, which is given by the functional

$$(3) \quad Q(\psi) = \frac{1}{2} \int |\psi|^2 dx.$$

The integrals H and Q are the only invariants of a dynamics in the class of equations we consider, apart from the momentum integral associated with x -translation invariance. To keep our theoretical development concise, we suppress the conservation of momentum by posing (1) in a bounded interval $0 < x < L$ and imposing the boundary conditions, $\psi(0) = \psi(L) = 0$.

Generally speaking, a statistical equilibrium theory of this kind is developed by (i) introducing a natural discretization of the dynamics having a finite number of degrees of freedom n , (ii) defining a Gibbs distribution on each n -dimensional phase space, and (iii) taking an appropriate continuum limit, $n \rightarrow \infty$. For the class of NLS systems we consider, however, this standard program has several unconventional aspects. First, the Gibbs canonical ensemble with respect to H and Q does not exist for a focusing nonlinearity, its partition function being divergent under the same conditions that ensure the existence of solitary waves. We therefore use a “mixed” ensemble, which is canonical in H and microcanonical in Q . Second, the ensemble mean energy, $\langle H \rangle = E$, tends to infinity with n at fixed temperature. We therefore rescale the temperature in the continuum limit, so that the ensemble represents the long-time average behavior of the turbulent wave system as it evolves from generic initial conditions with finite values of the invariants, $H(\psi^0) = E$ and $Q(\psi^0) = N$. Third, the underlying ergodic NLS dynamics realizes such an ensemble on a phase space of dimension n after a finite time T , and a definite relation $n = n(T)$ is exhibited by direct numerical simulations of the dynamics [13]. We therefore recognize that the continuum limit, $n \rightarrow \infty$, is approached in the limit as $T \rightarrow \infty$. Accordingly, when validating the theory, we compare the predictions of the model with large, finite n to the averages of numerical solutions at a corresponding finite T .

In these respects our approach differs from previous applications of equilibrium statistical mechanics to the NLS equation. In particular, the Gibbs distributions constructed by other investigators [16, 18, 2] all have infinite mean energy. While these Wiener-type measures have interesting probabilistic features, our rescaled continuum limit has the double advantage that it is directly relevant to the time-average behavior of regular solutions and that it admits an asymptotically exact mean-field approximation. These properties of our theoretical approach allow us to deduce quantitative predictions from the statistical equilibrium model that can be checked by numerical experiments. Moreover, our continuum limit is ideally suited to rigorous analysis by large deviation techniques. Namely, we invoke the theory of large deviations to demonstrate that the ground state solitary waves are the most probable macroscopic states for the statistical equilibrium model. In turn,

we use this variational characterization of the equilibrium states to give a simple and intuitive proof of the nonlinear stability of these coherent structures.

Although we limit our discussion to a class of prototype systems, our methods and results have the potential of wider applicability to what is sometimes referred to as “soliton turbulence” or “dispersive wave turbulence” [3, 17, 25, 6]. On the one hand, the same equilibrium statistical models could be defined for higher-dimensional equations with various boundary conditions, and for unbounded, but subcritical, nonlinearities. On the other hand, these models could be adapted to capture the quasi-equilibrium behavior on the large-scales of a turbulent wave system that is weakly forced and dissipated on the small scales. These extensions have not yet been much explored. Of course, the understanding of nonequilibrium effects, such as the universal form of direct or inverse cascades for strongly forced and dissipated systems, lies outside the range of applicability of these models.

Long-time behavior of solutions

Numerical simulations [6, 25, 13, 14] of the NLS equation (1) with either Dirichlet or periodic boundary conditions demonstrate the tendency of the system to form coherent structures. These long-time simulations exhibit a separation-of-scales behavior, in which the field ψ evolves from generic initial conditions into a final state consisting of a deterministic, coarse-grained coherent structure combined with a random, fine-grained fluctuations. For a focusing nonlinearity, the coherent structure takes the form of a spatially-localized solitary wave. At intermediate times before the relaxation to such a final state, the solution ψ typically consists of a collection of solitary waves, which undergo a succession of imperfect interactions. When two such waves interact, the smaller one decreases in amplitude while the larger one increases in amplitude, and some fine-grained wave radiation is produced. After a series of such wave interactions, a single soliton of large amplitude survives in a background of turbulent radiation. Figure (1), taken from [13], illustrates the evolution of the solution of (1) for the subcritical nonlinearity $f(|\psi|^2) = |\psi|$ and with periodic boundary conditions on the spatial interval $[0, 256]$. A qualitatively similar picture is found for saturated nonlinearities and Dirichlet boundary conditions [15].

These numerical investigations also indicate that the dynamical invariants H and Q play disparate roles in this slow relaxation process. On the one hand, the particle number Q is almost insensitive to the fine-grained fluctuations, and the constraint $Q = N$ controls the amplitude of the coarse-grained coherent structure. The freely-evolving solution exhibits a flux of particle number to large scales throughout the formation of the coherent structure. On the other hand, the energy H contains a term involving $|\psi_x|^2$, to which the fine-grained waves make a significant contribution, and a term involving $F(|\psi|^2)$, to which they make a negligible contribution. Thus, in the equilibrium state the energy splits into a coherent part and a turbulent part. In the process of relaxation toward this equilibrium, as the dynamics excites fluctuations on progressively smaller scales with correspondingly smaller amplitudes, the solution exhibits a net flux of energy to small scales. This separation-of-scales behavior, which is supported by many simulations under a variety of conditions, motivates our particular choice of statistical equilibrium ensemble, as well as our mean-field approximation. These theoretical issues are taken up in the next sections.

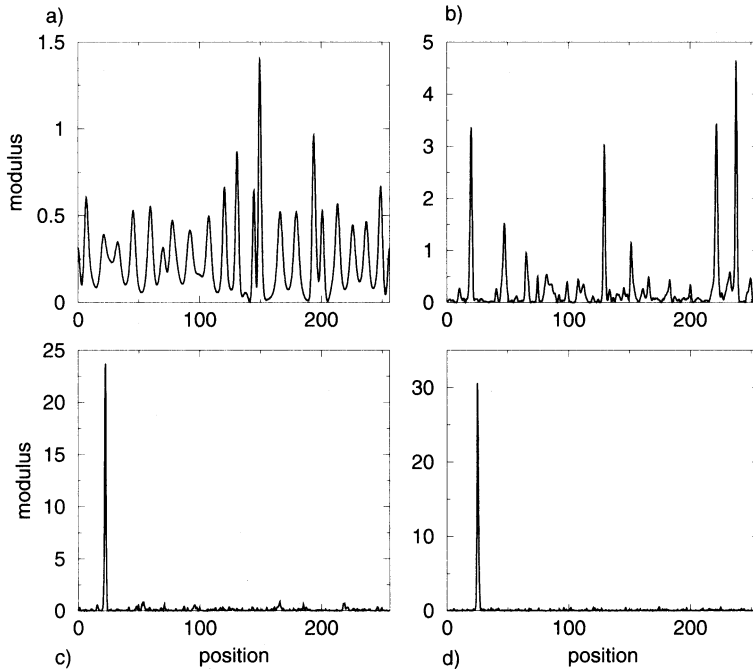


FIGURE 1. Profile of the modulus $|\psi|^2$ at four different times for the system (1) with nonlinearity $f(|\psi|^2) = |\psi|$ and periodic boundary conditions on the interval $[0, 256]$. The initial condition is $\psi(x, t = 0) = A$, with $A = 0.5$, plus a small random perturbation. The numerical scheme used to approximate the solution is the split-step Fourier method. The grid size is $dx = 0.125$, and the number of modes is $n = 2048$. a) $t = 50$: Due to the modulational instability, an array of soliton-like structures separated by the typical distance $l_i = 2\pi/\sqrt{A/2} = 4\pi$ is created; b) $t = 1050$: The solitons interact and coalesce, giving rise to a smaller number of solitons of larger amplitude; c) $t = 15050$: The coalescence process has ended, and one large soliton remains; d) $t = 55050$: the amplitude of the fluctuations has diminished while the amplitude of the coherent structure has increased.

Statistical equilibrium description of NLS dynamics

In order to define a probabilistic model, it is necessary to introduce a sequence of a finite-dimensional approximations to the partial differential equation (1). For ease of presentation, we consider the NLS equation on an interval $\Omega = [0, L]$ with homogeneous Dirichlet boundary conditions, and we use a spectral truncation of the NLS dynamics. Nevertheless, the same ideas apply to other boundary conditions (such as periodic) and other discrete approximations (such as finite-difference).

Let $e_k(x) = \sqrt{2/L} \sin(\sqrt{\lambda_k}x)$ and $\lambda_k = (k\pi/L)^2, k = 1, 2, \dots$, denote the eigenfunctions and eigenvalues of the operator $-\frac{d^2}{dx^2}$ on Ω . With respect to this orthonormal basis for $L^2(\Omega)$, let $W_n = \text{span}\{e_1, \dots, e_n\}$ be the n -dimensional subspace

consisting of functions

$$(4) \quad \psi^{(n)}(x) = u^{(n)}(x) + iv^{(n)}(x) = \sum_{k=1}^n \psi_k e_k(x),$$

with arbitrary complex coefficients $\psi_k = u_k + iv_k$. For each fixed n , the field $\psi^{(n)} \in L^2$ corresponds to a microstate for the model, that is, a point $\psi = (\psi_1, \dots, \psi_n)$ in the phase space $\Gamma_n \doteq C^n = \mathbb{R}^{2n}$. The microscopic dynamics for this model is governed by

$$(5) \quad i\psi_t^{(n)} + \psi_{xx}^{(n)} + P^{(n)} \left(f(|\psi^{(n)}|^2) \psi^{(n)} \right) = 0,$$

where $P^{(n)}$ denotes the orthogonal projection from L^2 onto W_n . This spectral truncation of the NLS equation (1) is equivalent to a system of ordinary differential equations for the real Fourier coefficients u_k and v_k , $k = 1, \dots, n$, having a canonical Hamiltonian form [2, 26]; namely,

$$(6) \quad \frac{du_k}{dt} = \lambda_k v_k - \int_{\Omega} f((u^{(n)})^2 + (v^{(n)})^2) v^{(n)} e_k dx = \frac{\partial H_n}{\partial v_k},$$

$$(7) \quad \frac{dv_k}{dt} = -\lambda_k u_k + \int_{\Omega} f((u^{(n)})^2 + (v^{(n)})^2) u^{(n)} e_k dx = -\frac{\partial H_n}{\partial u_k},$$

with Hamiltonian

$$(8) \quad H_n(\psi) = H_n(u_1, v_1, \dots, u_n, v_n) = \frac{1}{2} \sum_{k=1}^n \lambda_k |\psi_k|^2 - \frac{1}{2} \int_{\Omega} F(|\psi^{(n)}|^2) dx.$$

In fact, $H_n(\psi) = H(\psi^{(n)})$, the restriction to W_n of the functional H defined in (2). The spectrally-truncated particle number, $Q_n(\psi) = Q(\psi^{(n)})$, is also an invariant of the microscopic dynamics (5), and

$$(9) \quad Q_n(\psi) = Q_n(u_1, v_1, \dots, u_n, v_n) = \frac{1}{2} \int_{\Omega} |\psi^{(n)}|^2 dx = \frac{1}{2} \sum_{k=1}^n |\psi_k|^2.$$

We define the statistical equilibrium model by a Gibbs ensemble on the $2n$ -dimensional phase space Γ_n with n large, in which H_n is treated canonically and Q_n is treated microcanonically. This particular choice of ensemble is motivated in part by the fact that H is sensitive to the random small-scale fluctuations, while Q depends solely on the large-scale coherent structure. Indeed, physical reasoning suggests that the ensemble be canonical in H , since energy is in contact with a “bath” of unresolved small-scale wave motions, and that it be microcanonical in Q , because the particle number is isolated from those motions, being trapped in the large-scale waves. We refer to this ensemble as the *mixed ensemble*, and we denote it by $P_{\beta}^N(d\psi)$, where $N > 0$ is a given particle number and $\beta > 0$ is a given inverse temperature. Formally, the mixed ensemble is the probability distribution

$$(10) \quad P_{\beta}^N(d\psi) = Z_n(\beta, N)^{-1} \exp(-\beta H_n(\psi)) \delta(Q_n(\psi) - N) \Pi_n(d\psi),$$

where the normalizing constant is the partition function

$$(11) \quad Z_n(\beta, N) = \int_{Q_n=N} \exp(-\beta H_n(\psi)) ds(\psi).$$

Here, $\Pi_n(d\psi) = \prod_k du_k dv_k$ is phase volume on Γ_n , and $ds(\psi)$ is hypersurface area on the sphere $Q_n(\psi) = N$, which is the support of the distribution (10).

Let us define this mixed ensemble precisely as a conditional probability measure. First, we take $\sigma > 0$ sufficiently large so that

$$H_n(\psi) \geq -\frac{\sigma}{2} Q_n(\psi) \quad \text{for all } \psi \in \Gamma_n.$$

It is easy to see that, for any saturated nonlinearity f , such a σ can be found and can be fixed independent of n as $n \rightarrow \infty$. (A more refined argument can be given for unbounded, but subcritical, nonlinearities.) We then construct the following σ -regularized canonical measure

$$(12) \quad P_\beta(d\psi) = Z_n(\beta)^{-1} \exp(-\beta[H_n(\psi) + \sigma Q_n(\psi)]) \Pi_n(d\psi),$$

which exists and is normalizable. By contrast, with $\sigma = 0$ it is known that the partition function $Z_n(\beta)$ in (12) diverges for typical focusing nonlinearities, since H_n goes to $-\infty$ in some directions of the phase space Γ_n [16, 15]. Finally, we define the mixed ensemble to be

$$(13) \quad P_\beta^N(d\psi) = P_\beta(d\psi | Q_n(\psi) = N),$$

namely, the conditional distribution of the regularized canonical measure for H_n with respect to the microcanonical constraint $Q_n = N$. It is evident that the mixed ensemble (13) is independent of the choice of σ , and that it coincides with the formal expression (10). Technically, the condition $Q_n = N$ ought to be replaced by the thickened condition $Q_n \in [N - \epsilon, N + \epsilon]$, and then a second limit $\epsilon \rightarrow 0$ taken after $n \rightarrow \infty$. But, to keep the exposition clear, we ignore this minor point.

Our goal is to study the mixed ensemble (13) in a continuum limit $n \rightarrow \infty$, holding N fixed and scaling $\beta = \beta_n$ with n so that the ensemble mean energy $\langle H_n \rangle$ tends to a finite limit E . Before giving a rigorous analysis of this limit based on large deviation principles, we first introduce and investigate a mean-field ensemble that approximates the mixed ensemble (13). This mean-field theory has the advantage that its governing ensemble is explicitly calculable for finite n , and yet is asymptotically exact in the continuum limit. Consequently, it gives definite predictions about the coherent structure and the fluctuations, which can be compared with the results of direct numerical simulations to validate the theory.

Mean-field theory

We seek a tractable approximation to the mixed ensemble (13) for large but finite n , with a fixed particle number $Q_n = N$ and a fixed mean energy $\langle H_n \rangle = E$. The numerical simulations described above suggest a procedure for making such an approximation, since they show that in the statistical equilibrium state the variance of the computed solution, $\text{var } \psi^{(n)}(x)$, at any point $x \in \Omega$ tends to zero as $n \rightarrow \infty$. Furthermore, this conclusion is consistent with the notion that with respect to the mixed ensemble the energy of the fluctuations equipartitions over the n modes ψ_k , so that $\lambda_k \text{var } \psi_k = O(1/n)$.

In view of these asymptotic properties, we are led to an approximation of the form

$$(14) \quad P_\beta^N(d\psi) \approx \rho^{(n)}(\psi) \Pi_n(d\psi),$$

in which the probability density $\rho^{(n)}$ on Γ_n is defined by maximizing over all admissible probability densities ρ on Γ_n the entropy functional

$$(15) \quad S(\rho) = - \int_{\Gamma_n} \rho \log \rho \Pi_n(d\psi),$$

subject to the constraints

$$(16) \quad \left\langle \frac{1}{2} \sum_{k=1}^n \lambda_k |\psi_k|^2 \right\rangle - \frac{1}{2} \int_{\Omega} F(|\langle \psi^{(n)}(x) \rangle|^2) dx = E,$$

$$(17) \quad \frac{1}{2} \int_{\Omega} |\langle \psi^{(n)}(x) \rangle|^2 dx = N.$$

In these constraints, $\langle \cdot \rangle$ denotes expectation with respect to an admissible density ρ . This variational characterization of the mean-field ensemble (14) derives from the well-known principle that a canonical ensemble maximizes entropy subject to a mean constraint, while a microcanonical ensemble maximizes entropy subject to an exact constraint. Accordingly, the mixed ensemble (13) is characterized by maximizing $S(\rho)$ subject to the constraints $\langle H_n \rangle = E$ and $Q_n = N$. The constraints (16) and (17) for the mean-field ensemble result from expanding the corresponding constraints for the mixed ensemble in terms of the small fluctuation $\psi^{(n)} - \langle \psi^{(n)} \rangle$, and then retaining only the leading term. The validity of this expansion technique is verified a posteriori by proving that, asymptotically as $n \rightarrow \infty$, the mean-field ensemble is equivalent to the mixed ensemble [15].

Solutions $\rho = \rho^{(n)}$ to the constrained variational problem defining the mean-field ensemble are found to have the form

$$(18) \quad \rho^{(n)}(\psi) = \prod_{k=1}^n \frac{\beta^{(n)} \lambda_k}{2\pi} \exp\left(-\frac{\beta^{(n)} \lambda_k}{2} |\psi_k - \langle \psi_k \rangle|^2\right),$$

with

$$(19) \quad \langle \psi_k \rangle = \frac{1}{\lambda_k} \int_{\Omega} f(|\langle \psi^{(n)}(x) \rangle|^2) \langle \psi^{(n)}(x) \rangle e_k(x) dx - \frac{\mu^{(n)}}{\beta^{(n)} \lambda_k} \langle \psi_k \rangle,$$

Here, $\beta^{(n)}$ and $\mu^{(n)}$ are the Lagrange multipliers associated with the constraints (16) and (17), respectively.

The predictions of the mean-field theory can now be deduced from the explicit expression (18). As these results are discussed in detail elsewhere [15, 13], we merely summarize the main predictions here.

We see immediately that $u_1, v_1, \dots, u_n, v_n$ are mutually independent Gaussian random variables with means satisfying (19) and variances given by

$$(20) \quad \text{var}(u_k) = \text{var}(v_k) = \frac{1}{\beta^{(n)} \lambda_k}.$$

The mean field, $\phi^{(n)} \doteq \langle \psi^{(n)} \rangle$, is determined implicitly by (19). Setting $\lambda^{(n)} \doteq -\mu^{(n)}/\beta^{(n)}$, the equation for the mean-field reduces to

$$(21) \quad \phi_{xx}^{(n)} + P^{(n)}\left(f(|\phi^{(n)}|^2)\phi^{(n)}\right) + \lambda^{(n)}\phi^{(n)} = 0,$$

where $P^{(n)}$ is the projection onto the span W_n of e_1, \dots, e_n . We recognize this form of the mean-field equation as the spectral truncation of the ground state equation for the continuous NLS system (1); that is, the equation satisfied by $\bar{\phi}$ when the standing wave, $\psi(x) = \bar{\phi}(x) \exp(-i\lambda t)$, is substituted into (1). Like the ground states, $\phi^{(n)}$ is determined only up to an arbitrary phase-shift factor $e^{i\theta}$.

For each N the mean-field is, in fact, an absolute minimizer of H_n given the constraint $Q_n = N$ [15]. From this variational characterization, we infer that the family of coherent structures $\phi^{(n)}$ can be parametrized by the particle number N .

Moreover, the corresponding Lagrange multiplier, $\lambda^{(n)}$, in this variational problem is uniquely determined by the mean-field solution, and hence it can be parametrized by N . This parametrization is more natural in the statistical equilibrium theory than the usual approach of bifurcation theory, in which branches of solutions $\phi^{(n)}$ to the nonlinear eigenvalue problem (21) are parametrized by $\lambda^{(n)}$.

For each finite n , the difference between the energy of the coherent structure, $\bar{E}_n \doteq H_n(\phi^{(n)})$, and the ensemble mean energy, E , resides in the turbulent fluctuations having the temperature

$$(22) \quad \frac{1}{\beta^{(n)}} = \frac{E - \bar{E}_n}{n}.$$

The particle number spectral density is therefore given by:

$$(23) \quad \frac{1}{2} \langle |\psi_k|^2 \rangle = \frac{1}{2} |\langle \psi_k \rangle|^2 + \frac{E - \bar{E}_n}{n \lambda_k}.$$

Since $\phi^{(n)}$ is a spectral truncation of a smooth solution to the ground state equation, its spectrum decays rapidly in k . Hence, for large wavenumbers $k \gg 1/L$, we have the approximation $\frac{1}{2} \lambda_k \langle |\psi_k|^2 \rangle \approx (E - \bar{E}_n)/n$. This expression shows that, as may be anticipated from a statistical equilibrium theory, the contribution to the energy from the fluctuations is equipartitioned among the n modes.

Figure (2) shows the agreement between the spectrum predicted by the mean-field theory and the spectrum obtained by averaging numerical solutions to the underlying NLS equation over the final 1000 time units and over 16 initial conditions with the same energy E and particle number N . This simulation is for the subcritical power-law nonlinearity $f(|\psi|^2) = |\psi|$, but the same sort of results are obtained for saturated nonlinearities [12]. For small wavenumbers the computed spectrum follows that of the ground state, while for large wavenumbers it realizes the predicted equipartition of turbulent energy. In this remarkably good fit, all the parameters determining the theoretical spectrum are deduced from the given values of E and N .

The numerical investigations in [13] demonstrate that the time T required for the spectrally truncated NLS system (5) with n modes to reach a statistical equilibrium state scales like $T \sim n^4$. That is, the truncated dynamics ergodically samples the mean-field ensemble $\rho^{(n)}$ with given E and N at times t of the order of this characteristic time T . As time progresses the equilibrium coherent structure remains almost unchanged, while the turbulent dynamics excites smaller and smaller scales. The continuum limit of the model is approached in an asymptotic sense as $T \rightarrow \infty$. A fuller discussion of this behavior is given in [13].

Large deviation principle

Both the mean-field theory and the numerical simulations suggest that, in the continuum limit as $n \rightarrow \infty$ with fixed E and N , the random field $\psi^{(n)}$ approaches the set of ground states $e^{i\theta} \phi(x)$ of the NLS equation (1). Now, we formulate this statement precisely as a large deviation principle for the $L^2(\Omega)$ -valued stochastic process $\psi^{(n)}$ defined by (4) with respect to the mixed ensemble (13). Broadly speaking, a large deviation principle is an exponential-order refinement of the law of large numbers [5, 7]. We expect the random field $\psi^{(n)}(x)$ to have this kind of limit behavior because it is the sum of component fields $\psi_k e_k(x)$ that are asymptotically independent.

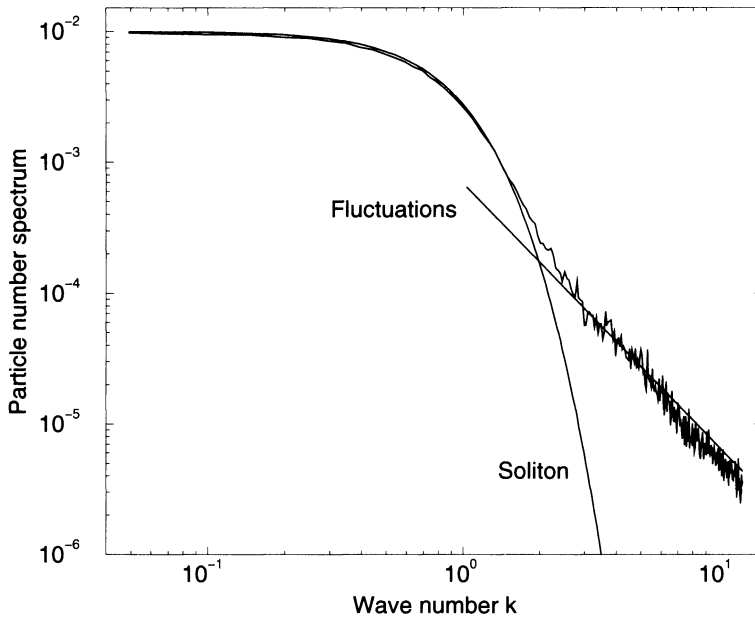


FIGURE 2. Particle number spectral density $|\psi_k|^2$ as a function of k for $t = 1.1 \times 10^6$ unit time (upper curve). The lower curve (smooth one) is the particle number spectral density for the solitary wave that contains all the particles of the system. The straight line drawn for large k corresponds to the mean-field prediction for the spectral density for large wavenumbers. The numerical simulation has been performed with $n = 512$, $dx = 0.25$, $N = 20.48$ and $E = -5.46$.

We are interested in the asymptotics of the mixed ensemble $P_{\beta_n}^N(d\psi)$ in the limit where the inverse temperature β_n goes to infinity as $n \rightarrow \infty$. This particular scaling is motivated by the fact that $\beta^{(n)} \sim \beta^* n$ for large n at fixed E , according to the mean-field theory (22). In such a limit, the process $\psi^{(n)}$ satisfies a large deviation principle, which is essentially expressed by the following limit formula:

For any continuity set $B \subset L^2(\Omega)$,

$$(24) \quad \lim_{n \rightarrow \infty} \frac{1}{\beta_n} \log P_{\beta_n}^N \{ \psi^{(n)} \in B \} = \bar{E}(N) - \inf \{ H(\phi) : Q(\phi) = N, \phi \in B \},$$

where

$$(25) \quad \bar{E}(N) \doteq \min \{ H(\phi) : Q(\phi) = N, \phi \in H_0^1(\Omega) \}.$$

By a “continuity set” we mean a Borel subset B of L^2 having the property that in (24) the same infimum is achieved over the interior of B as over the closure of B . In practical applications of this result, it suffices to use such continuity sets B . A more general statement holds in the form of an upper bound for closed sets B and a lower bound for open sets B . The sequence $\beta_n \rightarrow +\infty$ is called the sequence of scaling constants in the large deviation limit. The so-called rate function is the

extended functional on $L^2(\Omega)$:

$$(26) \quad I^N(\phi) = \begin{cases} H(\phi) - \bar{E}(N) & \text{for } \phi \in H_0^1(\Omega), Q(\phi) = N \\ +\infty & \text{otherwise} \end{cases}$$

Heuristically, the large deviation principle means that the states $\bar{\phi}$ that minimize H given the constraint $Q = N$ are the overwhelmingly most probable states with respect to the mixed ensemble. This set of constrained minimizers is the set of equilibrium states, or ground states; we denote it by \mathcal{E}^N . For an equilibrium state $\bar{\phi}$, $I^N(\bar{\phi}) = 0$; however, for any state ϕ satisfying $Q(\phi) = N$ that is not an equilibrium state, $I^N(\phi) > 0$. Thus, if we choose B to be the complement of an r -neighborhood of the equilibrium set \mathcal{E}^N , we infer from (24) that

$$P_{\beta_n}^N \{ \text{dist}(\psi^{(n)}, \mathcal{E}^N) \geq r > 0 \} \leq e^{-\beta_n J(r)/2} \rightarrow 0 \quad \text{as } n \rightarrow \infty,$$

where $J(r) = \inf\{I^N(\phi) : \text{dist}(\phi, \mathcal{E}^N) \geq r > 0\} > 0$; the distance is taken in the L^2 -norm. Thus, any state $\phi \in L^2(\Omega)$ that is not an equilibrium state has an exponentially small probability of being observed in this continuum limit.

The proof of the large deviation principle (24) relies on recent results about microcanonical ensembles and associated mixed ensembles developed in [8]. The general results in that paper allow us to derive (24) from a corresponding large deviation principle for $\psi^{(n)}$ with respect to the σ -regularized canonical ensemble $P_{\beta_n}(d\psi)$ defined in (12). The required asymptotic statement is essentially:

$$(27) \quad \lim_{n \rightarrow \infty} \frac{1}{\beta_n} \log P_{\beta_n} \{ \psi^{(n)} \in B \} = - \inf \{ H(\phi) + \sigma Q(\phi) : \phi \in B \},$$

for any continuity set $B \subset L^2(\Omega)$. The rate function for this large deviation principle is $I(\phi) = H(\phi) + \sigma Q(\phi)$ for $\phi \in H_0^1$, extended to be $+\infty$ for $\phi \in L^2 \setminus H_0^1$. By virtue of the choice of σ , I is a convex functional on L^2 having a unique minimum at 0, with $I(0) = 0$. As is demonstrated in [8], the rate function I^N for (24) is constructed from I by imposing the microcanonical constraint $Q = N$; that is, $I^N(\phi) = I(\phi) - \inf\{I : Q = N\}$, if $Q(\phi) = N$, and $I^N(\phi) = +\infty$, otherwise. This construction produces the formula (26), which is independent of σ .

In turn, the proof of the large deviation limit (27) without the microcanonical constraint follows from standard results [5, 7]. First, the Hamiltonian $H(\psi)$ is separated into the Dirichlet integral, $D(\psi) = \frac{1}{2} \int_{\Omega} |\psi_x|^2 dx$, and the remaining integral, $\Phi(\psi) = -\frac{1}{2} \int_{\Omega} F(|\psi|^2) dx$, involving the nonlinear potential. In terms of this decomposition, the canonical distribution (12) is a perturbation of a Gaussian distribution, in the sense that the following asymptotic approximation holds for large n :

$$P_{\beta_n}(d\psi) \sim Z_n^{-1} \exp(-\beta_n [\Phi(\psi^{(n)}) + \sigma Q(\psi^{(n)})]) G_{\beta_n}(d\psi)$$

where

$$G_{\beta_n}(d\psi) = C_n^{-1} \exp(-\beta_n D_n(\psi)) \Pi_n(d\psi).$$

The desired large deviation principle for $P_{\beta_n}(d\psi)$ is therefore a consequence of Varadhan's asymptotics of integrals [7, 24], combined with the elementary fact that $\psi^{(n)}$ satisfies a large deviation principle with respect to the rescaled Wiener-type measure $G_{\beta_n}(d\psi)$, for which the rate function is D . The latter result is a special case of a general theory of asymptotics for Gaussian integrals [10]. In this way, the proof of (24) is completed. Full details are given in [9].

It is worth noting that the large deviation principle for $\psi^{(n)}$ depends crucially on the fact that the functionals Q and Φ are continuous with respect to

the L^2 -topology, and hence that the necessary approximations $Q_n(\psi) \approx Q(\psi^{(n)})$ and $\Phi_n(\psi) \approx \Phi(\psi^{(n)})$ hold for large n . This fact is intimately related to the properties needed to justify the mean-field theory, which amounts to terminating these approximations at the first order. For this reason, the large deviation estimates can be used to give a rigorous justification of the mean-field approximation.

Ground states and their stability

The equilibrium states, $\bar{\phi} \in \mathcal{E}^N$, for the mixed ensemble (13) are the ground states of the underlying NLS equation (1). Indeed, for any such $\bar{\phi}$, we have $H(\bar{\phi}) = \bar{E}(N)$, the value function for the optimization problem defining the ground states (25). This “coherent energy” function, $\bar{E}(N)$, plays the role of the basic thermodynamic function in the statistical equilibrium theory. We now indicate how the properties of the ground states $\bar{\phi}$ – especially their nonlinear stability – are deduced from the properties of $\bar{E}(N)$.

The first-order variational condition for $\bar{\phi}$ is $\delta(H - \lambda Q)(\bar{\phi}) = 0$, where λ is the Lagrange multiplier for the constraint $Q = N$. A standard calculation shows that this condition is equivalent to the familiar equation for a ground state, namely,

$$(28) \quad \bar{\phi}_{xx} + f(|\bar{\phi}|^2)\bar{\phi} + \lambda\bar{\phi} = 0.$$

Exponential decay of the solitary wave $\bar{\phi}$ away from its peak requires that λ be negative. The coherent energy is therefore a decreasing function of N , since

$$\frac{d\bar{E}}{dN} = \lambda < 0.$$

Moreover, $\bar{E}(N) \rightarrow -\infty$ as $N \rightarrow \infty$. This property follows from the fact that, in the absence of the constraint $Q = N$ with fixed N , H is unbounded from below on $H_0^1(\Omega)$. In this way, we see again that the existence of a ground state solitary wave depends crucially on the particle number constraint.

In general, the ground state $\bar{\phi}$ is not a local minimizer of the corresponding Lagrangian functional $L \doteq H - \lambda Q$. Rather, the second-order variational condition for $\bar{\phi}$ is: $\delta^2(H - \lambda Q)(\bar{\phi}) \geq 0$ for all variations $\delta\bar{\phi}$ satisfying the linearized constraint, $\delta Q = 0$. An easy calculation shows that typically this second variation is negative when the restriction $\delta Q = 0$ is violated. This fact has an interesting relation to the proof of nonlinear stability of the ground state by a Lyapunov argument. A natural choice of Lyapunov functional for $\bar{\phi}$ is the Lagrangian L itself, and indeed standard proofs of stability make use of this functional [21, 23]. However, the indefiniteness of the Lagrangian at $\bar{\phi}$ requires that such proofs somehow take into account the particle number constraint $Q = N$, which plays a crucial role in controlling the growth of perturbations. Consequently, the known proofs of stability tend to be rather complicated. We now sketch a simple proof of nonlinear stability of the ground state that overcomes this difficulty by using a central concept in constrained optimization theory, the “augmented Lagrangian” [1].

The augmented Lagrangian in question is defined by

$$(29) \quad L_\gamma(\phi) = H(\phi) - \lambda Q(\phi) + \frac{\gamma}{2}[Q(\phi) - N]^2,$$

for some positive constant γ . Clearly, the idea is to add a quadratic penalty term for the constraint $Q = N$ to the Lagrangian L . In fact, it is possible to fix γ sufficiently large so that L_γ has a nondegenerate, unconstrained minimum at the ground state $\bar{\phi}$. Since L_γ is composed of functionals that are conserved quantities for the NLS

equation (1), L_γ is a Lyapunov functional for $\bar{\phi}$, and so nonlinear stability of the ground state follows.

The choice of the penalization constant γ is determined by the second-order properties of the coherent energy function $\bar{E}(N)$. Generically, the rate of spatial decay, $\sqrt{-\lambda}$, of a localized solitary wave increases with increasing amplitude, N ; this behavior means that

$$\frac{d^2 \bar{E}}{dN^2} = \frac{d\lambda}{dN} < 0.$$

In fact, this inequality coincides with the known stability condition for NLS solitary waves [21, 23]. In this situation, we construct the desired Lyapunov functional L_γ by choosing γ large enough so that $-\gamma < d^2 \bar{E}/dN^2$ at $N = Q(\bar{\phi})$. Then, locally near N the coherent energy function \bar{E} has a supporting parabola, in the sense that for $N' \neq N$

$$\bar{E}(N') > \bar{E}(N) + \lambda(N' - N) - \frac{\gamma}{2}(N' - N)^2.$$

This inequality together with the definition of \bar{E} in (25) imply the desired property of L_γ ; namely, that for any perturbation ϕ of $\bar{\phi}$ in L^2 ,

$$\begin{aligned} L_\gamma(\phi) &\geq \bar{E}(Q(\phi)) - \lambda Q(\phi) + \frac{\gamma}{2}[Q(\phi) - N]^2 \\ &> \bar{E}(N) - \lambda N = L_\gamma(\bar{\phi}). \end{aligned}$$

The stability of the ground state $\bar{\phi}$ in the L^2 -norm therefore follows. Technically, it is also necessary to verify that $\delta^2 L_\gamma(\bar{\phi})$ is positive-definite. The complete argument is given in [9].

In conclusion, we comment that the large deviation principle (24) can be viewed as a stability property of the ground states with respect to microscopic perturbations. That is, it guarantees that the macroscopic field $\psi^{(n)}$ remains close in the L^2 -norm to the set of ground states \mathcal{E}^N with very high probability, while the microstates ψ sample the invariant distribution $P_{\beta_n}^N$. In other words, as an ergodic microscopic dynamics explores the phase space in Γ_n compatible with the energy and particle number constraints, the fluctuations in the random field $\psi^{(n)}$ appear negligible in the L^2 -norm. A finite fraction of the total energy is however contained in these turbulent fluctuations, and consequently the typical microstate lies a finite distance from the ground states in the H^1 -norm. This weak stability property is a statistical characteristic of freely-evolving NLS turbulence. By contrast, the strong, or Lyapunov, stability property of the ground states pertains to the deterministic evolution of perturbations that are finite in the L^2 -norm. Nevertheless, the same Lyapunov argument shows that the macroscopic field $\psi^{(n)}$ remains close in the L^2 -norm to the ground states, even if a fraction of the perturbation energy goes into fine-grained turbulent fluctuations. Thus, we find that that ground states are stable in both the microscopic sense and the macroscopic sense.

Acknowledgments

The authors wish to thank Richard Ellis, Christophe Josserand and Craig Zirbel for their collaborations on the research described in this note.

References

- [1] D. P. Bertsekas. *Constrained optimization and Lagrange multiplier methods*. Academic Press, New York-London, 1982.
- [2] J. Bourgain. Periodic nonlinear Schrödinger equation and invariant measures. *Commun. Math. Phys.*, 166:1–26, 1994.
- [3] D. Cai, A. J. Majda, D. W. McLaughlin, and E. G. Tabak. Spectral bifurcations in dispersive wave turbulence. *Proc. Nat. Acad. Sci.*, 96:14216–14221, 1999.
- [4] D. Cai and D. W. McLaughlin. Chaotic and turbulent behavior of unstable 1D nonlinear dispersive waves. *J. Math. Phys.*, 41:4125–4153, 2000.
- [5] A. Dembo and O. Zeitouni. *Large deviations techniques and applications*. Jones and Bartlett, Boston, 1993.
- [6] S. Dyachenko, V. E. Zakharov, A. N. Pushkarev, V. F. Shvets, and V. V. Yan'kov. Soliton turbulence in nonintegrable wave systems. *Soviet Phys. JETP*, 69:1144–1147, 1989.
- [7] R. S. Ellis. *Entropy, large deviations and statistical mechanics*. Springer-Verlag, New York, 1985.
- [8] R. S. Ellis, K. Haven, and B. Turkington. Large deviation principles and complete equivalence and nonequivalence results for pure and mixed ensembles. *J. Statist. Phys.*, 2000. To appear.
- [9] R. S. Ellis, R. Jordan, and B. Turkington. In preparation.
- [10] R. S. Ellis and J. S. Rosen. Laplace's method for Gaussian integrals with an application to statistical mechanics. *Ann. Probab.*, 10:47–66, 1982.
- [11] A. Hasegawa. Self-organization processes in continuous media. *Adv. Phys.*, 34:1–42, 1985.
- [12] R. Jordan and C. Josserand. 2000. Unpublished.
- [13] R. Jordan and C. Josserand. Self-organization in nonlinear wave turbulence. *Phys. Rev. E*, 61:1527–1539, 2000.
- [14] R. Jordan and C. Josserand. Statistical equilibrium states for the nonlinear Schrödinger equation. *Math. Comp. Simulation*, 2000. To appear.
- [15] R. Jordan, B. Turkington, and C. L. Zirbel. A mean-field statistical theory for the nonlinear Schrödinger equation. *Physica D*, 137:353–378, 2000.
- [16] J. L. Lebowitz, H. A. Rose, and E. R. Speer. Statistical mechanics of a nonlinear Schrödinger equation. *J. Stat. Phys.*, 50:657–687, 1988.
- [17] A. J. Majda, D. W. McLaughlin, and E. G. Tabak. A one-dimensional model for dispersive wave turbulence. *J. Nonlinear Sci.*, 7:9–44, 1997.
- [18] H. P. McKean. Statistical mechanics of nonlinear wave equations IV. Cubic Schrödinger. *Commun. Math. Phys.*, 168:479, 1995.
- [19] J. C. McWilliams. The emergence of isolated vortices in turbulent flow. *J. Fluid Mech.*, 146:21–43, 1984.
- [20] D. Mihalache, R. G. Nazmitdinov, and V. K. Fedyanin. Nonlinear optical waves in layered structures. *Soviet J. Part. Nucl.*, 20:86–92, 1989.
- [21] J. J. Rasmussen and K. Rypdal. Blow-up in nonlinear Schroedinger equations—I: A general review. *Physica Scripta*, 33:481–504, 1986.
- [22] E. Segre and S. Kida. Late states of incompressible 2d decaying vorticity fields. *Fluid Dyn. Res.*, 23:89–112, 1998.
- [23] W. A. Strauss. *Nonlinear wave equations*. AMS, Providence, RI, 1989.
- [24] S. R. S. Varadhan. Asymptotic probabilities and differential equations. *Commun. Pure Appl. Math.*, 19:261–286, 1966.
- [25] V. E. Zakharov, A. N. Pushkarev, V. F. Shvets, and V. V. Yan'kov. Soliton turbulence. *JETP Lett.*, 48:83–86, 1988.
- [26] P. E. Zhidkov. On an invariant measure for a nonlinear Schrödinger equation. *Soviet Math. Dokl.*, 43:431–434, 1991.

DEPARTMENT OF MATHEMATICAL SCIENCES, WORCESTER POLYTECHNIC INSTITUTE, WORCESTER, MA 01609-2280

E-mail address: rjordan@wpi.edu

DEPARTMENT OF MATHEMATICS AND STATISTICS, UNIVERSITY OF MASSACHUSETTS, AMHERST, MA 01003

E-mail address: turk@math.umass.edu

This page intentionally left blank

Is there a 2D cascade in 3D convection?

Robert M. Kerr

ABSTRACT. The boundary layer in simulations of classical Rayleigh-Bénard convection in a wide box with no mean flow is used to study the third order structure function $S_3(r)$ and the associated longitudinal and transverse second order structure functions, $S_2^L(r)$ and $S_2^T(r)$. At small scales $S_3(r)$ is consistent with the -4/5 law for three-dimensional turbulence. At large scales $S_3(r)$ is found to be linearly increasing and eventually positive, which is similar to a 2D backward energy cascade. However, the magnitude of $S_3(r)$ is too large for its origin to be a 2D backward energy cascade. The relationship to atmospheric observations is discussed.

Introduction

While all geophysical fluid systems are fundamentally three-dimensional, there are a number of geophysical constraints that suggest that two-dimensional effects might be present in many situations. These constraints include stratification, rotation, and the large aspect ratio (width/height) of many geophysical systems. However, there is no conclusive evidence for any two-dimensional behavior that does not involve the third dimension. The most commonly quoted evidence is the existence of a -5/3 energy spectrum at large scales in the stratosphere [Q], which could be consistent with a backward energy cascade [N]. The stratospheric measurements come from commercial aircraft and show a -5/3 spectrum between $k = 0.001\text{km}^{-1}$ and 0.01km^{-1} and a steeper -3 spectrum at larger scales. [Q].

This evidence for a two-dimensional cascade has recently been called into question. Using analysis of the longitudinal third-order structure function $S_3(r) = S_3^L(r)$ and comparison of the longitudinal and transverse second-order structure functions $S_2^{L,T}(r)$ to their expected isotropy relationship, it is found that S_3 is an order of magnitude too large to be due to a two-dimensional cascade [O]. Another -5/3 energy spectrum over a wide range of scales has recently been shown [T] in three overlapping sources of observational data in the atmospheric boundary layer over the tropical ocean. The range of scales is between 1000 km and 1 km. Each set of observations is within the boundary layer where none of the traditional mechanisms for two-dimensionality such as stratification or rotation should apply. That

1991 *Mathematics Subject Classification.* Primary 54C40, 14E20; Secondary 46E25, 20C20.
Key words and phrases. Turbulence, Atmospheric Sciences.

NCAR is supported by the National Science Foundation. I wish to thank R. Milliff and C. Wikle for their analysis of the third-order structure function in the tropical atmospheric boundary layer data.

is, the atmosphere over the tropical ocean is convecting, it is not strongly stratified, and being at the equator, rotational effects should be minimal.

In a manner similar to the atmospheric boundary layer, in classical Rayleigh-Bénard convection between two flat plates a $-5/3$ horizontal kinetic energy spectrum was found numerically [K]. In that work, the observation was explained as a three-dimensional forward cascade, but the large horizontal scales over which a $-5/3$ spectrum is obeyed brings up the question of whether this could also be related to a two-dimensional backward cascade of energy. Again, no traditional mechanism for two-dimensionality exists.

There are thus three flows showing $-5/3$ spectra that are much wider than they are deep and for which the traditional forwards cascade mechanism would be difficult to apply. This paper will examine the structure function properties of the simulated flow to gain insight into what might be the origin of these $-5/3$ spectra. The paper will be organized as follows. First there will be a discussion of the properties of the structure functions and the mechanisms that have been proposed for suppressing the third direction in geophysical flows. Then there will be a detailed examination of the structure functions for the numerical simulations of convection in a wide, flat box at several vertical levels.

The conclusions will be similar to Lindborg's observations for the stratosphere. That is, there exists a regime where $S_3(r)$ is roughly linear and positive, but neither $S_2^T(r)$ nor $S_3(r)$ are consistent with two-dimensional predictions based upon $S_2^L(r)$. How this might relate to the atmospheric boundary layer measurements [T] will be discussed.

1. Two-dimensional relations.

The p -th order longitudinal structure function is the correlation

$$S_p^L(r) = \overline{(\vec{u}(\vec{x} + \vec{r}) - \vec{u}(\vec{x}))^p} \quad (1.1)$$

where $r = |\vec{r}|$, \vec{u} and \vec{r} are in the same direction and the average is over all \vec{x} . The transverse structure functions $S_p^T(r)$ are obtained when \vec{u} is perpendicular to \vec{r} . The second-order longitudinal structure function $S_2(r) = S_2^L(r)$ is related to the one-dimensional energy spectrum such that where

$$E_{11}(k) = \frac{1}{2} u_1^2(k) = C_1 |\Pi_u| k^{-5/3} \quad (1.2)$$

then

$$S_2^L(r) = S_2 = C_1 |\Pi_u| r^{2/3} \quad (1.3)$$

where C_1 is the one-dimensional Kolmogorov constant and $|\Pi_u|$ is the energy cascade rate. For a three-dimensional forward energy cascade, $|\Pi_u|$ is the energy dissipation rate. For both two and three dimensional flows, C_1 must be determined experimentally. The relationship for the third-order structure function S_3 for an ideal three-dimensional forward energy cascade, known as Kolmogorov's $4/5$ law [M, G], is

$$S_3(r) = -\frac{4}{5} \epsilon r \quad (1.4)$$

That is negative and linear.

What Lindborg [O] suggests is that there should be a similar relationship for S_3 for the backward two-dimensional energy cascade that is positive and linear

$$S_3(r) = \frac{3}{2} |\Pi_u| r \quad (1.5)$$

where the $3/2$ coefficient comes from simulations [S] and spectral closure calculations [H].

Both the 2D and 3D relationships are linear, but one is negative and the other is positive. Furthermore, if there is a $-5/3$ spectrum and if linear, positive $S_3(r)$ were due to a back cascade of two-dimensional turbulence, then from our knowledge of two-dimensional turbulence and $S_2^L(r)$, $|\Pi_u|$ can be determined and the magnitude of $S_3(r)$ could be predicted. What newer stratospheric data shows [O] is that $S_3(r)$ is positive and plausibly linear, but has the wrong magnitude if it is a result of a backwards cascade in two-dimensional turbulence.

The test using second order structure functions relies upon the following isotropy relation for isotropic D -dimensional turbulence,

$$S_2^T = S_2^L + (r/(D-1)) \frac{d}{dr} S_2^L \quad (1.6)$$

For an $r^{2/3}$ regime, in two dimensions this reduces to $S_2^T = (5/3)S_2^L$ and in three dimensions to $S_2^T = (4/3)S_2^L$. The stratospheric observations show instead that $S_2^T \approx S_2^L$.

In order to invoke two-dimensional arguments for fundamentally three-dimensional systems, some dynamical mechanism for suppressing the effects of the third dimension must be invoked. The objective is to develop a justification for balanced models such as quasi-geostrophy, where the fundamental motion is two-dimensional and any remaining three dimensional effects gradually disappear as the strength of the confining dynamical mechanism is increased. Three mechanisms have been proposed. Stratification, rotation, and thin domains. In the convective boundary layer near the equator the existing arguments for two-dimensionality by stratification [F, P] and rotation [B, E, C] do not apply. The third mechanism, thin domains, might apply since the boundary layer is capped by large-scale subsidence, but the current analysis [R, A] only applies only to thin periodic domains, which is not found in the atmosphere. For the stratosphere, another suggestion [U] is that a $-5/3$ regime could be due to gravity wave saturation.

There could be many mechanisms that yield $-5/3$ and the particular power law could just represent how nearly singular structures of the correct dimensionality and power law scale near their cusp to give $-5/3$. In the language of multi-fractals, these determining parameters would be the Hausdorff dimension and the Lifshitz condition for the nearly singular structures. If one wants to claim that a particular $-5/3$ spectral regime is due to an inverse energy cascade, some additional test besides the spectral shape is necessary. The claim is that examination of the second $S_2(r)$ and third order $S_3(r)$ structure functions could provide such tests [O].

2. Flat numerical convection

The numerical data set in this study is a simulation of classical Rayleigh-Bénard convection between two plates with periodic sidewalls and a large aspect ratio (width over height) in both horizontal directions of $6 : 6 : 1$ [K]. The original purpose of this simulation was to test some of the scaling proposals for boundary

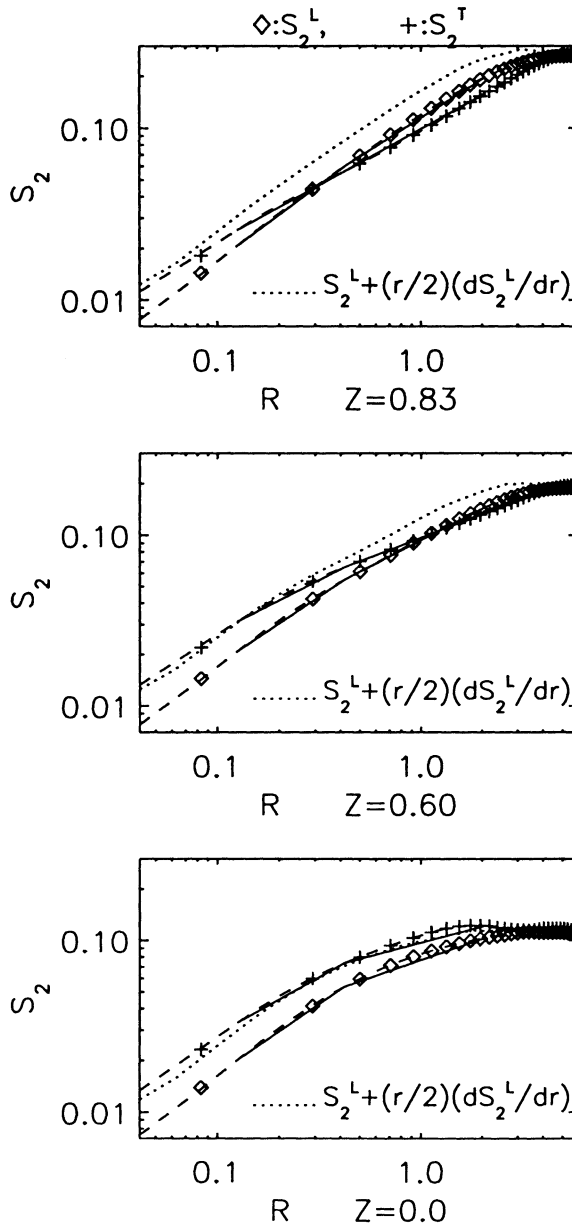


FIGURE 1. Comparison of longitudinal and transverse second order structure functions at three heights in Rayleigh-Bénard convection at $Ra = 2 \times 10^7$. The three heights represent the top of the boundary layer $Z = 0.83$, roughly 1/2 the way to the center $Z = 0.6$, and the center $Z = 0$. Shown are $S_2^L(r)$, $S_2^T(r)$ and the 3D prediction for $S_2^T(r)$ based upon $S_2^L(r)$. Here, the smallest $\Delta r = 0.04$ and only every 4th point starting at $r = 0.08$ is shown with a symbol. Near the wall ($Z=0.83$) $S_2^T(r) \approx S_2^L(r)$ for all except the smallest r . As one moves into the interior, the 3D prediction covers a larger range of r , until in the center the 3D prediction is satisfied for all r .

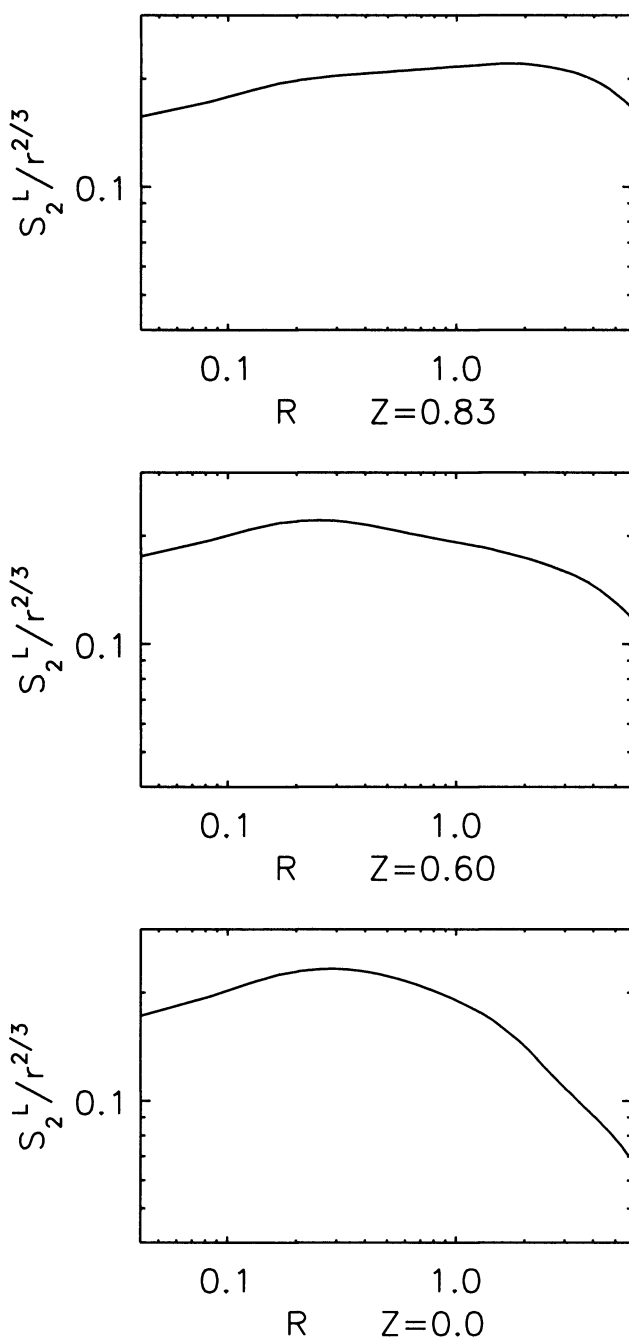


FIGURE 2. $S_2^L(r)/r^{2/3}$ at three heights for the same data as in Fig. 1. Although the 3D relation between S_2^L and S_2^L is true for all r only in the center, the strongest $r^{2/3}$ regime in S_2^L is found at $Z = 0.83$, at the top of the boundary layer.

layers associated with the $\beta_T = 2/7$ law for the normalized heat flux or Nusselt number as a function of the Rayleigh number $Nu \sim Ra^{2/7}$. Unlike most of the experiments and simulations for this problem, a large aspect ratio was chosen so as to be closer to the linear theory, to test how universal the $2/7$ law was, and to be closer to geophysical convection. Along with a detailed discussion of issues such as resolution, the spectrum was shown to be close to $-5/3$ and was related to a three-dimensional forward cascade of energy. The evidence that was given for a three-dimensional cascade was consistency with the experimental and numerical evidence [I] that says that when there is a three-dimensional energy cascade that the normalized enstrophy stretching rate

$$S_{\omega\epsilon\omega} = C \frac{\omega_i e_{ij} \omega_j}{(\epsilon/\nu)^{3/2}} \approx 0.5 \quad . \quad (2.1)$$

This term is cubic, as is $S_3(r)$, and is related to the $r \rightarrow 0$ limit of $S_3(r)$.

The present use for this data set will be to investigate the behavior of $S_2^L(r)$, $S_2^T(r)$ and $S_3(r)$ for a situation that clearly obeys none of the assumptions associated with constraining a three-dimensional flow to be two-dimensional turbulence, but still exhibits a $-5/3$ spectrum at scales too large for there to be a forwards cascade of turbulence. $S_2^L(r)$ and $S_2^T(r)$ will be discussed first, going from small to large scales at different heights. For reference, Fig. 3 shows the time-averaged temperature and horizontal velocity fluctuation profiles. Mean velocity profiles are not shown because they are insignificant. The averages are over several convective timescales [K] and the equivalent distances from the top and bottom walls have been averaged. If the wall is at $Z = 1$ and the center is at $Z = 0$, three heights away from the wall will be shown. These are chosen to be at the top of the boundary layer ($Z = 0.83$), on the central side of the boundary layer ($Z = 0.60$) and in the center ($Z = 0$).

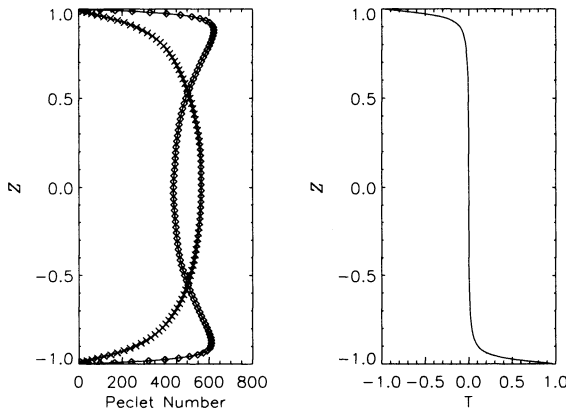


FIGURE 3. \diamond : mean u'^2 , \times : mean w'^2 , and T profiles for the flat box calculation.

As $r \rightarrow 0$, $S_2(r) \sim r^2$ is expected. Rather, at all Z , the dominant trend up to $r = 0.4$ in the log-log plots in Fig. 1 is slightly less than linear behavior, although linear plots show a slight trend towards quadratic r^2 over the first 3 mesh points

(to $r = .125$). The transverse structure function does obey the 3D isotropy relation (1.6) at the smallest scale for all three Z and for all r at the center. Therefore the smallest scales at all Z obey the three-dimensional isotropy relations. One might speculate that near the wall that it is three dimensional only at the smallest scales because the third direction of motion is only the height of the boundary layer.

At $Z = 0.83$, not only does $S_2^T(r)$ not obey either the 2D or 3D isotropy relationships for most r , but instead $S_2^T(r) \approx S_2^L(r)$.

Fig. 2 shows $S_2^L(r)/r^{2/3}$ to determine over what r for different Z that $S_2^L(r) \sim r^{2/3}$. Although the spectral equivalent of $r^{2/3}$, $k^{-5/3}$ is found when spectra are averaged over the entire flow [K], $r^{2/3}$ appears for at most a few points at moderate r for $Z = 0$ and $Z = 0.60$. Only for $Z = 0.83$ and within the boundary layer (not plotted) is $S_2^L(r) \sim r^{2/3}$ approximately obeyed at large scales.

Therefore, the boundary layer behavior of S_2^L is similar to the stratospheric results [O] in that where $S_2^L(r) \sim r^{2/3}$ when $S_2^T(r) \approx S_2^L(r)$.

Figure 4 plots the third-order longitudinal structure function for the same three Z levels. Recall 3D would be negative and 2D would be positive. The comparison of $S_2^T(r)$ and $S_2^L(r)$ suggested that at the smallest scales for all three Z in Fig. 1 the flow is 3D, so one might expect $S_3(r) < 0$ at these scales. For the center $Z = 0$, one might expect 3D behavior for all r , although there would still be a question of how this could occur for $r > 2$, the height of the domain.

What is observed in Fig. 4 is that, as predicted, $S_3(r) < 0$ for $r < 1$ for all Z . Furthermore for $Z = 0$ for $r < 0.5$, $S_3(r) = -4/5\epsilon r$. For $Z = 0.6$ this is also approximately true. The evidence for a three-dimensional cascade at small scales, obtained by comparing $S_2^T(r)$ and $S_3(r)$ to $S_2^L(r)$, is consistent with the observation that $S_{\omega e \omega} \approx 0.5$.

To find evidence for two-dimensional behavior, we want to look where $S_3(r) > 0$. For all three Z , this is observed. But only for $Z = 0.83$ is there a long range of r for which there is a strongly linear and positive increase from a negative value. The positive rate of increase at $Z = 0.83$ and 0.6 is much greater than the prediction based upon the value of Π_u predicted using $S_2^L(r)$. In this sense, the boundary layer results are again similar to the stratospheric data [O].

The conclusion is that in or just above the boundary layer, at the large scales, $S_2^T(r)$ and $S_3(r)$ have similar relationships to $S_2^L(r)$ as in the stratospheric measurements.

3. Discussion

The primary result of this paper is that in convective simulations in a wide domain without a mean flow, relationships for second and third-order structure functions at larger scales within the boundary layer do not match the expectations of either two or three dimensional dynamics. Instead, as in stratospheric observations $S_2^T(r) \approx S_2^L(r)$ and $S_3(r)$ is increasing linearly and becomes positive over the regime where a $-5/3$ spectrum, or $S_2 \sim r^{2/3}$, is observed. The maximum of $S_3(r)/S_2^{3/2} \approx 0.2$, which is not as large as the stratospheric value of about 0.5, but is still much larger than the value expected for a 2D backward cascade of energy of about 0.03.

Despite the absence of truly two-dimensional dynamics in this simulation, a linearly, increasing $S_3(r)$ suggests some sort of upscale energy transfer mechanism. One might ask whether this could be calculated directly. With periodic boundary

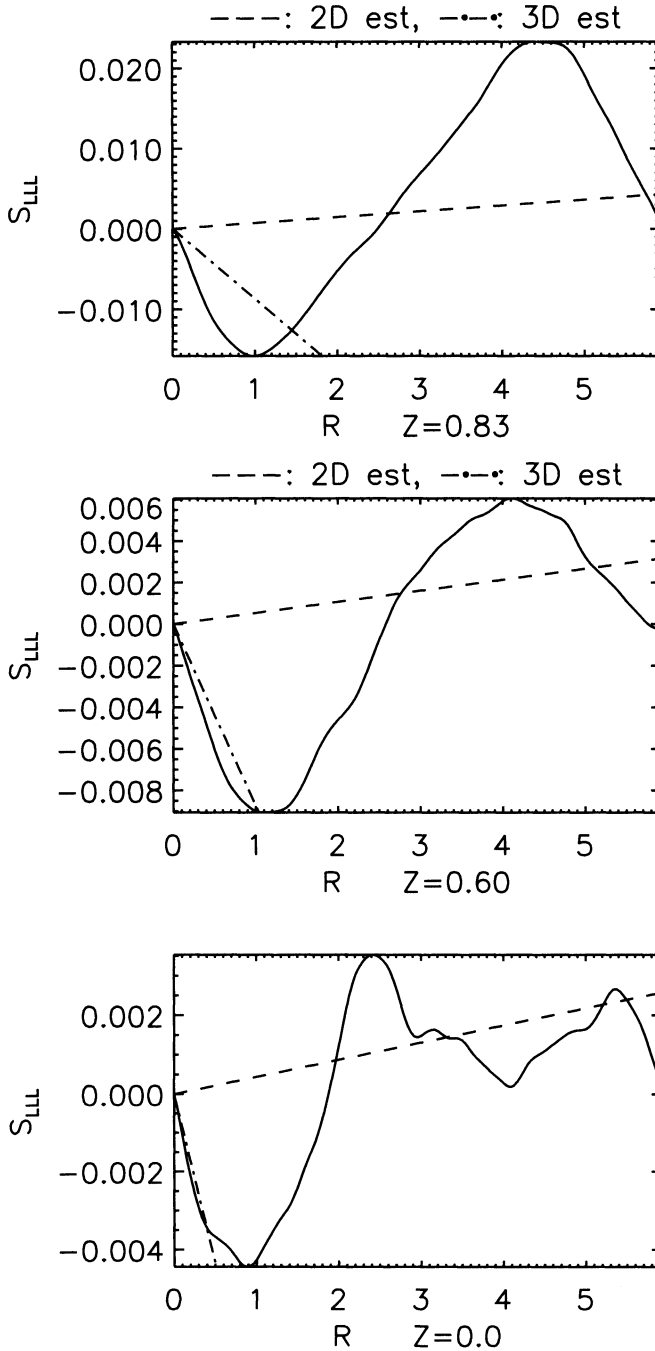


FIGURE 4. Comparison of 3rd order structure functions at three heights in Rayleigh-Bénard convection at $Ra = 2 \times 10^7$. Dot-dashed is the $-\frac{4}{5}\epsilon r$ 3D prediction. The dashed line is the $\frac{3}{2}|\Pi_u|r$ 2D prediction.

conditions where a Fourier decomposition can be applied, or if the velocity had free-slip boundary conditions in any direction so that sine and cosine transforms could be used, we know how to calculate the spectral energy transfer directly [J]. However, for no-slip boundary conditions and Chebyshev transforms in the vertical, this is not feasible.

While the existence of an upscale transfer mechanism is only suggested by the behavior of $S_3(r)$, from visualizations of this flow there is a good reason to believe that such a mechanism exists. Visualizations of this convective flow show fine-scale motions superimposed upon a large-scale pattern [K]. In the boundary layer, the fine-scale motions consist of numerous small plumes whose vertical velocity is small and locally induced. Since the only source of energy is the heating which is originally transferred from the walls to the fluid through these small-scale plumes, the small-scale boundary layer motions are probably the energy source for the large-scale pattern. Therefore, the energy in the small-scale plumes must be transferred upscale to the large-scale flow.

For an upscale energy transfer to occur in the boundary layer, and for direct transfer to small-scales and dissipation through a three-dimensional cascade to be suppressed, it still seems that there should be some source of two-dimensionality. This new source of two-dimensionality could not be either stratification or rotation. Possible sources of two-dimensionality in the boundary layer could be sweeping and strong horizontal velocities along the boundary layer due to the large-scale flow, or the large-scale motion pushing into one boundary that originates with the small-scale convective generated on the opposite boundary. This needs to be investigated further.

What initially inspired this analysis of the flat, convection calculations was the observation of an extensive $-5/3$ spectrum in the atmospheric boundary layer over the tropical ocean. While the mechanism behind the $-5/3$ spectrum and a linearly increasing S_3 in these simulations has not been identified, a reasonable question to ask would be whether similar analysis of the atmospheric boundary layer data [T] between 1 km and 1000 km might yield similar results. This analysis has been performed and as in the stratospheric observations and the simulations, for the second order structure functions are nearly equal, $S_2^T(r) \approx S_2^L(r)$. However, while $|S_3(r)/S_2^{L3/2}| \gg 0.03$, the sign of S_3 is not constant at large scales and furthermore depends on whether the meridional or zonal direction is taken.

In order to understand the origin of these effects in the atmospheric boundary layer, simulations must address several significant differences between the large-scale flow in the tropical atmosphere and the flat convection simulations. The primary difference is that there is a large zonal (east-west) flow over the tropical ocean and this could affect the nature of the boundary layer flow [D]. Therefore, a convection simulation with a large-scale flow would be necessary. Some preliminary analysis of a convection simulation with a large-scale flow, but in an aspect ratio 1 box (a cube, not flat) [L], shows that the sign of S_3 in the boundary layer can be affected by the presence of a mean shear at the top of the boundary layer.

References

- [A] A. Babin, A. Mahalov & B. Nicolaenko, *Global regularity of 3D rotating Navier-Stokes equations for resonant domains*. Indiana Univ. Math. Journal **48** (1999), 1133-1176.
- [B] P. Bartello, O. Metais & M. Lesieur *Coherent structures in rotating three-dimensional turbulence*. J. Fluid Mech. **273** (1995), 1-29.

- [C] P. Bartello *Geophysical and Astrophysical Convection*. Gordon and Breach Scientific Publishers (ed. R.M.Kerr and P.A.Fox), Potential vorticity, resonance, and dissipation in rotating convective turbulence., (2000), pp. 309–340.
- [D] C. Deser *Diagnosis of the surface momentum balance over the tropical Pacific ocean..* J. Climate **6** (1993), 64–74.
- [E] P. Embid & A. Majda *Averaging over fast gravity waves for geophysical flows with arbitrary potential vorticity..* Comm. Part. Diff. Eqs. **21** (1996), 619–; P. Embid & A. Majda *Low Froude number limiting dynamics for stably stratified flow with small or fixed Rossby numbers..* Geophys. Astro. Fluid Dyn. **to appear** (1997), –.
- [F] A. M. Fincham, T. Maxworthy & G. R. Spedding, *Energy dissipation and vortex structure in freely decaying, stratified grid turbulence..* Dyn. Atmos. Oceans **23** (1996), 155–169.
- [G] U. Frisch *Turbulence: The legacy of A.N. Kolmogorov..* Cambridge Univ. Press, 296 pp..
- [H] J. R. Herring *Theory of two-dimensional anisotropic turbulence..* J. Atmos. Sci. **32** (1975), 2254–2271.
- [I] R. M. Kerr *Higher-order derivative correlations and the alignment of small-scale structures in isotropic numerical turbulence..* J. Fluid Mech. **153** (1985), 31–58.
- [J] R. M. Kerr *Velocity, scalar and transfer spectra in numerical turbulence..* J. Fluid Mech. **211** (1990), 309–332.
- [K] R. M. Kerr *Simulation of High Rayleigh Number Convection..* J. Fluid Mech. **310** (1996), 139–179.
- [L] R. M. Kerr 2001 *The energy budget in Rayleigh-Bénard convection* Phys. Rev. Lett. (in press).
- [M] A. Kolmogorov *Dissipation of energy in locally isotropic turbulence..* Dokl. Akad. Nauk. SSSR **31** (1941), 99–101. (reprinted in *The Royal Society, London***434**, 9–13.)
- [N] D. K. Lilly *Two-dimensional turbulence generated by energy sources at two scales..* J. Atmos. Sci. **46** (1989), 2026–2030.
- [O] E. Lindborg *Can the atmospheric kinetic energy spectrum be explained by two-dimensional turbulence?.* J. Fluid Mech. **388** (1999), 259–288.
- [P] J. R. Herring & O. Metais, . J. Fluid Mech. **202** (1990), 97–115.; O. Metais & J.R. Herring, . J. Fluid Mech. **202** (1990), 117–148.
- [Q] G. D. Nastrom, K. S. Gage & W. H. Jasperson *Kinetic energy spectrum of large- and mesoscale atmospheric processes..* Nature **310** (1984), 36–; . J. Atmos. Sci. **36** (1979), 1950–1954.
- [R] L. M. Smith, J. Chasnov & F. Waleffe *Crossover from two- to three-dimensional turbulence..* Phys. Rev. Lett. **77** (1996), 2467–2470.
- [S] L. M. Smith & V. Yakhot, *Bose condensation and small-scale structure generation in a random force driven 2D turbulence..* Phys. Rev. Lett. **71** (1993), 352–355.
- [T] C. K. Wikle, R. F. Milliff & W. G. Large *Surface wind variability on spatial scales from 1 to 1000 km observed during TOGA COARE..* J. Atmos. Sci. **56** (1999), 2222–2231.
- [U] T. E. VanZandt *A universal spectrum of buoyancy wave in the atmosphere..* Geophys. Res. Lett. **9** (1982), 575–578.

NATIONAL CENTER FOR ATMOSPHERIC RESEARCH, BOULDER, COLORADO, 80307-3000

Current address: Department of Atmospheric Sciences, University of Arizona, Tucson, Arizona 85721-0081

E-mail address: kerr@atmo.arizona.edu

The Forced Inviscid Burgers Equation as a Model for Nonlinear Interactions among Dispersive Waves

Fernando Menzaque, Rodolfo R. Rosales, Esteban G. Tabak, and Cristina
V. Turner

ABSTRACT. The forced inviscid Burgers equation is studied as a model for the nonlinear interaction of dispersive waves. The dependent variable $u(x, t)$ is thought of as an arbitrary mode or set of modes of a general system, and the force is tuned to mimic the effects of other modes, which may be either near or far from resonance with u .

When the force is unimodal, a family of exact traveling waves fully describes the asymptotic behavior of the system. When the force is multimodal, with the frequencies of the various modes close to each other, the asymptotic solution is quasi-stationary, punctuated by faster intermittent events. The existence of these “storms” may have significant implications for energy transfer among modes in more general systems.

1. Introduction.

The nonlinear interaction among a large set of waves is a complex phenomenon. Among the issues involved are the tuning (or detuning) of sets of modes, depending of how far they are from perfect resonance. This issue is subtle though, since it depends on the time scale of the nonlinear interaction, which itself depends on the degree of tuning among modes.

A particularly subtle issue appears in the transition from discrete to continuous sets of waves: how to add up the effects of very many near resonances. Do they interfere destructively or constructively? In most theories of continuous spectra, the former is usually assumed, to the point of suppressing altogether the leading order effect of resonances, pushing them to higher orders than those appearing in discrete systems.

In systems that are both forced and damped, statistical cascades often appear, carrying energy among scales, from the scales associated with the forcing, to those where dissipation transfers the energy out of the system. When the scales of forcing

2000 *Mathematics Subject Classification.* Primary 35Q35.

Key words and phrases. Breaking waves, near-resonance, Burgers equation.

The work of Menzaque was partially supported by SECYT-UNC 98-275/00 CONICOR 465/99.

The work of Rosales was partially supported by NSF grant DMS-9802713.

The work of Tabak was partially supported by NSF grant DMS-9701751.

The work of Turner was partially supported by SECYT-UNC 98-275/00 CONICOR 465/99.

and dissipation are many decades apart, the intermediate scales span the so-called *turbulent inertial range*, where the system behaves effectively as a Hamiltonian one, and self-similar energy spectra are often observed. Attempts to understand the nature of these self-similar cascades gave rise to the theory of *Wave Turbulence* (e.g., see [1], [2], [5], and [11].) In order to close a very complex system, this theory makes a number of assumptions, such as phase decorrelation among the various modes, scale separation between linear and nonlinear phenomena, and infinite size of the system, giving rise to a continuum of modes. These assumptions are hard to justify, and the theory, despite its beauty, has a number of problems, such as internal inconsistencies — as when it predicts upscale energy fluxes— and a mixed record of agreement with observations and numerical simulations (e.g., see [3] and [6].)

In this work, we consider a simple model, where surrogates for resonances and near resonances can easily be built in: the forced inviscid Burgers equation,

$$(1.1.1) \quad u_t + \left(\frac{1}{2} u^2 \right)_x = f(x, t),$$

where $f = f(x, t)$ is some smooth forcing, and both f and u are periodic (of period 2π) in space and have vanishing mean.

Here the dependent variable $u(x, t)$ represents a mode (or set of modes) with linear frequency $\omega = 0$ (as follows from the zero mean condition.) On the other hand, the externally imposed force $f(x, t)$ represents other modes of the system, which (depending on the scale of their dependence on time) will be close or far from resonance with u .

A vastly different reduced model for resonant energy transfer among modes was developed in [7]. It is interesting to note that both models, though completely different in conception and structure, contain intermittent regimes — these are strong in [7] and much milder in the present work. It appears that intermittence is a natural occurrence in models of turbulent energy cascades.

The nonlinear term in (1.1.1) has two combined functions: to transfer energy among the various (Fourier) components of u , and to dissipate energy at shocks. Thus the “inertial cascade” and the system’s dissipation are modeled by a single term. This not only implies a big gain in simplicity, but could also in fact be a rather realistic model for fluid systems, where dissipation is almost invariably associated with some form of wave breaking.

The model equation (1.1.1) above is a simplified version of the equations describing the interaction among resonant triads involving a nondispersive wave [8]. The simplification consists in freezing the two dispersive members of the triad, thus making them act as a prescribed force on $u(x, t)$.

It would seem that a more general model, with a non-zero linear frequency ω , is the one given by the equation

$$(1.1.2) \quad u_t + \omega u_x + \left(\frac{1}{2} u^2 \right)_x = f,$$

which is equivalent to considering non-zero mean solutions to (1.1.1) — i.e.: write $u = \omega + \tilde{u}$, where ω is the mean¹ of u . However, this last equation can be reduced to equation (1.1.1) by the introduction of the new independent variable $x' = x - \omega t$.

A resonant force $f(x, t)$ in (1.1.1) is one that does not depend on time; a near-resonant one, on the other hand, evolves slowly. More precisely, a near resonance should be modeled by

$$(1.1.3) \quad u_t + \left(\frac{1}{2} u^2 \right)_x = \epsilon^2 f(x, \epsilon t),$$

where $0 < \epsilon \ll 1$ measures the degree of non-resonance. The reason for the factor ϵ^2 in front of the forcing term follows from considering a quasi-steady approximation to the solution to (1.1.3), namely:

$$u(x) \approx \epsilon \sqrt{2 \int^x f(s, \epsilon t) ds}.$$

This is not quite right, but indicates the correct result: a (slow) forcing of size $O(\epsilon^2)$ in (1.1.3), generally induces a response of amplitude ϵ in u . This shows that any force stronger than ϵ^2 in (1.1.3) would render its own modulation irrelevant, since the induced nonlinearity would act on a much faster time scale than that of the modulation.

Interestingly, the ϵ 's above in (1.1.3) can be scaled out by a simple transformation: let $\tilde{t} = \epsilon t$, and write $u = \epsilon \tilde{u}$. Then, in terms of these new variables, (1.1.3) becomes (1.1.1). Hence **near-resonances in (1.1.1) cannot be defined as an asymptotic limit involving a small parameter ϵ** ; if there is a distinction between near resonant and nonresonant forces, it will have to arise from a finite bifurcation in the behavior of the solutions to (1.1.1) — which in fact occurs, as we will show in section 2.

The fact pointed out in the prior paragraph is part of a more general property of equation (1.1.1), namely: it is a canonical system. For consider a model involving a more general nonlinearity, such as:

$$(1.1.4) \quad u_t + N(u)_x = f(x, t),$$

where, generically, we can assume that $N(u) = O(u^2)$ (since any linear term can be eliminated by a Galilean transformation.) Now consider a weakly nonlinear, nearly resonant, situation, where u is small, the force is small and the time scales are slow. Thus, take: $u = \epsilon \tilde{u}$, $f = \epsilon^2 \tilde{f}$, with the time dependence via $\tilde{t} = \epsilon t$, and $0 < \epsilon \ll 1$. Then it is easy to see that, in terms of \tilde{u} , \tilde{f} , \tilde{t} , and x , the leading order system is (1.1.1) — except for, possibly, a constant other than 1/2 in front of the nonlinear term. In fact, this reduction of the equations to (1.1.1) will occur even if we have a system (i.e.: u in (1.1.4) is a vector), as long as there is a single force (lined up with a single mode of the system.)

¹Note that, **because f has a vanishing mean, the mean of the solutions to (1.1.1) is a constant.**

Notation and general properties.

It is well known that the inviscid Burgers equation develops shocks. Throughout this work, we shall use the following notation for various quantities at shocks:

- A plus (respectively, minus) superscript (or subscript) stands for the value of the corresponding variable ahead (respectively, behind) of the shock.
- Brackets stand for the jump across the shock of the enclosed expression. Specifically: the value ahead (to the right) minus the value behind (to the left). Thus, for example:

$$[u] = u^+ - u^- ,$$

is the jump in u across the shock.

Shocks obey the following rules:

- The shock speed is given by the **Rankine-Hugoniot jump conditions**, namely:

$$S = \bar{u} = \frac{1}{2} (u^+ + u^-) .$$

where \bar{u} is the arithmetic mean of u at the shock, and S is the shock speed.

- Shocks must satisfy an **entropy condition**, which for (1.1.1) states that u should jump down across shocks, i.e.:

$$[u] \leq 0 .$$

Finally, equation (1.1.1) has an energy

$$E(t) = \int_0^{2\pi} \frac{1}{2} u^2(x, t) dx ,$$

which satisfies the equation

$$(1.1.5) \quad \frac{dE}{dt} - \sum \left(\frac{1}{12} [u]^3 \right) = \int_0^{2\pi} u(x, t) f(x, t) dx ,$$

where the sum on the left is over all the shocks in the solution. This sum accounts for the dissipation of energy at the shocks, and the right hand side represents the work by the forcing term f . That is, we have:

$$E_d = - \sum \left(\frac{1}{12} [u]^3 \right) > 0 \quad \text{and} \quad W_f = \int_0^{2\pi} u f dx ,$$

where E_d is the energy dissipated per unit time and W_f is the work done by the forcing.

Contents and plan of the paper.

Much of the contents of this paper will be concerned with the study of the energetic interplay between the dissipation at shocks and the work done by the forcing function. Our interest lies mostly in situations where $E(t)$ is close to stationary, so that the work done by the forcing and the dissipation at shocks approximately balance each other. Either of these then represents the amount of energy flowing through the system, and the dependence of this flux on the characteristics of $f(x, t)$ will teach us something about the nature of the energy exchange among near resonant modes.

This paper is organized as follows. In section 2, we study the asymptotic, long time solutions to (1.1.1), under unimodal forces $f(x, t) = f(x - \omega t)$. This long time asymptotic behavior is given by a family of exact traveling wave solutions. We

observe an interesting bifurcation between near resonant and nonresonant behavior, taking place at a critical value of ω (that depends on the form and size of the forcing f .) If $|\omega|$ is smaller than this critical value, the forcing does work on the solution; if $|\omega|$ is bigger, on the other hand, it does not. We sketch proofs for these results, which use a novel combination of Hamiltonian formalism with breaking waves.

In section 3, we study two-modal forcings, in which $f = g_1(x) + g_2(x - \omega t)$. For large values of ω , g_2 has vanishingly small effect on the asymptotic, long time, solution $u(x, t)$. For small values of ω , on the other hand, quasi-steady solutions $u = u(x, \tau)$ arise (where τ is a slow time), punctuated by intermittent events (which we call “storms”) with enhanced rates of energy exchange between the forcing and the solution, at an intermediate time scale (slow, but faster than τ .) The abnormal rate of energy exchange during storms hints at the possibility that nonlinear wave systems may have regimes where the energy exchange among modes is strongly influenced by fast, intermittent events, involving coherent phase and amplitude adjustments of the full spectrum, rather than by the slow evolution of individual resonant sets.

We can make the statement in the prior paragraph more precise, or at least more suggestive, as follows: We show in section 3 that the extra (integrated) energy exchange during a storm scales like $\omega^{-1/2}$. In our model, however, there are only a finite number of storms per period, which itself scales like ω^{-1} . Thus the average energetic impact of the storms is of order $\omega^{1/2}$, vanishing with ω . Yet, in more complex systems, there are a number of likely scenarios (involving, for instance, random or pseudo-random events), in which the number of storms per period will increase as the period does, at least as $\omega^{-1/2}$. When this is the case, the energetic impact of storms will be at least comparable to that of the quasi-steady parts of the solution, and we will find ourselves at the threshold of an energy cascade driven by intermittent events.

2. A Single Forcing Mode.

In this section, we consider the equation

$$(2.2.1) \quad u_t + \left(\frac{1}{2} u^2 \right)_x = f(x - \omega t),$$

where $f = f(z)$ and $u = u(x, t)$ are 2π -periodic in space, real functions, with zero mean. Here we will assume that f is a sufficiently smooth function, and that the initial conditions are such that the solution is, at all times, piece-wise smooth, with a finite number of shocks.

As explained earlier, the forcing term is resonant if $\omega = 0$, near resonant if ω is small and far from resonant if ω is big. Notice though that, from the argument above equation (1.1.4) in the introduction, we cannot give an asymptotic meaning to this distinction through the introduction of a small parameter, since this equation is the canonical model for the description of systems with a fluid-like nonlinearity, weakly forced near resonance. Interestingly, as we shall see below (remark 2.2), the equation admits exact solutions where there is a sharp transition between resonant and non-resonant behavior, at a critical value of the frequency $\omega = \omega_c$.

Below we consider a special set of solutions to equation (2.2.1), given by traveling waves. These solutions not only can be written exactly in closed form, but have special significance — since they describe the long time behavior for the general

solution. In subsections 2.2 and 2.3 we show –numerically and analytically– that the solution to the initial value problem for (2.2.1) above converges to the traveling wave solution as $t \rightarrow \infty$, which is generically unique.

2.1. Exact Traveling Solutions. We shall seek traveling wave solutions to (2.2.1) of the form

$$(2.2.2) \quad u(x, t) = G(z),$$

where $z = x - \omega t$. Then equation (2.2.1) becomes the O.D.E.

$$(2.2.3) \quad \frac{d}{dz} \left(\frac{1}{2}(G - \omega)^2 \right) = f(z).$$

This has the solutions

$$(2.2.4) \quad G(z) = \omega \pm \sqrt{2F(z)},$$

where $F = \int^z f(s)ds$, with the constant of integration selected so that $F(z) \geq 0$ everywhere.

$$(2.2.5) \quad \text{We shall define } F_{cr} \text{ to be the choice of } F \text{ such that } \min(F_{cr}) = 0.$$

These solutions can be used to produce exact (periodic) traveling wave solutions that both have a vanishing mean, and satisfy the entropy condition when they include shocks. Generically, three distinct cases can arise, with the **solution determined uniquely by ω if F_{cr} has a single minimum per period.** See figure 1 for illustrative examples.

Case 1. If F is strictly larger than F_{cr} , then the solution must be smooth — with only one sign selected in (2.2.4). This follows because the entropy condition for shocks only allows downward jumps; thus only jumps from the positive to the negative root are allowed. Given that G must be periodic, no shocks are possible when $\min(F) > 0$. In this case, the sign of the square root, and the value of the integration constant defining F , follow upon imposing the condition that the mean of $u = G$ must vanish.

We can write the solutions corresponding to this case as two families of solutions (one for $\omega > 0$ and another one for $\omega < 0$) parameterized by a single parameter $\delta > 0$, as follows:

$$(2.2.6) \quad u = \omega - \text{sign}(\omega) \sqrt{2(\delta + F_{cr}(z))},$$

$$(2.2.7) \quad \omega = \pm \frac{1}{2\pi} \int_0^{2\pi} \sqrt{2(\delta + F_{cr}(z))} dz,$$

where $z = x - \omega t$ and F (as defined above) is given by $F(z) = \delta + F_{cr}(z)$. These formulas show that

For $|\omega| > \omega_{cr}$, where ω_{cr} is defined below in equation (2.2.8), the traveling wave solutions are as smooth as F_{cr} . Furthermore, they are uniquely determined by the function f and the frequency ω .

Notice that **uniqueness, in this case where $|\omega| > \omega_{cr}$, does not depend at all on F_{cr} having a single minimum per period.**

Case 2. For values of $|\omega|$ smaller than

$$(2.2.8) \quad \omega_{cr} = \frac{1}{2\pi} \int_0^{2\pi} \sqrt{2F_{cr}(z)} dz,$$

no F can be found that will satisfy the zero mean condition. When this is the case, one must take $F = F_{cr}$, and allow the solution to jump between the positive and the negative roots. Then the solution can return (smoothly) to the positive root through the point where $F_{cr} = 0$, which is generically unique. In this case, the tunable parameter that one can use to adjust the solution so that $u = G$ has a vanishing mean, is the position $z = s$ of the shock (notice that, because u at the shock jumps from $u_- = \omega + \sqrt{2F_{cr}(s)}$ to $u_+ = \omega - \sqrt{2F_{cr}(s)}$, the shock's velocity is ω — therefore it remains fixed in the frame moving with the traveling wave.)

To be specific, **assume that F_{cr} has a single minimum per period**, and let $z = z_m$ be the position of the minimum. Then the equation for the shock position $z = s$ is given by:

$$(2.2.9) \quad \omega = -\frac{1}{2\pi} \int_{z_m}^s \sqrt{2F_{cr}(z)} dz + \frac{1}{2\pi} \int_s^{z_m+2\pi} \sqrt{2F_{cr}(z)} dz,$$

where $z_m \leq s < z_m + 2\pi$. Since the right hand side in this equation is a (strictly) monotone decreasing function of s (with the values ω_{cr} for $s = z_m$, and $-\omega_{cr}$ for $s = z_m + 2\pi$) there is a unique solution for s . Thus **the traveling wave solution is unique**.

REMARK 2.1. Notice that, in the (non-generic) case when F_{cr} has more than one minimum per period, uniqueness is lost when $\omega \leq \omega_{cr}$. This is because, in this case, there is more than one possible point where a smooth switch from the negative to the positive root in equation (2.2.4) can occur. This feature is at the root of the behavior reported in section 3 for the response to forcings with more than one frequency.

Case 3. In the limiting case when $\omega = \omega_{cr}$, the shock and the smooth transition from negative to positive root coalesce and disappear, leaving a corner moving at speed ω_{cr} as the only singularity of the solution.

Simple example; single harmonic forcing.

Consider the case with a single sinusoidal forcing: $f = f(z) = \sin z$ (with $z = x - \omega t$), for which $F_{cr} = 1 - \cos(z) = 2 \sin^2(z/2)$. Then the critical value for ω is given by:

$$(2.2.10) \quad \omega_{cr} = \frac{1}{2\pi} \int_0^{2\pi} 2 \left| \sin\left(\frac{z}{2}\right) \right| dz = \frac{4}{\pi},$$

and we have:

Solutions with shocks for the simple example: These occur for $|\omega| < \omega_{cr} = 4/\pi$, and have the form

$$(2.2.11) \quad u(x, t) = G(z) = \omega \pm 2 \left| \sin\left(\frac{x - \omega t}{2}\right) \right|.$$

In each period (say $0 \leq z < 2\pi$) there is a (continuous) switch from the minus to the plus sign as z crosses $z = 0$, and a switch from the plus to the minus sign (across a shock) at some position $z = s$. The position of this (single) shock follows from the zero mean condition (i.e.: equation (2.2.9) for this simple example)

$$(2.2.12) \quad 0 = \int_0^s G^+(z) dz + \int_s^{2\pi} G^-(z) dz = 2\pi\omega - 8 \cos(s/2),$$

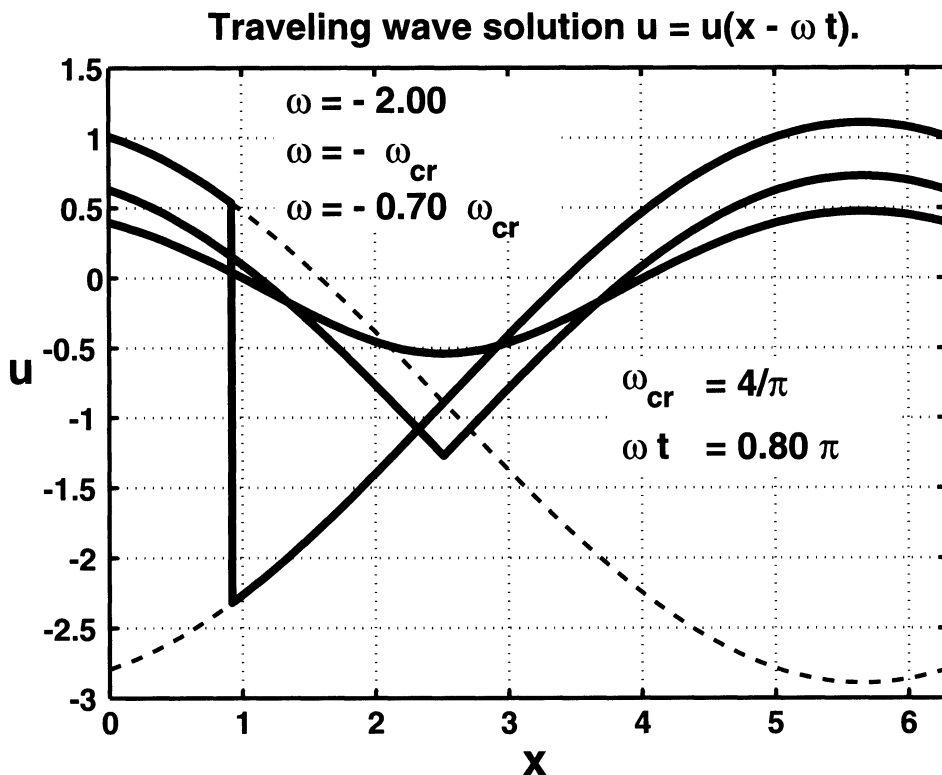


FIGURE 1. Examples of traveling waves for the equation $u_t + (0.5 u^2)_x = \sin(x - \omega t)$. Three solutions are shown:

- (a) Smooth solution, for $\omega = -2.00 < -\omega_{cr}$.
- (b) Critical solution, with a corner, for $\omega = -\omega_{cr} = -4/\pi$.
- (c) Solution with a shock, for $\omega = -0.70 \omega_{cr}$.

The "envelope" for the solution with a shock, given by $u = \omega \pm \sqrt{2F}$ is also shown (dashed line.) In each case, the solution is plotted for a time t such that $\omega t = 0.80 \pi$.

where $G^+ = \omega + 2 |\sin(z/2)|$, and $G^- = \omega - 2 |\sin(z/2)|$. Thus

$$(2.2.13) \quad s = 2 \arccos \left(\frac{\pi \omega}{4} \right), \quad \text{with } 0 \leq s < 2\pi.$$

We can also compute the work per unit time W_f done by the external force f on this exact solution. Since this work must agree with the energy E_d dissipated at

the shock (given that the solution is steady), we have:

$$(2.2.14) \quad W_f = \int_0^{2\pi} f u \, dx = E_d = -\frac{1}{12} [u]^3 = \frac{16}{3} \left\{ 1 - \left(\frac{\pi\omega}{4} \right)^2 \right\}^{3/2}.$$

A plot of the work done by the forcing is shown in figure 2.

REMARK 2.2. For $|\omega| \geq \omega_{cr} = 4/\pi$ the solutions have no shocks (see below) and there is no energy dissipation, nor work done by the forcing (i.e.: the solution is orthogonal to the forcing.) This indicates a rather abrupt change in behavior, which we interpret as the **boundary of resonance**. That is, a **sharp transition from resonant behavior** (with the forcing continuously pumping energy into the system, which is then dissipated by a shock) **to non-resonant behavior** (with no work done by the forcing) occurs at $|\omega| = \omega_{cr}$. It is easy to see that this behavior is general, and not particular to the special harmonic forcing of this simple example. It will occur for the traveling waves produced by any forcing of the form in equation (2.2.1). It is interesting to note that this behavior is analogous to a third order phase transition, with the collective behavior of the modes making up the solution switching from a dissipative configuration to a non-dissipative one.

Smooth solutions for the simple example: These occur for $|\omega| > \omega_{cr} = 4/\pi$, and have the form

$$(2.2.15) \quad u(x, t) = \omega \pm \sqrt{2(D - \cos(x - \omega t))},$$

where $D > 1$ and the sign of the square root follow from the condition on the mean:

$$\int_0^{2\pi} u(x, t) \, dx = 0.$$

It is actually easier to write ω as a function of D , as follows

$$(2.2.16) \quad \omega = \omega(D) = \pm \frac{1}{2\pi} \int_0^{2\pi} \sqrt{2(D - \cos z)} \, dz, \quad \text{where } D \geq 1.$$

This equation is the same as (2.2.7) for this simple example, with $D = 1 + \delta$.

Critical solutions for the simple example: These occur for $|\omega| = \omega_{cr} = 4/\pi$, and are given by:

$$(2.2.17) \quad u = \pm \left\{ \omega_{cr} - 2 \left| \sin \left(\frac{x \mp \omega_{cr} t}{2} \right) \right| \right\}.$$

2.2. Numerical Experiments. In subsection 2.3 we will show (analytically) that the solution to the general initial value problem for equation (2.2.1) converges asymptotically (for large times) to the traveling wave solution — at least in the case where the traveling wave solution is unique, i.e.: F_{cr} , as defined in (2.2.5), has a single minimum per period. In this section, we show the result of a numerical calculation illustrating the convergence process.

Numerical code: In both the calculations shown in this subsection, and those in section 3, we use a (second order in time) Strang [9] splitting technique, separating the equation into

$$u_t = f \quad \text{and} \quad u_t + \left(\frac{1}{2} u^2 \right)_x = 0.$$

Then we use a second order Runge–Kutta ODE solver for the first equation. For the second equation we use a second order Godunov [4] scheme, with the van Leer

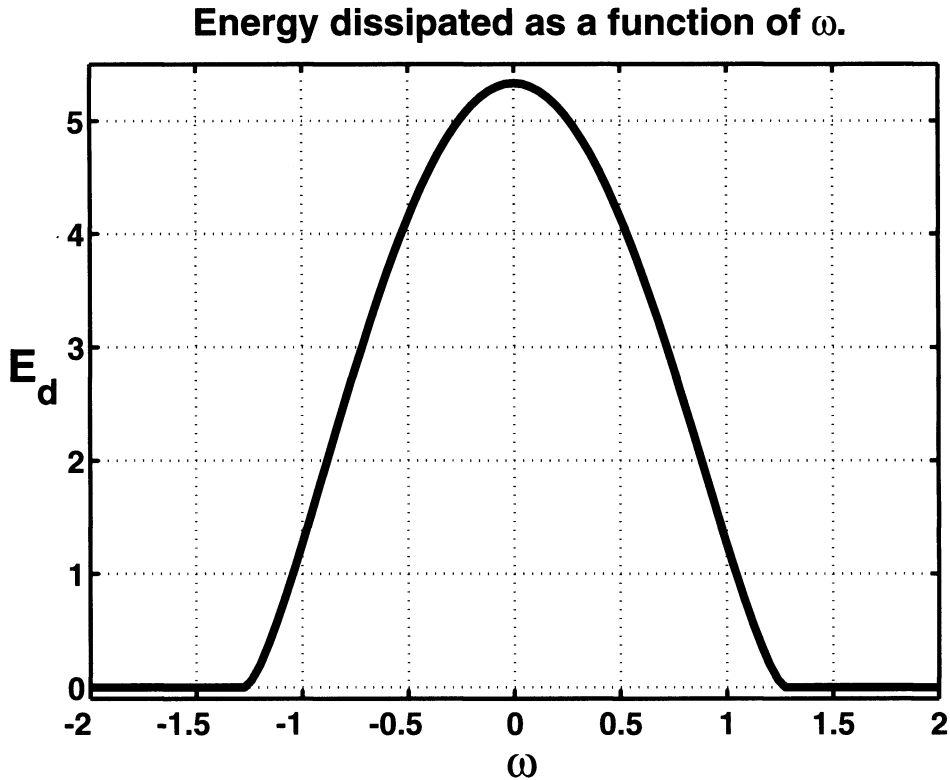


FIGURE 2. Energy dissipated (as a function of ω) by the traveling waves. The energy dissipated E_d (equal to the work W_f done by the external force f) for the equation $u_t + (0.5 u^2)_x = \sin(x - \omega t)$, is shown as a function of ω . Notice the sharp cutoff at $\omega = \pm \omega_{cr}$, beyond which no work is done by the force f . This result is general and does not depend on the particular forcing $\sin(x - \omega t)$ — it will occur for any forcing of the form $f = f(x - \omega t)$.

[10] monotonicity switches. This yields a fairly simple and robust shock capturing (second order, both in time and space) algorithm.

Example: Figure 3 shows an example of how a solution to equation (2.2.1) (with $f = \sin(x - \omega t)$ and “arbitrary” initial data) converges to a traveling wave as $t \rightarrow \infty$. Specifically, we take $\omega = 0.5 \omega_{cr}$ — where ω_{cr} is given in equation (2.2.10) — and $u(x, 0) = \sin(x)$.

The convergence to the traveling wave solution is done via the formation of shocks (only one in this case) that dissipate energy and force the solution to converge to its limiting shape. The arguments in subsection 2.3 give a more precise description of this process. Notice how fast the convergence is: the period in time of the forcing function is $T = 2\pi/\omega$, and (even though the initial condition is $O(1)$ away from

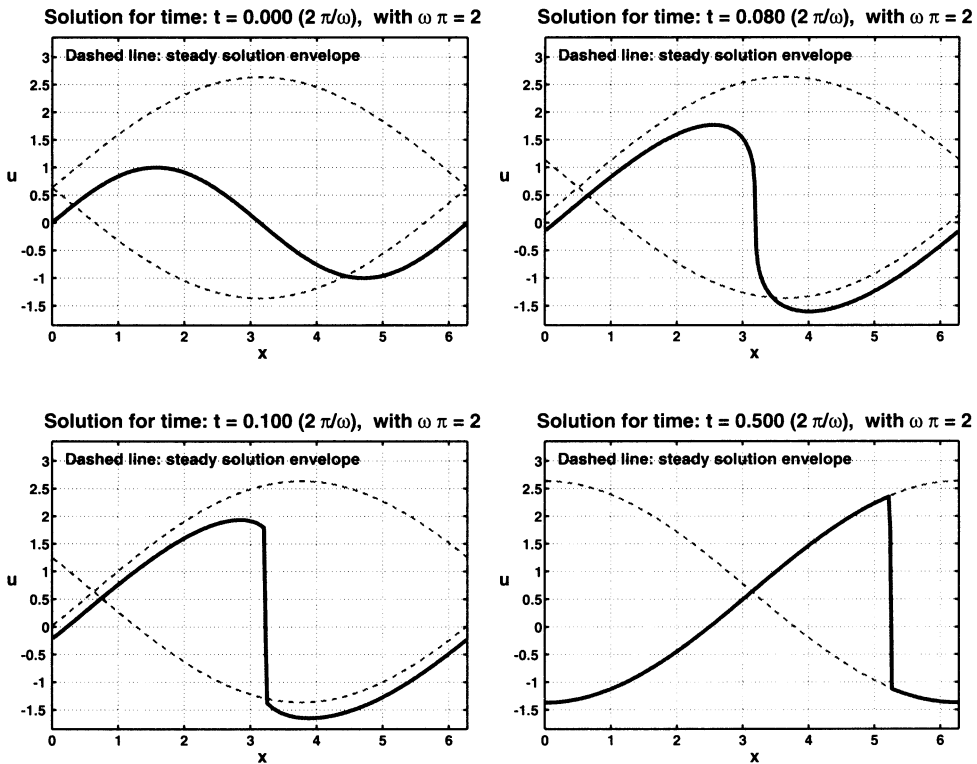


FIGURE 3. Forcing $f = \sin z$ in the equation, with $z = x - \omega t$ and $\omega = \omega_{cr}/2 = 2/\pi$. As $t \rightarrow \infty$ the solution converges to the traveling wave $u = \omega \pm 2 \sin(z/2)$, where the sign switch occurs at the shock position. The traveling wave has period $2\pi/\omega$ in time (same as the forcing.) From left to right and from top to bottom, we plot the solution and the "envelope" $\omega \pm 2 \sin(z/2)$ (dashed line) for the traveling wave: (a) Initial conditions for $t = 0$. (b) Time $t = 0.08 (2\pi/\omega)$, shortly before the formation of the shock. (c) Time $t = 0.10 (2\pi/\omega)$, shortly after the formation of the shock. (d) Time $t = 0.50 (2\pi/\omega)$, once the solution has converged to the traveling wave.

the traveling wave) by $t = T/2$ the solution is indistinguishable from the traveling wave.

2.3. Asymptotic behavior of the solutions. In this subsection, we show (analytically) that the exact solutions of subsection 2.1 yield the large time ($t \rightarrow \infty$) asymptotic behavior of the solutions to equation (2.2.1), for any initial data. First, we show that this result holds for $|\omega| > \omega_{cr}$, and initial data relatively close to the corresponding smooth exact solution. Next we present arguments for the case $|\omega| \leq \omega_{cr}$, and arbitrary initial data. The same type of reasoning that we use in

this second part can be used to show global convergence when $|\omega| > \omega_{cr}$, but we shall not carry out the details of such argument here.

The main mechanism involved in the convergence (as $t \rightarrow \infty$) to the traveling wave solution when $|\omega| \leq \omega_{cr}$ (see remark 2.5) is much more “efficient” than the mechanism involved in the case when $|\omega| > \omega_{cr}$. This is because the first mechanism involves $O(1)$ shocks at all times, while the second has shocks of vanishing amplitude as $t \rightarrow \infty$. The calculation displayed in figure 3 illustrates how efficient the mechanism in the case $|\omega| \leq \omega_{cr}$ is, as pointed out at the end of subsection 2.2. By contrast, in numerical calculations done for $|\omega| > \omega_{cr}$, we observed a very slow approach to the limiting behavior.

REMARK 2.3. We shall restrict our arguments to the case when F_{cr} , given by equation (2.2.5), has only two extremal points per period: a single zero, and a single maximum. The single zero condition guarantees a unique traveling wave solution. The single maximum condition is technical and simplifies the arguments — it is not really needed, as we point out later (see remark 2.6.)

When the single zero condition is not satisfied, so that the traveling wave solution for $|\omega| \leq \omega_{cr}$ is not unique, our numerical experiments still show convergence to a traveling wave as $t \rightarrow \infty$, which depends on the initial conditions. Actually, the arguments in this section for the case $|\omega| > \omega_{cr}$ do not depend on F_{cr} having a single zero, while the arguments for $|\omega| \leq \omega_{cr}$ indicate convergence to some traveling wave, even if it is not unique.

Case: $|\omega| > \omega_{cr}$. Local convergence to the smooth exact solution.

Preliminaries.

Let $u_{ex} = u_{ex}(z)$ (where $z = x - \omega t$) be the exact solution introduced in subsection 2.1 — see equations (2.2.6 – 2.2.7). Then equation (2.2.1) can be written in the form

$$(2.2.18) \quad v_t + \left(\frac{1}{2}v^2 - F \right)_z = 0,$$

where $v = v(z, t) = u - \omega$, and $F = F(z) = \frac{1}{2}(u_{ex} - \omega)^2$ is the function defined earlier in subsection 2.1. We note that

$$\min(F) > 0, \quad \frac{dF}{dz} = f,$$

and that v must be a 2π -periodic function of z , with $\text{Mean}(v) = -\omega$. Finally, let

$$v_{ex} = u_{ex} - \omega = -\text{sign}(\omega) \sqrt{2F(z)}$$

be the exact solution of equation (2.2.18) corresponding to u_{ex} — i.e.: the traveling wave. We shall now **assume that** $\omega < -\omega_{cr}$, since the case $\omega > \omega_{cr}$ can be obtained from the symmetry, in equation (2.2.1), given by: $\omega \rightarrow -\omega$, $u \rightarrow -u$, $f(z) \rightarrow -f(-z)$, and $x \rightarrow -x$. Then we can write

$$(2.2.19) \quad v_{ex}(z) = \sqrt{2F}.$$

The argument of convergence to the traveling wave solution as $t \rightarrow \infty$, in this $|\omega| > \omega_{cr}$ case, is divided in two parts. In part I we show that the initial data can be restricted so that the solution remains positive (and bounded away from zero) for all times, and that such solutions always break and develop shocks — with the

sole exception of the traveling wave (which has no shocks.) In part II we construct a (convex) Hamiltonian functional, which decreases for solutions with shocks, and is minimized by the traveling wave solution.

Case: $|\omega| > \omega_{cr}$. **Part I.**

Along characteristics, equation (2.2.18) takes the form

$$(2.2.20) \quad \frac{dz}{dt} = v, \quad \text{and} \quad \frac{dv}{dt} = \frac{dF}{dz}(z).$$

This can be written in the Hamiltonian form

$$(2.2.21) \quad \frac{dz}{dt} = \frac{\partial h}{\partial v}, \quad \text{and} \quad \frac{dv}{dt} = -\frac{\partial h}{\partial z},$$

with Hamiltonian

$$(2.2.22) \quad h = h(z, v) = \frac{1}{2}v^2 - F(z).$$

This is the standard Hamiltonian for a particle in a one-dimensional potential field $V(z) = -F(z)$. We shall use this Hamiltonian formulation to derive the following two results:

$$(2.2.23) \quad \left\{ \begin{array}{l} \text{I. We can constrain the initial data } v = v(z, 0), \text{ so that } v = \\ v(z, t) \text{ remains positive (and bounded away from zero) for all} \\ \text{times } t \geq 0. \\ \text{II. Smooth initial data } v = v(z, 0), \text{ different from } v_{ex} \text{ (but con-} \\ \text{strained so that } v > 0 \text{ for all } t \geq 0), \text{ necessarily develop} \\ \text{shocks.} \end{array} \right.$$

These two results will be used in Part II to show convergence of v to v_{ex} , as $t \rightarrow \infty$.

For both results, we turn to the phase plane for the Hamiltonian system (2.2.21) (see figure 4). To prove the first result, notice that, because the characteristic evolution is given by this Hamiltonian system, if the initial data are such that $v(z, 0) \geq v_0(z)$ (where $v = v_0(z) > 0$ is an orbit for the system), then $v \geq v_0$ for all times (hence it remains positive and bounded away from zero.) This is easy to see from the example in figure 4. Therefore, we shall (from now on) **assume that v is greater than zero.**

To prove the second result, notice that, because here we consider only values of v greater than zero, all centers are excluded, and the trajectories of (2.2.21) are all open in the plane (though, of course, closed in the cylinder defined by the 2π periodicity of z). Several such trajectories, corresponding to different values of h , are displayed in figure 4. The point we need to make is that any two such trajectories always have different periods, for the period $T(h)$ is given by

$$T(h) = \frac{1}{\sqrt{2}} \int_0^{2\pi} \frac{dz}{\sqrt{h + F(z)}},$$

so that

$$\frac{dT}{dh} = -\frac{1}{2\sqrt{2}} \int_0^{2\pi} \frac{dz}{(h + F(z))^{3/2}} < 0.$$

This means that any two characteristics with different values of h necessarily meet (the one with the shorter period catches up to the other one.) Therefore a shock must form (since two values of h at a single position z imply two distinct values of v .)

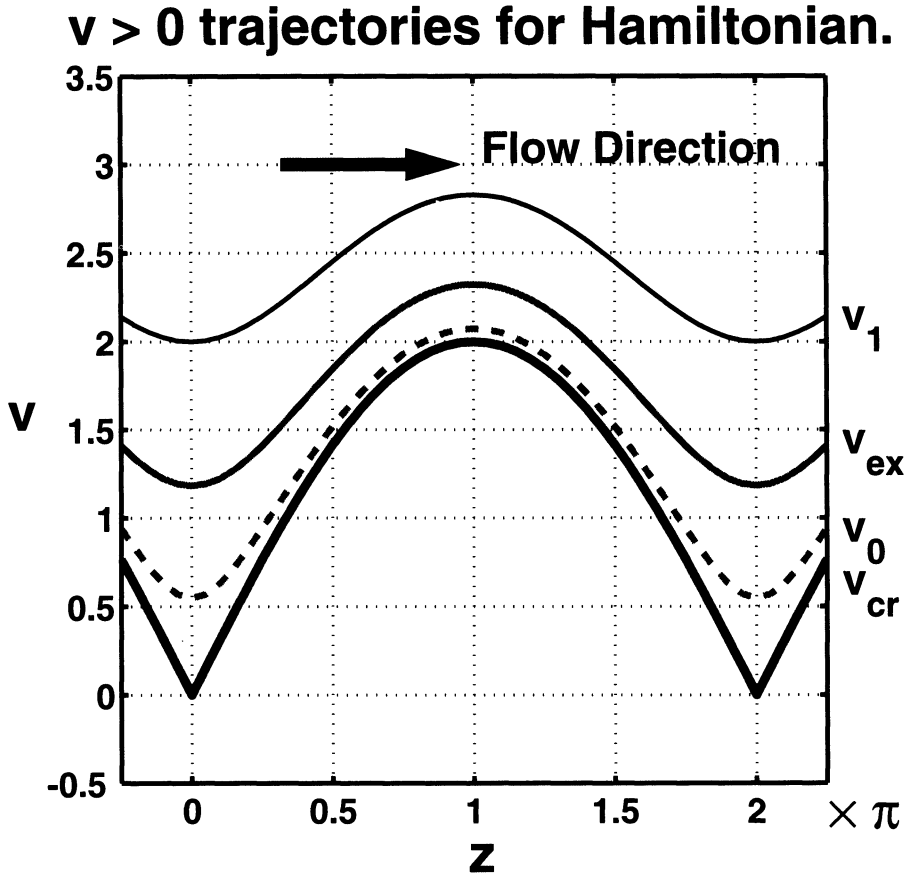


FIGURE 4. Unbounded, $v > 0$ trajectories, for the system with Hamiltonian $h = \frac{1}{2}v^2 + \cos z - 1$. These occur for $v > v_{cr}(z) = \sqrt{2F_{cr}(z)}$, where $F_{cr} = (1 - \cos z)$. (a) Critical trajectory v_{cr} , connecting the saddle points (thick solid line.) (b) A trajectory v_0 , slightly above critical (dashed line.) (c) Two typical trajectories v_{ex} and v_1 (solid lines.) For the P.D.E. $v_t + (\frac{1}{2}v^2 + \cos z)_z = 0$, whose characteristic form is given by this Hamiltonian system, it is clear that: If the initial data for v are above a curve such as v_0 , then the solution remains above v_0 for all times.

Hence the only case in which characteristics do not cross is the one in which the initial data lies on a contour line $h = \text{constant}$. However, such initial data is given by

$$v(z, 0) = \sqrt{2(F + h)},$$

and the condition that the average of v be equal to $-\omega$ implies that $h = 0$, i.e., $v = v_{ex}$. Hence all initial data different from v_{ex} develop shocks.

Case: $|\omega| > \omega_{cr}$. Part II.

For the second part of the argument, we need a different Hamiltonian structure, the one given by the integral

$$(2.2.24) \quad H = \int_0^{2\pi} \left(\frac{1}{6} v^3 - v F \right) dz .$$

Using H , equation (2.2.18) can be written in the Hamiltonian form

$$(2.2.25) \quad v_t = - \frac{\partial}{\partial z} \left(\frac{\delta H}{\delta v} \right) .$$

We notice that H is convex for positive functions $v = v(z)$ (of mean equal to $-\omega$), with a unique absolute minimum given by $v(z) = \sqrt{2F} = v_{ex}$. Furthermore, because of the Hamiltonian structure (2.2.25), H is conserved while $v(z, t)$ remains smooth. On the other hand (see equation (2.2.27) below) H is dissipated at shocks. Hence, since all v 's different from v_{ex} develop shocks (as shown earlier in part I), H cannot settle down until it reaches its minimum value, corresponding to $v = v_{ex}$.

We show now that H decreases when there are shocks. We have:

$$(2.2.26) \quad \frac{dH}{dt} = \sum_{j=1}^N \left(\int_{s_j}^{s_{j+1}} \frac{\delta H}{\delta v} v_t dz - \frac{ds_j}{dt} \left[\frac{1}{6} v^3 - v F \right]_j \right) ,$$

where we have assumed that there are N shocks per period (for some N), with $s_j = s_j(t)$ the position of the j -th shock, $s_1 < s_2 < \dots < s_N$, and $s_{N+1} = s_1 + 2\pi$ (from the periodicity.) Substitute now into this last expression v_t from (2.2.25), and the Rankine-Hugoniot jump conditions for the shock velocities:

$$\frac{ds_j}{dt} = \frac{1}{2} (v_j^- + v_j^+) ,$$

where v_j^\pm denote the values of v ahead and behind the shock. Then

$$\begin{aligned} \frac{dH}{dt} &= - \frac{1}{2} \sum_{j=1}^N \left(\int_{s_j}^{s_{j+1}} \left(\left(\frac{\delta H}{\delta v} \right)^2 \right)_z dz + (v_j^- + v_j^+) \left[\frac{1}{6} v^3 - v F \right]_j \right) \\ &= \frac{1}{2} \sum_{j=1}^N \left(\left[\left(\frac{\delta H}{\delta v} \right)^2 - \frac{1}{6} v^4 + v^2 F \right]_j - \frac{1}{6} v_j^- v_j^+ [v^2]_j \right) \\ &= \frac{1}{12} \sum_{j=1}^N \left(\left[\frac{1}{2} v^4 \right]_j - v_j^- v_j^+ [v^2]_j \right) \\ (2.2.27) \quad &= \frac{1}{24} \sum_{j=1}^N [v]_j^2 [v^2]_j < 0 . \end{aligned}$$

The last inequality follows from the entropy condition, that states that v (therefore v^2 , since $v > 0$) decreases from left to right across shocks. This concludes the argument of convergence to the traveling wave in the case $|\omega| > \omega_{cr}$.

Case: $|\omega| \leq \omega_{cr}$. *Global convergence to the non-smooth traveling waves.*

Here we shall consider the case with $|\omega| \leq \omega_{cr}$ (when $F = F_{cr} \geq 0$) and general initial data. We shall require that the zero value of F_{cr} be achieved only once per period in z (for concreteness take this value to be $z = 0$.) The reason for this restriction — which is satisfied by generic functions $F_{cr} = F_{cr}(z)$ — is that: when F_{cr} vanishes at more than one position per period, there is more than one steady solution to equation (2.2.1), and this renders the issue of ultimate convergence to one of the steady solutions more cumbersome. We shall also require that F_{cr} have only one local maximum per period, since this simplifies the arguments (but this condition is not strictly needed, as we point out later, in remark 2.6.)

We shall use the following functional G , a modification of the Hamiltonian H in (2.2.24):

$$(2.2.28) \quad G = \int_0^{2\pi} \left(\frac{1}{6}|v|^3 - |v| F_{cr} \right) dz.$$

Notice that G is minimized pointwise by functions of the form $v(z) = \pm\sqrt{2F_{cr}} = \pm|v_{ex}|$. In particular, the exact steady solution to equation (2.2.1) is the only minimizer of G consistent with the entropy condition for shocks (v never jumps upwards) and with the requirement that its average be equal to $-\omega$. This follows from the condition that there is only one point where $F_{cr}(z) = 0$, which is the only place at which $v(z)$ can switch smoothly from negative to positive. Hence there can be only one shock switching $v(z)$ back to negative. The position of this shock is then determined by the condition that $v(z) + \omega$ must have a vanishing mean. In particular, for $|\omega| = \omega_{cr}$, this last condition determines that the sign of $v(z)$ never changes, and the only singularity of the solution is a corner at the position of the zero of F_{cr} (with no shocks.)

The argument for convergence to v_{ex} will be based on the fact that, after an initial transient period, G necessarily decays when $v(z, 0) \neq v_{ex}$.

Unlike H , G is not a Hamiltonian, yet it allows us to write equation (2.2.18) in the following pseudo-Hamiltonian form (valid wherever $v \neq 0$):

$$(2.2.29) \quad v_t = -\sigma \frac{\partial}{\partial z} \left(\frac{\delta G}{\delta v} \right),$$

where

$$\sigma = \text{sign}(v) = \begin{cases} 1 & \text{if } v > 0. \\ 0 & \text{if } v = 0. \\ -1 & \text{if } v < 0. \end{cases}$$

Assume now that there are N shocks per period, with $s_j = s_j(t)$ the location of the j -th shock, where $s_1 < s_2 < \dots < s_N$ and $s_{N+1} = s_1$ (periodicity.) Furthermore, introduce the functions $h = h(z, t) = \frac{1}{2}v^2 - F_{cr}$ and $g = \frac{1}{6}|v|^3 - |v|F_{cr}$. We notice that

$$v_t = -h_z, \quad \frac{\partial g}{\partial v} = \sigma h, \quad \text{and} \quad \sigma h h_z = \left(\frac{1}{8}\sigma v^4 - \frac{1}{2}\sigma v^2 F_{cr} \right)_z + \frac{1}{2}\sigma (F_{cr}^2)_z,$$

where the last equation applies away from the shocks (in particular, it is valid when σ is discontinuous due to a zero of v .)

Using the formulas above, we write below an equation for the time evolution of the functional G . Here, as usual, the brackets stand for the jump — front to back — of the enclosed quantities across the shock, the superscripts \pm are used to indicate values immediately ahead and behind a shock, and a subscript j indicates evaluation at the j -th shock. We have:

$$\begin{aligned}
 \frac{dG}{dt} &= - \sum_{j=1}^N \left(\int_{s_j}^{s_{j+1}} \sigma h h_z dz + \frac{ds_j}{dt} [g]_j \right) \\
 &= - \frac{1}{2} \int_0^{2\pi} \sigma (F_{cr}^2)_z dz - \frac{1}{2} \sum_{j=1}^N [\sigma F_{cr}^2]_j + \\
 &\quad \sum_{j=1}^N \left(\left[\frac{1}{8} \sigma v^4 - \frac{1}{2} \sigma v^2 F_{cr} + \frac{1}{2} \sigma F_{cr}^2 \right]_j - \frac{1}{2} (v_j^+ + v_j^-) [g]_j \right) \\
 &= - \frac{1}{2} \int_0^{2\pi} \sigma (F_{cr}^2)_z dz - \frac{1}{2} \sum_{j=1}^N [\sigma F_{cr}^2]_j + \\
 &\quad \sum_{j=1}^N \left(\left[\sigma \left(\frac{1}{24} v^4 + \frac{1}{2} F_{cr}^2 \right) \right] - v^+ v^- \left[\sigma \left(\frac{1}{12} v^2 - \frac{1}{2} F_{cr} \right) \right] \right)_j \\
 (2.2.30) \quad &= S_1 + S_2 + S_3 + S_4,
 \end{aligned}$$

where

$$\begin{aligned}
 S_1 &= - \frac{1}{2} \int_0^{2\pi} \sigma (F_{cr}^2)_z dz - \frac{1}{2} \sum_{j=1}^N [\sigma F_{cr}^2]_j, \\
 S_2 &= \frac{1}{24} \sum_{\text{local}} (\sigma [v]^2 [v^2])_j, \\
 S_3 &= \sum_{\text{transonic}} \left\{ v^+ v^- \left(\frac{1}{6} \overline{v^2} - F_{cr} \right) - \left(\frac{1}{12} \overline{v^4} + F_{cr}^2 \right) \right\}_j,
 \end{aligned}$$

and

$$S_4 = \sum_{\text{to zero}} \left[\sigma \left(\frac{1}{24} v^4 + \frac{1}{2} F_{cr}^2 \right) \right]_j.$$

Here the sum S_2 is carried over all the “local” shocks (where v^+ and v^- both have the same sign: $v^+ v^- > 0$), the sum S_3 is carried over all the “transonic” shocks (where $v^+ < 0 < v^-$), the sum S_4 is carried over all shocks where either v^+ or v^- vanishes, and the overbars indicate the average value across the shock of the appropriate quantity.

REMARK 2.4. Notice that only the values of F_{cr} at the points where σ jumps, and are not shocks, contribute to S_1 (that is, the places where v changes sign “smoothly”.) This is because only the points where σ jumps contribute to the integral that appears in the definition of S_1 , with the sum in the same definition subtracting any contributions that arise at the shocks. In fact, (generically) we can

write:

$$S_1 = \frac{1}{2} \left(\sum_{n \in D} [\sigma F_{cr}^2]_n - \sum_{j=1}^N [\sigma F_{cr}^2]_j \right) = \frac{1}{2} \left(\sum_{n \in D} ([\sigma] F_{cr}^2)_n - \sum_{j=1}^N ([\sigma] F_{cr}^2)_j \right),$$

where D is a set of indexes for all the positions across which v switches sign.

It should be clear that

- S_1 does not have a definite sign, since its overall sign depends on the relative sizes of F_{cr}^2 at the places where v crosses zero upwards (from negative to positive, so that $[\sigma] = 2$) versus the places where it crosses zero downwards, so that $[\sigma] = -2$.
- On the other hand, S_2 is **always non-positive, vanishing only when there are no local shocks** (as it is the case for the exact traveling wave solution v_{ex} .) This follows because, when $v \geq 0$ on both sides of the shock: $\sigma = 1$ and the entropy condition yields $[v^2] < 0$. Similarly, when $\sigma = -1$, the entropy condition yields $[v^2] > 0$.
- S_3 is **always non-positive, vanishing only when $v^- = \sqrt{2F_{cr}}$ and $v^+ = -\sqrt{2F_{cr}}$ (or there are no transonic shocks)**, as it is the case for the exact solution v_{ex} . We shall only need this last result for $v^- \geq \sqrt{2F_{cr}}$ and $v^+ \leq -\sqrt{2F_{cr}}$. In this case, the proof is quite straightforward, since S_3 can be rewritten in the form:

$$S_3 = - \sum_{\text{trans}} \left((a + b + 2\sqrt{F_{cr}}) (a^2 + b^2) \sqrt{F_{cr}} + \frac{1}{6} (a^4 + b^4 + 2ab^3 + 2a^3b) \right) \leq 0,$$

$$\text{where } a = \frac{v^-}{\sqrt{2}} - \sqrt{F_{cr}} \geq 0, \text{ and } b = - \left(\frac{v^+}{\sqrt{2}} + \sqrt{F_{cr}} \right) \geq 0.$$

- Finally, S_4 is **always non-positive, vanishing only when there are no shocks in the summation**. This is obvious, since each shock in the summation contributes an amount $\sigma_+ A_+ - \sigma_- A_-$, where $A_{\pm} > 0$ and either: $\sigma_+ = -1$ and $\sigma_- = 0$, or $\sigma_+ = 0$ and $\sigma_- = 1$.

The argument for convergence to the exact traveling wave solution v_{ex} (in this $\omega \leq \omega_{cr}$ case) will be based on the phase plane for the characteristic equations (2.2.21), corresponding to the Hamiltonian h in equation (2.2.22) — with $F = F_{cr}$. This phase plane, displayed again in figure 5, is partitioned into two domains by the separatrix $h = 0$: a **domain D containing the closed periodic orbits, and its complement $C(D)$ containing the open orbits**. We will assume here that F_{cr} has a single maximum per period, so that there is a single critical point in D (a center), with all the other orbits being closed and periodic (as shown in figure 5.) We shall first argue that:

(2.2.31) **The asymptotic behavior for the solutions to (2.2.18) cannot include any values in the interior of the domain D .**

The argument for this goes as follows:

- A.** First we note that: any two characteristics starting in the interior of D cross in finite time — even if they lie on the same contour line (orbit) for h . Furthermore: for any compact subdomain D_c of D , the crossing time can be uniformly bounded.

Bounded trajectories for Hamiltonian.

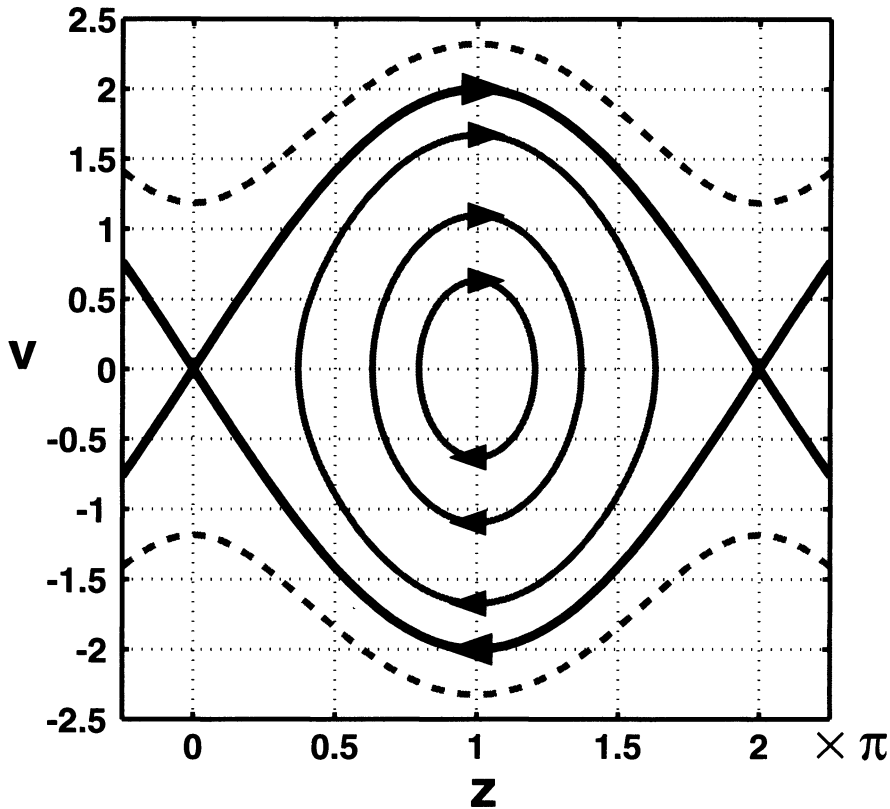


FIGURE 5. Bounded trajectories for the system with Hamiltonian $h = \frac{1}{2}v^2 + \cos z - 1$. These occur in the region $|v| < v_{cr}(z) = \sqrt{2F_{cr}(z)}$, where $F_{cr} = (1 - \cos z)$. The critical trajectories $v = \pm v_{cr}$, connecting the saddle points (thick solid lines), and several periodic orbits are shown, in addition to a couple of unbounded orbits (dashed lines.) Notice that, in cases where F_{cr} has more than one maximum per period, the bounded orbit region will be more complicated, with saddles and more than one center in it.

This is obvious from figure 5. A formal argument goes as follows: let $z_1 = z_1(t)$ and $z_2 = z_2(t)$ be any two characteristics corresponding to orbits in D , with z_1 the characteristic for the outermost orbit in D . Then both z_1 and z_2 are periodic functions of time, with $\max(z_1) \geq \max(z_2)$ and $\min(z_1) \leq \min(z_2)$. Then $\max(z_1 - z_2) \geq \max(z_1) - \max(z_2) \geq 0$ and $\min(z_1 - z_2) \leq \min(z_1) - \min(z_2) \leq 0$, so that $z_1 - z_2$ must vanish somewhere, in fact: at least twice per z_1 -period. Thus: a uniform bound on the crossing time

is given by the maximum of the orbit periods over the domain D_c . Note that: **as the distance of D_c to the boundary of D gets smaller, the crossing time bound goes to infinity**, because the orbit period grows unboundedly as the separatrix is approached (points on the separatrix take an infinite amount of time to move from saddle to saddle, while points inside D move on orbits with a finite period.)

- B.** Using the result in **A**, we argue now that any part of the initial data contained in a compact subdomain D_c of D , ceases to influence the solution after a finite time. This second result, of course, implies (2.2.31).

The argument here is as follows: suppose that there is a characteristic connecting some point on the solution with the initial data in D_c . But then some neighborhood of this point (possibly one-sided, if the point is on a shock), connected with the initial data in D_c by a “beam” of characteristics, would exist. This is clearly impossible after the time given by the uniform bound in part **A** above.

REMARK 2.5. The result in (2.2.31) is easy to visualize graphically (in terms of what the solution to equation (2.2.18) does as it evolves in time) using the phase plane for the evolution by characteristics in (2.2.21) — as illustrated by figure 5. It should be clear that any part of the solution curve $v = v(z, t)$, contained inside D , will be stretched and “rolled up” (as illustrated in figure 6) by the characteristic evolution along the periodic orbits of the Hamiltonian

$$h = \frac{1}{2}v^2 - F_{cr}(z).$$

This then leads to multiple values, which are resolved by the introduction of shocks. It should also be clear that, in this roll up process, the upper and lower envelope of the solution curve will be produced by stretching of the parts of the initial solution curve closest to the separatrix $h = 0$ — which will then be the only parts surviving after the shocks are introduced.

Notice that this is a very “efficient” mechanism for the elimination of any part of the solution curve contained inside D . For all practical purposes, the elimination of these parts occurs in a finite time (roughly, the average “turn over” time for the periodic orbits), after which only a very small region near the critical level curve $h = 0$ can remain. As pointed out at the beginning of this subsection, this fact is clearly seen in the numerical experiments we conducted, with a very sharp separation of scales between the convergence times for the cases $|\omega| > \omega_{cr}$ and $|\omega| < \omega_{cr}$.

REMARK 2.6. The prior remark should make it clear that the key element in obtaining (2.2.31) is the existence of a small “band” of periodic orbits in D close to the separatrix. This is true even if F_{cr} has more than two extremal points per period — leading to several critical points inside D , not just a center.

The critical thing to notice is that the initial data solution curve $v = v(z, 0)$ must be periodic in z . Thus it is clear that: if any part of this curve ends up inside D , then there will have to be points where the curve crosses the separatrix $h = 0$ going from $C(D)$ to D , and vice versa. The neighborhoods of these points inside D will then be stretched and “rolled up” by the characteristic evolution, so that they are the only surviving parts of the initial data inside D (after some time.) Hence (2.2.31) will be valid, even if F_{cr} has many extremal points.

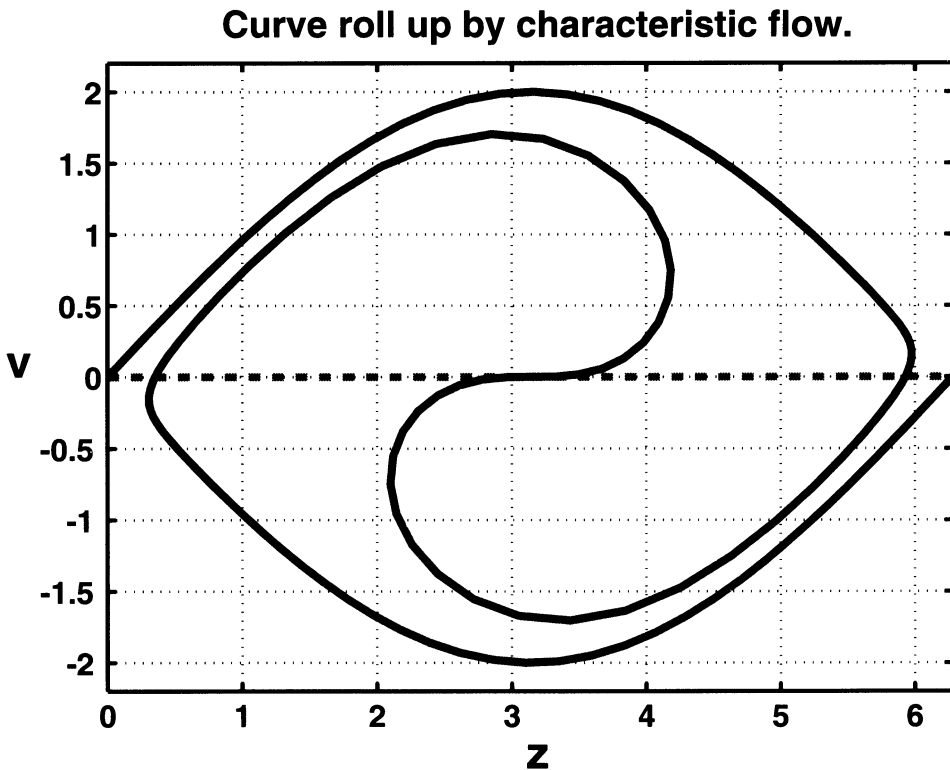


FIGURE 6. Solution curve roll up by the characteristic flow with the Hamiltonian $h = \frac{1}{2}v^2 + \cos z - 1$, and initial condition $v(z, 0) = 0$. The figure shows the initial conditions (dashed line) and the curve, as evolved by the characteristic flow, for time $t = 2\pi$. The parts of the curve near the saddles stretch to fill the critical $h = 0$ orbit (as $t \rightarrow \infty$), which is the only thing that survives after the shock is put in place.

The result in (2.2.31) shows that, after a long enough time, the solution can cross the line $v = 0$ smoothly **only** in an arbitrarily small neighborhood of $z = 0$, where F_{cr} vanishes (notice that a crossing is needed when $|\omega| < \omega_{cr}$, since the condition $\text{Mean}(v) = -\omega$ cannot be satisfied if either $v \geq v_{cr} = \sqrt{2F_{cr}}$ or $v \leq -v_{cr} = -\sqrt{2F_{cr}}$.) If there is such a crossing, it must be upwards, with v returning to negative values through a transonic shock. Moreover, the solution needs to lie entirely on $C(D)$ or at most, if within D , in an arbitrarily small neighborhood of the separatrix $h = 0$.

Once in the situation described in the prior paragraph, S_1 in equation (2.2.30) becomes arbitrarily small (see remark 2.4). Since (as shown earlier) S_2, S_3 , and S_4 are non-positive, it follows that the functional G , defined in (2.2.28), can no longer

increase: it remains constant for solutions that are either smooth or only have shocks from $\sqrt{2F_{cr}}$ to $-\sqrt{2F_{cr}}$, and decreases for all other solutions. Furthermore, the same argument we used for the case $|\omega| > \omega_{cr}$ can be used to show that any parts of the solution (in $C(D)$) not lying on a single contour line $h = \text{constant}$, necessarily break and form shocks. Hence, as long as $v(z, t)$ stays away from v_{ex} , G decreases. Again, we conclude that the long time ($t \rightarrow \infty$) asymptotic limit of the solution $v = v(x, t)$ must be given by $v_{ex}(z)$ (which minimizes G .)

3. Two Forcing Modes.

In this section, we study the effects — on the solutions to equation (1.1.1) — of a forcing term consisting of the sum of two traveling waves of different speeds. For concreteness, we shall only consider the case in which one of these speeds is zero, corresponding to a perfect resonance, and we shall observe the changes in behavior as the other speed ranges from zero to infinity. To be specific, we will consider the equation

$$(3.3.1) \quad \left\{ \begin{array}{l} u_t + \left(\frac{1}{2}u^2\right)_x = f(x, t), \\ \text{where} \\ f(x, t) = g_1(x) + g_2(x - \Omega t) \end{array} \right.$$

Ω is a constant, g_1 and g_2 are 2π periodic smooth functions with vanishing mean, and $u = u(x, t)$ is 2π periodic in space, with zero mean. We will **assume** $\Omega > 0$, since the case $\Omega < 0$ can be reduced to this one using the symmetry: $x \rightarrow -x$, $u \rightarrow -u$, and $f \rightarrow -f$.

When Ω is small, the two forcing modes oscillate at nearly the same [resonant] frequency. Our interest in this situation arises from the general question of the effects of the superposition of many near resonant interactions in general systems. In order to estimate the combined effect of the interaction of a mode with very many others, one needs to assess the degree of phase coherence among the corresponding forcing terms. Such assessment depends fundamentally on the consideration of three issues:

- $$(3.3.2) \quad \left\{ \begin{array}{l} 1. \text{ How close to each other are the linear frequencies of the forcing} \\ \text{modes.} \\ 2. \text{ How much these linear frequencies are affected [“renormalized”]} \\ \text{by nonlinear effects.} \\ 3. \text{ How often do strong [intermittent] nonlinear events effectively} \\ \text{reinitialize the phases of the various forcing modes. Also, do} \\ \text{these reinitializations tend to randomize or rather further cor-} \\ \text{relate the various phases?} \end{array} \right.$$

It should be quite clear that these questions are not easy to answer. Moreover, once answers are assumed (see next paragraph), one has only defined the nature of the forcing; its effects on the evolution of the forced mode still need to be assessed. Furthermore, since the forcing arises from combinations of other modes which are also similarly forced, the problem has an enormously complicated nature.

Attempts to bypass this great complexity often rely on universal assumptions, such as randomization of the phases and separation of the linear and nonlinear scales, which are very difficult to justify. Typically, these closures are sometimes successful — in that their predictions agree with the observed behavior of the system under

study — and sometimes a radical failure, with the reasons for this disparity open to debate.

Here we isolate the issue of the response to a given force, by prescribing the form of the forcing term. Moreover, we consider only two forcing modes, and prescribe their form and frequency as if they were not subject to nonlinear interactions themselves. By so reducing the complexity of the problem, we are able to resolve some questions regarding the effects of the degree of coherence of the forcing modes on the behavior of the forced mode.

The plan of this section is the following: First we describe certain general features of the solution to equation (3.3.1). Then we study separately two limiting regimes, corresponding to Ω either very large or very small. In each case we study (analytically and numerically) the behavior of the corresponding solutions.

Let us start by noticing that the forcing term in (3.3.1) is periodic in time, of period $2\pi/\Omega$. Since (3.3.1) is dissipative — though only through shocks, which are not necessarily present all the time — we expect that **the solution $u(x, t)$ will converge to a periodic pattern of the same periodicity.** We have checked this numerically, by computing the quantity

$$(3.3.3) \quad D = \int_0^{2\pi} \left(u(x, t + \frac{2\pi}{\Omega}) - u(x, t) \right)^2 dx.$$

In all the numerical experiments that we performed, D decreased rapidly, becoming effectively zero in about one or two periods of the forcing function.

We shall now distinguish two distinct extreme regimes, with the general case behavior interpolating between these two. Of the two terms in the forcing, $g_1 = g_1(x)$ is in resonance with $u(x, t)$, since the latter has a vanishing mean (hence zero linear frequency in the unforced case.) On the other hand, the forcing $g_2 = g_2(x - \Omega t)$ will be close to —or far from— resonance depending on the size of Ω . When $\Omega \gg 1$, we expect the leading order effect of $g_2(x - \Omega t)$ on $u(x, t)$ to cancel, due to averaging. When $0 < \Omega \ll 1$, on the other hand, the effect of g_2 can no longer be neglected. In this second case we expect g_1 and g_2 to combine into a single, quasi-steady force, yielding a quasi-steady solution $u = u(x, \Omega t)$ — very much a modulated version of the steady solution to (2.2.1), studied in section 2, for $\omega = 0$. Namely, in this last case we expect:

$$(3.3.4) \quad \left(\frac{1}{2} u^2 \right)_x \approx g_1(x) + g_2(x - \Omega t).$$

That this is roughly the case, yet with some interesting qualifications, will become clear in the analysis that follows.

3.1. Case: $\Omega \gg 1$; g_2 far away from resonance. In this subsection, we show that, when Ω is large, the solution $u = u(x, t)$ to (3.3.1) is close to the solution that one would obtain if the only forcing term were $g_1(x)$ — that is (to leading order) g_2 has no effect. To see this, introduce the small parameter

$$\epsilon = \frac{1}{\Omega}.$$

Then equation (3.3.1) takes the form

$$(3.3.5) \quad u_t + \left(\frac{1}{2} u^2 \right)_x = g_1(x) + g_2(x - \tau),$$

where $\tau = \frac{t}{\epsilon}$ is a fast time variable. We now propose the following asymptotic expansion:

$$(3.3.6) \quad u = u_0(x) + \epsilon u_1(x, \tau) + O(\epsilon^2),$$

where the dependence on τ is 2π -periodic. Then, at leading order, equation (3.3.5) yields

$$(3.3.7) \quad \frac{\partial u_1}{\partial \tau} + \left(\frac{1}{2} u_0^2 \right)_x = g_1(x) + g_2(x - \tau) = \frac{\partial G_1(x)}{\partial x} - \frac{\partial G_2(x - \tau)}{\partial \tau},$$

where G_1 and G_2 are the integrals of g_1 and g_2 , respectively (uniquely defined by the condition that both should have a vanishing mean.) We will assume the (generic) condition that G_1 **has a single minimum per period**.

Integrating equation (3.3.7) over one period (in τ), we obtain

$$(3.3.8) \quad \left(\frac{1}{2} u_0^2 \right)_x = \frac{\partial G_1(x)}{\partial x} \implies u_0(x) = \pm \sqrt{2(D + G_1(x))},$$

where $D = -\min(G_1)$, the solution crosses (continuously) from the negative to the positive root at the position of the minimum of G_1 , and has a shock (jumping from the positive to the negative root) at a position determined by the requirement that the average of $u_0 = u_0(x)$ should vanish. This leading order solution agrees with the solution that one would obtain if the forcing consisted exclusively of g_1 (see section 2, for $\omega = 0$.)

Substituting (3.3.8) into (3.3.7) we then find that

$$(3.3.9) \quad u_1(x, \tau) = -G_2(x - \tau) + p(x),$$

where $p = p(x)$ is a 2π -periodic function of vanishing mean, that is determined at the next order in the asymptotic expansion. Numerical experiments — not shown here — corroborate the results of this asymptotic analysis.

3.2. Case: $0 < \Omega \ll 1$; quasi-steady forcing. When $0 < \Omega \ll 1$, we can (in principle) think of the solution to equation (3.3.1) as frozen in time near each value $t = t_0$. This yields a quasi-steady leading order solution $u = u(x, \Omega t)$, where $u(x, \Omega t_0)$ is given by the steady state solution (section 2, case $\omega = 0$) to the case with a single forcing mode, with $f = f(x) = g_1(x) + g_2(x - \Omega t_0)$. In this subsection, we shall discuss this quasi-steady solution in some detail.

We begin with a simple asymptotic expansion that implements the idea in the paragraph above. Using Ω as the small parameter, we write

$$(3.3.10) \quad u(x, t) = u_0(x, \tau) + \Omega u_1(x, \tau) + O(\Omega^2),$$

where the dependence on τ is 2π -periodic and $\tau = \Omega t$ is a slow time variable. Then, at leading order, (3.3.1) yields

$$(3.3.11) \quad \left(\frac{1}{2} u_0^2 \right)_x = g_1(x) + g_2(x - \tau).$$

Thus

$$(3.3.12) \quad u_0(x, \tau) = \pm \sqrt{2G(x, \tau)},$$

where $G = G(x, \tau)$ is defined (for each τ) by

$$(3.3.13) \quad \frac{\partial G}{\partial x} = g_1(x) + g_2(x - \tau) \quad \text{and} \quad \min_{0 \leq x < 2\pi} (G) = 0.$$

In each period $0 \leq x < 2\pi$ the solution crosses (continuously) from the negative to the positive root at the point $x = x_m(\tau)$ where $G = 0$, and has a shock (jumping from the positive to the negative root) at a position $x = s(\tau)$, chosen so that the mean of u_0 vanishes.

The solution (3.3.12) above works as long as G has a single minimum per period, in which case $x_m = x_m(\tau)$ and $s = s(\tau)$ are well defined and depend smoothly on τ . However, there will generally be some special times, $\tau = \tau_c$, at which this fails. Generically G will have several local minimums, evolving in time, with one of them smaller than all the others. The (generic) special times occur when two local minimums exchange the property of being the global minimum. At these times x_m ceases to be smooth, jumps discontinuously from one position to another, and the expansion in (3.3.10) becomes inconsistent and fails.

REMARK 3.1. As pointed out at the beginning of subsection 2.3 (and remark 2.5) the convergence of the solution to a steady state — when the forcing is time independent — is generally very fast. Thus, we can be pretty sure that (3.3.10) will describe the behavior of the solution away from the critical times τ_c . The question (which we will address below) now becomes: what happens for $\tau \approx \tau_c$?

On each side of a critical time τ_c , the expansion in (3.3.10) is valid, but the position of the shock ($x = s(\tau)$) and the zero ($x = x_m(\tau)$) jump across $\tau = \tau_c$, implying a discontinuous global change in the solution u . Hence, there is a set of discrete times when the solution u needs to adjust “rapidly” from one quasi-steady state to another ($O(1)$ away) one. The existence of these **adjustment processes, which we will call “storms”**, raises the following questions:

$$(3.3.14) \quad \left\{ \begin{array}{l} \mathbf{1.} \text{ What is the time-scale (i.e., the duration) of a storm?} \\ \mathbf{2.} \text{ During a storm: are there significant effects in the energy} \\ \text{exchange between the forcing function } f = f(x, t) \text{ in (3.3.1)} \\ \text{and the solution } u = u(x, t)? \text{ That is to say: is the work per} \\ \text{unit time} \\ \\ W_f = \int_0^{2\pi} f u \, dx, \\ \\ \text{done by the external force, significantly affected by the storm?} \end{array} \right.$$

REMARK 3.2. Notice that the total energy (as follows from equation (3.3.12))

$$(3.3.15) \quad E \approx \int_0^{2\pi} \frac{1}{2} u_0^2(x, \tau) \, dx = \int_0^{2\pi} G(x, \tau) \, dx$$

is a continuous function of τ for the quasi-steady solution, even though u_0 itself is not. This implies that any extra energy exchange between u and the forcing f during a storm will need to be matched by extra dissipation over the course of the storm.

REMARK 3.3. Away from the storms, the asymptotic solution in (3.3.10) shows that there is a leading order balance between the work W_f done by the forcing f on the solution u , and the energy E_d dissipated at the shocks. Namely:

$$(3.3.16) \quad E_d - W_f = O(\Omega).$$

This, of course, is in agreement with the fact that the total energy E is a slow function of time ($E = E(\tau)$, as shown by equation (3.3.15).) This suggests the following extra question, related to **2** in (3.3.14) above: **How is the balance in (3.3.16) affected by a storm?**

Before attempting to answer these questions analytically, let us set up a simple example, that will help both make the discussion concrete, and verify its results through numerical experiments. Let us select a forcing term of the form

$$(3.3.17) \quad f(x, t) = \sin(x) + 2 \sin(2(x - \Omega t)),$$

in equation (3.3.1). Then G , as defined in (3.3.13), is given by:

$$(3.3.18) \quad G = \int f(x, t) dx = C(\Omega t) - (\cos(x) + \cos(2(x - \Omega t))),$$

where $C = \max_x(\cos(x) + \cos(2(x - \Omega t)))$. The critical times at which the zero of G jumps are given by

$$(3.3.19) \quad t_n = \frac{(2n + 1)\pi}{2\Omega},$$

where n is an integer. At these times

$$(3.3.20) \quad G(x, \Omega t_n) = \frac{1}{8} (1 - 4 \cos(x))^2,$$

and

$$(3.3.21) \quad u_0(x, \Omega t_n) = \pm \frac{1}{2} |1 - 4 \cos(x)|,$$

with two candidate crossings of zero.

At the critical times t_n (of which there is one per period), there are two solutions $u_0(x)$ of the form (3.3.21), in which u_0 switches from negative to positive at one of the zeros, has a corner at the other, and switches once from positive to negative through a shock, at a position determined by the condition that u_0 has a vanishing average. The quasi-steady solution given by the asymptotic expansion in (3.3.10) approaches one (or the other) of these two solutions as $t \rightarrow t_n$ from below (or above.)

REMARK 3.4. In addition to the two special solutions mentioned in the prior paragraph, there is a full one-parameter family of solutions (of which the two solutions just described are extreme cases.) In this family, both zeros of u_0 are used for upward (negative to positive) crossings, and there are consequently two shocks switching the solution back to negative. The positions of these two shocks are related by the constraint on the average of u_0 , which leaves one free parameter. The relevance of this one parameter family of solutions is that, during a “storm”, the actual solution $u(x, t)$ sweeps this family, one member at a time, at an intermediate rate, faster than $O(\Omega t)$, but slower than $O(t)$. Before showing this curious result through an asymptotic expansion, we illustrate it with a numerical solution.

Figure 7 displays the [numerical] solution to equation (3.3.1) with the forcing given by (3.3.17), starting from the asymptotic solution shortly before the critical time t_1 , for a value of the frequency $\Omega = 0.01$, not exceedingly small. The dotted line gives the envelope for the asymptotic, quasi-steady solution $u_0(x, \tau)$ (i.e.: the curves $u = \pm\sqrt{2G}$.) In this figure we can see the actual solution $u = u(x, t)$ switching its upward crossing point from one zero of $G(x, \Omega t_1)$ to the other, through a relatively fast transition, involving the development, growth, travel and eventual disappearance of a second shock. During this transition, the solution sticks very closely to the envelope of the quasi-steady solution. The slight disagreement, most visible in frame (e), is due to the finite size of Ω : as Ω gets smaller, the full “storm” takes place with the envelope nearly constant, and we should compare it with the “critical” envelope (that has two zero crossings per period.)

Figure 8 shows the total energy of the solution as a function of time, for a full period² in time π/Ω , and four values of the frequency, from $\Omega = 1/50$ to $\Omega = 1/400$. Note that this figure shows the energy converging to a function of time with a corner at t_1 , as the frequency Ω tends to zero (the limit is the function given by equation (3.3.15), for this special case when G is given by (3.3.18).) Such a cornered energy function corresponds to an instantaneous storm, which changes the phase of the solution discontinuously at $t = t_1$.

A more thorough understanding of the energetics of a storm is gained by looking at either the energy dissipation rate $E_d = E_d(t)$ (caused by the shocks), or the work $W_f = W_f(t)$ done by the forcing (see figures 9 and 10). Both show a marked spike during the storm, approximately duplicating the regular amount of work and dissipation. The doubling of the energy dissipation rate is easily explained as arising from the appearance of an extra shock during a storm, of a size comparable to the regular one. The close agreement between the energy dissipated and the work performed by the forcing, on the other hand, can be explained by the slow evolution of storms, faster than the regular $O(\Omega t)$ rate, but clearly slower than a $O(t)$ rate. Hence, at any particular time, the energy input and output need to be in balance to leading order. In other words: **even during a storm the solution is quasi-steady** (as we will show below.)

The points just raised bring us back to the natural question of what is the time-scale for a storm (namely, question 1 in (3.3.14).) Quantifying this time-scale will tell us how significant storms are from the viewpoint of energy exchange: fast storms do not have time to affect the energy exchange significantly, while slower storms do. Notice that the storms have a very definite duration in figures 9 and 10: they start and end rather abruptly. Measuring these durations suggests that they scale with the square-root of the frequency Ω . That this is precisely the case can be inferred from the following asymptotic argument:

Consider, during a storm³ an asymptotic expansion of the form

$$(3.3.22) \quad u(x, t) = u_0(x, T) + \delta u_1(x, T) + O(\delta^2),$$

where $T = \delta(t - t_c)$, and $\Omega \ll \delta \ll 1$ is a small parameter to be determined (δ gives the storm time scale.) The right hand side $f = f(x, \tau)$ in equation (3.3.1)

²Note that, because g_2 in (3.3.17) has period π , in this case the long time asymptotic solution to (3.3.1) has period π/Ω in time — not $2\pi/\Omega$, as in the general case.

³Taking place for $t \approx t_c = \tau_c/\Omega$, where τ_c is defined below equation (3.3.13).

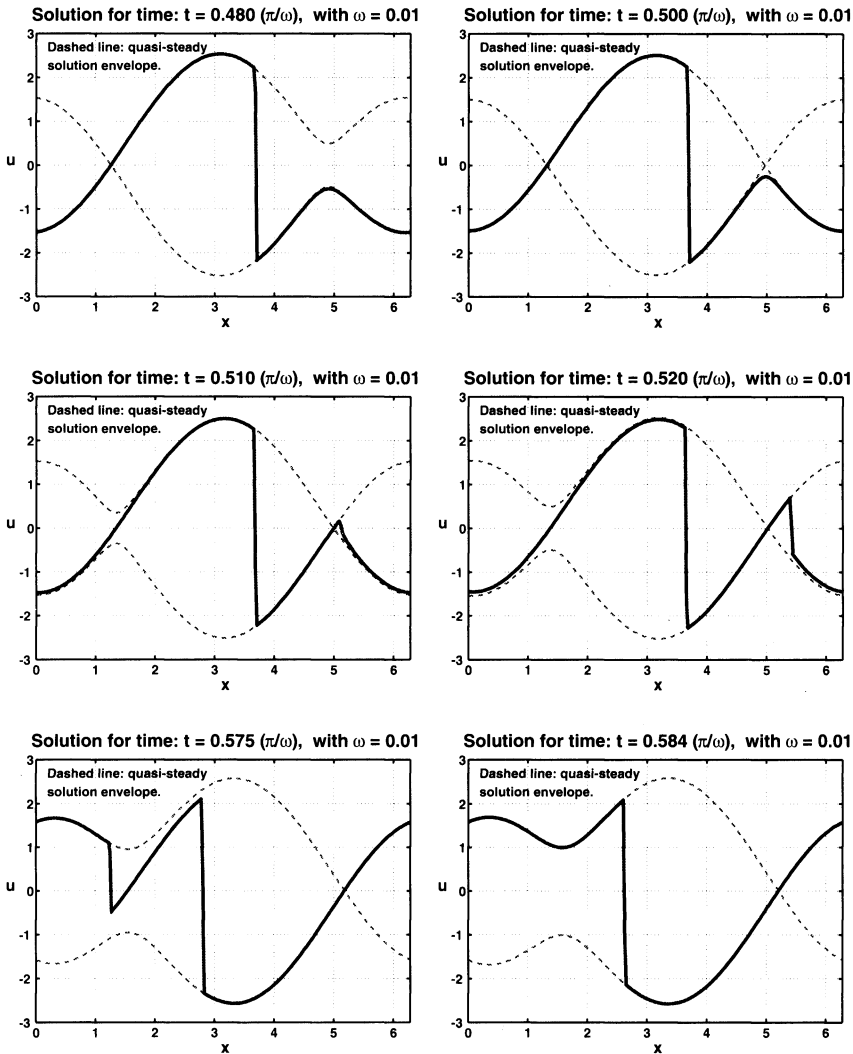


FIGURE 7. Asymptotic $t \rightarrow \infty$ solution to the equation $u_t + (\frac{1}{2} u^2)_x = \sin(x) + 2 \sin(2(x - \Omega t))$, with $\Omega = 0.01$. Time slices of the solution are shown for t near the critical time $t_c = \pi/(2\Omega)$, when F_{cr} has a double zero. The asymptotic solution is periodic in time, of period π/Ω . Because Ω is small, the solution is quasi-steady at all times. The plots here illustrate the evolution in the time scale $O(\sqrt{\Omega}t)$, with corrections of order $O(\sqrt{\Omega})$, for t near t_c (when a double shock arises.) For t away from t_c the solution is close to the unique quasi-steady solution of the problem. For t close to t_c the solution evolves following the one parameter family of quasi-steady solutions possible when $t = t_c$. Two shocks arise in this stage. Left to right and top to bottom, the figures show the solution (and the envelope $\pm \sqrt{2F_{cr}}$ for the quasi-steady solution, in a dashed line) for the times: (a) $t = 0.480 (\pi/\Omega)$, (b) $t = 0.500 (\pi/\Omega)$, (c) $t = 0.510 (\pi/\Omega)$, (d) $t = 0.520 (\pi/\Omega)$, (e) $t = 0.575 (\pi/\Omega)$, and (f) $t = 0.584 (\pi/\Omega)$.

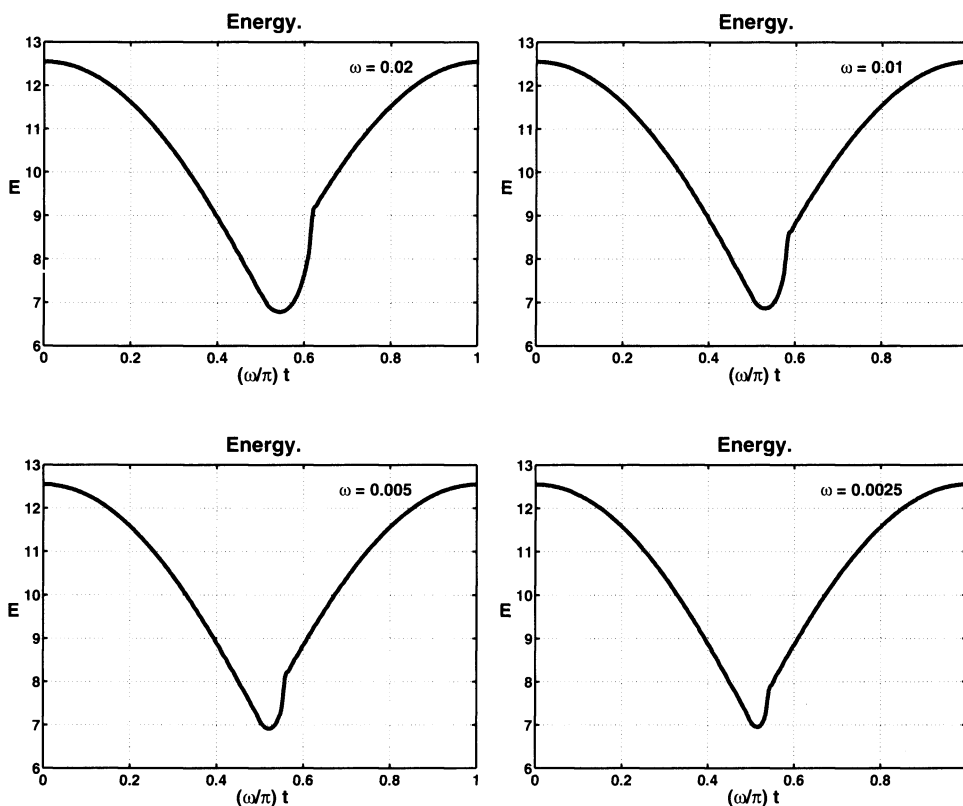


FIGURE 8. Energy $E = E(t)$ — shown over one period $0 \leq (\Omega/\pi)t \leq 1$ in time — for the $t \rightarrow \infty$ asymptotic solution for the equation $u_t + (\frac{1}{2} u^2)_x = \sin(x) + 2 \sin(2(x - \Omega t))$. Left to right and top to bottom, plots for the cases $\Omega = 1/50$, $\Omega = 1/100$, $\Omega = 1/200$, and $\Omega = 1/400$ are shown.

can expanded in the form

$$(3.3.23) \quad f(x, \tau) = f(x, \tau_c) + \frac{\Omega}{\delta} T f_\tau(x, \tau_c) + \dots,$$

where $\tau = \Omega t$, as in the expansion in (3.3.10). Substituting (3.3.22) and (3.3.23) into equation (3.3.1) we obtain, to leading order:

$$(3.3.24) \quad u_0(x, T) = \pm \sqrt{2G_c(x)},$$

where $G_c = G(x, \tau_c)$, and G is as in (3.3.13). Because $\tau = \tau_c$, generically G_c will have two zeros per period, and the dependence of u_0 on T is through the position of the two shocks in (3.3.24). That is: u_0 must be a member of the one parameter family of solutions that the steady state problem has at the critical times (see remark 3.4), with the parameter a function of T .

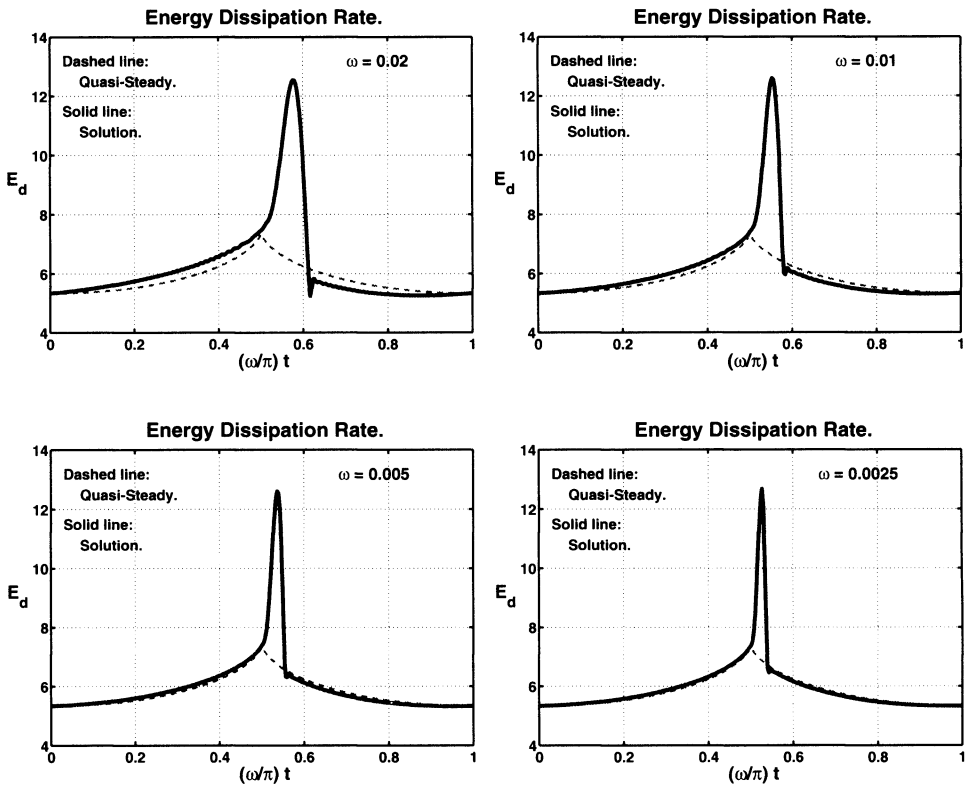


FIGURE 9. Energy dissipation rate $E_d = E_d(t)$ — shown over one period $0 \leq (\Omega/\pi)t \leq 1$ in time — for the $t \rightarrow \infty$ asymptotic solution for the equation $u_t + (\frac{1}{2} u^2)_x = \sin(x) + 2 \sin(2(x - \Omega t))$. Left to right and top to bottom, plots for the cases $\Omega = 1/50$, $\Omega = 1/100$, $\Omega = 1/200$, and $\Omega = 1/400$ are shown. The width of the dissipation spike near the time where the shock in the quasi-steady solution changes location, behaves like $\Delta t \approx 1/\sqrt{\Omega}$. The energy dissipation rate for the quasi-steady solution is shown by the dotted line.

At the next order in the expansion we have, on each side of the equation:

$$(3.3.25) \quad \delta (u_{0T} + (u_0 u_1)_x) = \frac{\Omega}{\delta} T f_\tau(x, \tau_c),$$

which requires $\delta = \sqrt{\Omega}$ in order to balance. Hence the (intermediate) time-scale, valid during storms, is given by $T = \sqrt{\Omega}t$, as suggested by the numerical experiments.

Answers to the questions posed earlier.

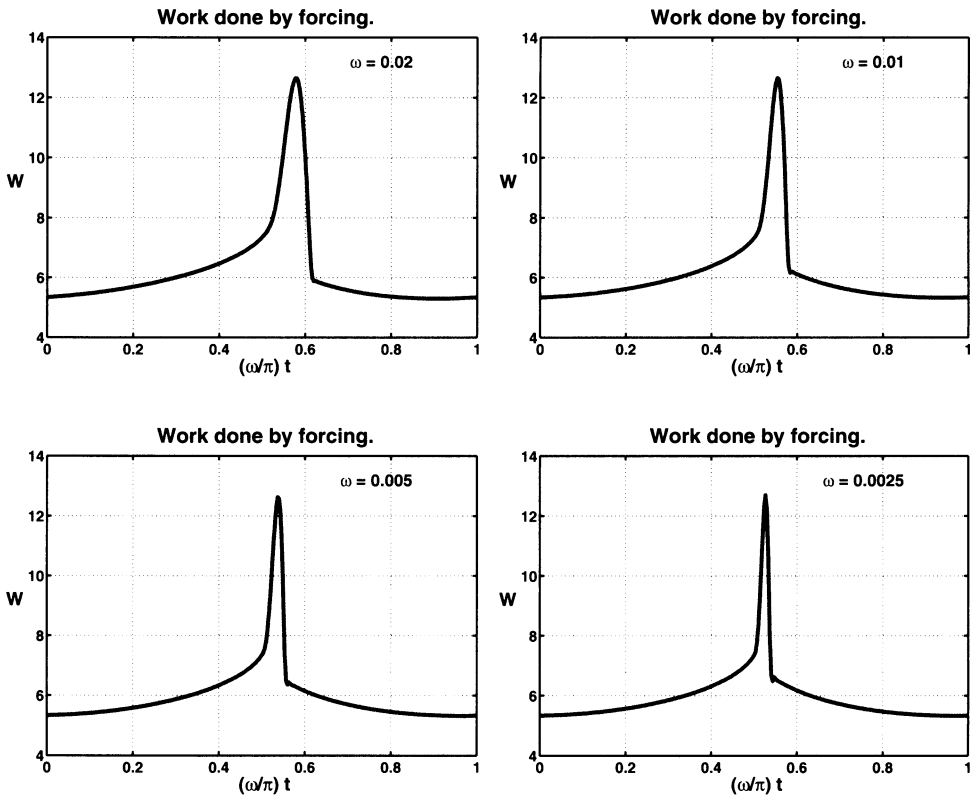


FIGURE 10. Work done by the forcing $W_f = W_f(t)$ — shown over one period $0 \leq (\Omega/\pi)t \leq 1$ in time — for the $t \rightarrow \infty$ asymptotic solution for the equation $u_t + (\frac{1}{2} u^2)_x = \sin(x) + 2 \sin(2(x - \Omega t))$. Left to right and top to bottom, plots for the cases $\Omega = 1/50$, $\Omega = 1/100$, $\Omega = 1/200$, and $\Omega = 1/400$ are shown. Note how closely the work done and the dissipation match, as a consequence of the fact that the solution, at all times, is fairly close to a quasi-steady solution.

We can now answer the questions that were posed earlier in this subsection as follows:

- (3.3.26) {
- A. Storms have a typical duration $\Delta t = 1/\sqrt{\Omega}$, evolving on an (intermediate slow) time-scale $T = \sqrt{\Omega} t$ (question 1 in (3.3.14).)
 - B. During a storm both: the work per unit time W_f by the force f , and the energy dissipation rate E_d by the shocks are (roughly) twice as large as their values away from a storm, since the solution has two shocks during a storm, and only one away from it (question 2 in (3.3.14).)
 - C. Combining the answers in A and B, we see that the **overall excess dissipation caused by a storm is $O(1/\sqrt{\Omega})$** .
 - D. Storms alter the balance between dissipation and work given by (3.3.16), replacing it by
- $$E_d - W_f = O(\sqrt{\Omega}).$$

As pointed out in the introduction to this paper, the fact that the effects caused by a storm scale with $\sqrt{\Omega}$, not Ω , may have important consequences when considering the effects of a complex set of near-resonances (something that escapes the scope of this present paper, and which we plan on investigating in future work.)

References

- [1] Benney, D.J. and Newell, A.C., “Random wave closures”, *Stud. Appl. Math.*, vol. 48 (1969), 29–53.
- [2] Benney, D.J., and Saffman, P.G., “Nonlinear interactions of random waves in a dispersive medium”, *Proc. Roy. Soc. A*, vol. 289 (1965), 301.
- [3] Cai, D., Majda, A.J., McLaughlin, D.W. and Tabak, E.G., “Spectral Bifurcations in Dispersive Wave Turbulence” *PNAS*, vol. 96 (1999), 14216–14221.
- [4] Godunov, S. K., “A difference scheme for numerical computation of discontinuous solutions of equations of fluid dynamics”, *Mat. Sb.*, vol. 47 (1959), 271–306.
- [5] Hasselmann, K., “On the nonlinear energy transfer in a gravity wave spectrum. Part I: General theory”, *J. Fluid Mech.*, vol. 12 (1962), 481–500.
- [6] Majda, A.J., McLaughlin, D.W. and Tabak, E.G., “A one-dimensional model for dispersive wave turbulence”, *J. Nonlinear Sci.*, vol. 7 (1997), 9–44.
- [7] Milewski, P.A., Tabak, E.G. and Vanden Eijnden, E., “Resonant wave interaction with random forcing and dissipation”, to appear in *Stud. Appl. Math.* (2001).
- [8] Rosales, R.R., Tabak, E.G. and Turner, C.V., “Resonant triads involving a nondispersive wave”, to appear in *Stud. Appl. Math.* (2001).
- [9] Strang, G., “On the construction and comparison of difference schemes”, *SIAM J. Num. Anal.*, vol. 5 (1968), 506–517.
- [10] van Leer, B., “Towards the ultimate conservative difference scheme V. A second order sequel to Godunov’s method”, *J. Comput. Phys.*, vol. 32 (1979), 101–136.
- [11] Zakharov, V.E., Lvov, V. and Falkovich, G., **Wave Turbulence**, Springer, New York, 1992.

F. A. M. A. F. , UNIVERSIDAD NACIONAL DE CÓRDOBA, CÓRDOBA, ARGENTINA
E-mail address: Menzaque@mate.uncor.edu

DEPARTMENT OF MATHEMATICS, MASSACHUSETTS INSTITUTE OF TECHNOLOGY, CAMBRIDGE, MA 02139
E-mail address: rrr@math.mit.edu

COURANT INSTITUTE OF MATHEMATICAL SCIENCES, NEW YORK UNIVERSITY, NEW YORK, NY 10012
E-mail address: tabak@cims.nyu.edu

F. A. M. A. F. — CIEM-CONICET, UNIVERSIDAD NACIONAL DE CÓRDOBA, CÓRDOBA, ARGENTINA
E-mail address: turner@mate.uncor.edu

Traveling surface elastic waves in the half-plane

Panayotis Panayotaros

ABSTRACT. We develop a perturbation theory for small amplitude traveling surface elastic waves in the half-plane, and apply the theory to various non-linear hyperelastic materials. For such media the traveling wave problem has a variational structure and we use this structure to study an equation for the first approximation to the shape of the waves. We find evidence for traveling wave solutions where the elastic displacement has cusps at the boundary.

1. Introduction

In this contribution we study small amplitude non-linear traveling surface elastic waves in a solid occupying the half-plane. These traveling waves describe elastic displacements that are translated with uniform velocity in the direction parallel to the surface of the medium.

Our main motivation for considering the problem is related to the common interpretation of traveling waves of permanent form as solutions bifurcating from the trivial solution. This viewpoint has been very useful in proving existence of periodic traveling wave solutions in dispersive wave equations, and can be thought of as a rigorous version of Stokes' perturbation theory for water waves. On the other hand, linear surface elastic waves in the half-plane are non-dispersive, and traveling wave solutions would correspond to solutions bifurcating from an eigenvalue of infinite multiplicity (this eigenvalue is the square of the speed of the linear traveling waves).

To study the possibility of such a bifurcation we have developed (see [Pa]) a systematic perturbation theory that is formally analogous to solving the bifurcation and complementary equations appearing in Liapunov-Schmidt reduction order by order in a suitable small parameter. The bifurcation equation is here replaced by an infinite set of solvability conditions. The first solvability condition is a non-linear equation for the lowest order part of the traveling wave solution, and coincides with equations originally derived and studied numerically by [PT] and [La]. The second and higher order solvability conditions are linear and share a common structure, involving the linearization of the first solvability equation around its solutions. The

1991 *Mathematics Subject Classification.* Primary 74J15, 35L67 ; Secondary 35B10,35Q72.

Key words and phrases. Surface elastic waves, traveling waves.

The author was supported in part by NSF Grant DMS-9810751.

solvability equations are infinite dimensional, but involve the boundary values of the elastic displacement, i.e. the displacement inside the domain can be at each order determined by its boundary values.

For hyperelastic materials the traveling wave equations as well as the solvability conditions have the structure of a constrained variational problem. This observation is particularly useful in studying the first solvability condition, where there has been some controversy regarding the limits of the numerical solutions of [PT] (see [HIZ]). Here we consider three hyperelastic materials and we find evidence for numerical solutions with non-trivial limits. An interesting feature of these solutions is that they describe surface elastic displacements with discontinuities in their first derivative, specifically, cusps in the horizontal component of the surface elastic displacement.

2. The traveling wave problem

We consider a homogeneous elastic medium occupying in its undeformed state the half-plane $H = \{(y_1, y_2) \in \mathbf{R}^2 : y_2 \geq 0\}$. A deformation of the body will take a point originally at (y_1, y_2) to a new position $y_i + u_i(y_1, y_2)$, $i = 1, 2$, and we can describe time dependent elastic motions by the evolution of the displacement vector field u defined on H . Elastic forces are described by the (first Piola-Kirchhoff) stress tensor $\tau_{i,j}$, $i, j = 1, 2$, a specified function of the derivative ∇u of the elastic displacement, and the equations of motion of elasticity have the general form

$$(2.1) \quad \partial_{tt} u_i = \sum_{j=1}^2 \partial_{y_j} \tau_{ij}, \quad i = 1, 2, \quad \text{in } H.$$

In the problem of traveling waves of permanent form we are seeking solutions that have the form $u_i(y_1 - ct, y_2)$, $i = 1, 2$, with c the unknown velocity. If we also require that no external forces be applied at ∂H , traveling wave solutions must then satisfy

$$(2.2) \quad c^2 \partial_{x_1 x_1} u_i = \sum_{j=1}^2 \partial_{x_j} \tau_{ij}, \quad \text{in } H, \quad \sum_{j=1}^2 \tau_{ij} \hat{n}_j = 0 \quad \text{at } \partial H, \quad i = 1, 2,$$

where $x_1 = y_1 - ct$, $x_2 = y_2$, and \hat{n} is the outward unit normal at ∂H . We will also impose the decay condition

$$(2.3) \quad \lim_{x_2 \rightarrow \infty} u(x_1, x_2) = 0, \quad \forall x_1 \in \mathbf{R},$$

and periodicity in the horizontal direction, i.e.

$$(2.4) \quad u(x_1 + 2\pi, x_2) = u(x_1, x_2), \quad \forall (x_1, x_2) \in H.$$

With these boundary conditions we will be working in the half-cylinder D obtained by identifying $x_2 = \pi$ and $-\pi$.

We are particularly interested in the traveling wave problem for hyperelastic materials, where the stress $\tau_{i,j}$ is given by

$$(2.5) \quad \tau_{ij} = \frac{\partial W(\nabla u)}{\partial u_{i,j}}, \quad \text{with } u_{i,j} = \partial_{x_i} u_j, \quad i, j = 1, 2.$$

Physically, W is the potential energy density. We will write $W = W^L + W^{NL}$, with W^L quadratic and W^{NL} cubic or higher order in ∇u . The linear part of the traveling wave equations will be here specified by

$$(2.6) \quad W^L = \frac{\lambda}{2}(\text{tr}\gamma)^2 + \mu\text{tr}(\gamma^2), \quad \text{where } \gamma = \frac{1}{2}[\nabla u + (\nabla u)^T],$$

and $\lambda, \mu > 0$ are the Lamé constants. (2.6) is the quadratic part of the most general potential energy for isotropic materials. We will also denote the stresses corresponding to W^L, W^{NL} through (2.5) by τ^L, τ^{NL} respectively.

The linear traveling wave problem corresponds to the choice $\tau = \tau^L$ in (2.5). The problem was considered by Rayleigh (see e.g. [Lo]), and we summarize the solution as follows. First, there exists a unique speed of propagation $c^2 = c_0^2$ (depending on λ, μ). Also, all solutions have the form $u_i(x_1, x_2) = \sum_{k \in \mathbf{Z}} a_k e^{ikx_1} \hat{v}_i(k, x_2)$, $i = 1, 2$, with

$$(2.7) \quad \hat{v}_1(k, x_2) = i \frac{k}{|k|} \left(-Ae^{-|k|Ax_2} + \frac{2A}{A^2 + 1} e^{-|k|Bx_2} \right), \quad k \in \mathbf{Z} \setminus \{0\},$$

$$(2.8) \quad \hat{v}_2(k, x_2) = \left(e^{-|k|Ax_2} - \frac{2AB}{A^2 + 1} e^{-|k|Bx_2} \right), \quad k \in \mathbf{Z} \setminus \{0\},$$

and $a_k \in \mathbf{C}$ arbitrary ($a_{-k} = \bar{a}_k$ for real displacements). The constants A, B are given by $A^2 = 1 - \frac{c_0^2}{\mu}$, $B^2 = 1 - \frac{c_0^2}{\lambda + 2\mu}$. For $k = 0$ we have the trivial solution $\hat{v}_i(0, x_2) \equiv 0, i = 1, 2$.

Therefore, the space of solutions to the linear problem is infinite dimensional and all solutions propagate at the same speed. Also note that linear traveling solutions are determined by their value at $\partial D = S^1$.

In the perturbation theory we develop in the next section we will also consider the inhomogeneous linear traveling wave equation

$$(2.9) \quad \nabla \cdot \tau^L(u) - c_0^2 \partial_{x_1}^2 u = F \quad \text{in } H, \quad \tau^L(u) \cdot \hat{n} = f \quad \text{at } \partial H,$$

with the decay and periodicity conditions (2.3), (2.4). The functions $F = [F_1, F_2] : H \rightarrow \mathbf{R}^2$ and $f = [f_1, f_2] : \partial H \rightarrow \mathbf{R}^2$ are also assumed to be 2π -periodic in x_1 , and F decays as $x_2 \rightarrow \infty$. In order for (2.9) to have a solution, it is necessary that F and f satisfy

$$(2.10) \quad \int_0^\infty \hat{v}^*(k, x_2) \cdot \hat{F}(k, x_2) dx_2 - \hat{v}^*(k, 0) \cdot \hat{f}(k) = 0, \quad \forall k \in \mathbf{Z} \setminus \{0\},$$

where the $\hat{v}(k, x_2) = [\hat{v}_2(k, x_2), \hat{v}_1(k, x_2)]$ are as in (2.7), (2.8), and F_k, f_k are the Fourier coefficients of F, f respectively. Assuming that the solvability condition is satisfied, we can explicitly construct a solution w of (2.9) (see [Pa], Appendix A), so that the general solution will have the form $u = w + v$, with v an arbitrary solution of the homogeneous system.

3. Small amplitude non-linear traveling waves

To obtain a formal expansion for non-linear traveling waves we look for solutions of (2.2) of the form

$$(3.1) \quad u = \alpha u^{[1]} + \alpha^2 u^{[2]} + \alpha^3 u^{[3]} + \dots, \quad c^2 - c_0^2 = \alpha \lambda_1 + \alpha^2 \lambda_2 + \alpha^3 \lambda_3 + \dots,$$

with the $u^{[i]}$ satisfying the periodicity and decay conditions (2.3), (2.4). Physically, the “small parameter” α is the ratio of the boundary displacement (u_1 or u_2) to the horizontal period. To simplify the notation we will assume that $\tau^{NL} = \tau^{NL}(u, u)$ is quadratic in the displacement. Using the expressions of (3.1) in (2.2), and setting the coefficients of powers of α to zero, we obtain a sequence of linear equations for the $u^{[i]}$ and λ_i . At order α^1 we have

$$(3.2) \quad \nabla \cdot \tau^L(u^{[1]}) - \rho c^2 \partial_{x_1}^2 u^{[1]} = 0, \quad \text{in } H, \quad \tau^L(u^{[1]}) \cdot \hat{n} = 0 \quad \text{at } \partial H,$$

so that we can set $u^{[1]} = v^{[1]}$, with $v^{[1]}$ an arbitrary solution of the homogeneous linear traveling wave equation. At order α^2 we have

$$(3.3) \quad \nabla \cdot \tau^L(u^{[2]}) - c_0^2 \partial_{x_1}^2 u^{[2]} = -\nabla \cdot \tau^{NL}(v^{[1]}, v^{[1]}) + \lambda_1 \partial_{x_1}^2 v^{[1]} \quad \text{in } H,$$

$$(3.4) \quad \tau^L(u^{[2]}) \cdot \hat{n} = -\tau^{NL}(v^{[1]}, v^{[1]}) \cdot \hat{n} \quad \text{at } \partial H.$$

The solvability condition (2.9) for this inhomogeneous system for $u^{[2]}$ will then give us a non-linear equation for $v^{[1]}$ and λ_1 , and it is this equation that selects the lowest order terms in the expansion (3.1). Assuming that the solvability condition has solutions we can construct explicitly a formal solution $w^{[2]}$ of (3.3), (3.4). The general solution of (3.3), (3.4) will then have the form $u^{[2]} = w^{[2]} + v^{[2]}$, with $v^{[2]}$ an arbitrary solution of the homogeneous linear traveling wave equation, to be determined together with λ_2 by the solvability condition for the equation for $u^{[3]}$. The procedure can be thus iterated to higher orders. At each order α^r , $r \geq 2$, we have the inhomogeneous linear traveling wave equation for $u^{[r]}$, with the right hand side depending on a solution $v^{[r-1]}$ of the homogeneous problem, λ_{r-1} , and previously determined terms. The $v^{[r-1]}$, λ_{r-1} will be determined by the solvability condition (2.9), and the solution will have the form

$$(3.5) \quad u = \alpha v^{[1]} + \alpha^2 (v^{[2]} + w^{[2]}) + \alpha^3 (v^{[3]} + w^{[3]}) + \dots,$$

with the $w^{[r]}$ explicitly given solutions of the inhomogeneous equations.

The main question is whether we can use the above scheme to produce the formal expansion (3.1). The key lies in finding the $v^{[r]}$ and λ_r , $r \geq 1$ through the solvability conditions, and we start our discussion with some observations and comments regarding the general structure of these equations.

First, note that the solvability conditions are equations for solutions of the homogeneous linear traveling wave equations and are thus equations on S^1 . Although we are reducing the spatial dimension of the problem we have to solve an infinite sequence of integro-differential equations (it will be more convenient here to write the spectral form of these equations).

The first solvability condition, which we abbreviate as $S^{[1]}(v^{[1]}, \lambda_1) = 0$, is quadratic in $v^{[1]}$ and homogeneous in $v^{[1]}$, λ_1 . The solvability conditions for the higher order terms $v^{[r]}$, λ_r , $r > 1$ are linear equations for the $v^{[r]}$, and all have the form

$$(3.6) \quad Lv^{[r]} = G^{[r]} + \lambda_r \tilde{L}v^{[r]}, \quad r > 1,$$

where L is the derivative of $S^{[1]}(v^{[1]}, \lambda_1)$ with respect to the first argument, evaluated at a solution of the first solvability condition, and $G^{[r]}$ depends on previously determined terms (ultimately on $v^{[1]}$). Also, the k -th Fourier coefficient of $(\tilde{L}v^{[r]})$ is $\int_D v_k^* \cdot \partial_{x_1}^2 v^{[r]}$.

Another general observation, shown in [Pa], is that in the case of hyperelastic materials, all the solvability conditions have a variational structure and can be written as

$$(3.7) \quad \nabla_{\bar{c}^{[r]}} V_r(v^{[r]}) = \lambda_r \nabla_{\bar{c}^{[r]}} I_r(v^{[r]}), \quad r \geq 1,$$

with $c^{[r]}$ the Fourier coefficients of $v^{[r]}$, and V_r, I_r appropriate functionals.

The above observations also apply to non-linearities with cubic and higher order terms. The first solvability condition will involve only the quadratic terms, while the higher order solvability conditions will have the form of (3.7). The higher order non-linearities will be absorbed in the part $G^{[r]}$ that depends on previously determined terms of the expansion.

The formal analogy of the procedure we described with Liapunov-Schmidt reduction is through the decomposition (3.5) of the solution to a component belonging to the kernel of the linear traveling wave operator and a component solving the inhomogeneous system. A similar perturbation theory has also been used in problems of static elasticity (see [CPG]).

4. The first solvability condition

By (2.9) and (3.3), (3.4) the first solvability condition is the set of equations

$$(4.1) \quad S_k^{[1]}(v^{[1]}, \lambda_1) = - \int_D \hat{v}^*(k) \cdot (\nabla \cdot \tau^{NL}(v^{[1]}, v^{[1]})) + \int_{\partial D} \hat{v}^*(k) \cdot (\tau^{NL}(v^{[1]}, v^{[1]}) \cdot \hat{n}) + \lambda_1 \rho \int_D \hat{v}^*(k) \cdot \partial_{x_1}^2 v^{[1]} = 0, \quad k \in Z \setminus \{0\}$$

Writing

$$(4.2) \quad v^{[1]} = \sum_{k \in Z \setminus \{0\}} c_p^{[1]} e^{ipx_1} \hat{v}(p, x_2),$$

with $\hat{v}(p, x_2) = [\hat{v}_1(p, x_2), \hat{v}_2(p, x_2)]$ as in (2.7), (2.8), we can solve (4.1) numerically by considering its Galerkin (spectral) projections. In the case of hyperelastic materials, (4.1) is also equivalent to

$$(4.3) \quad \nabla_{\bar{c}^{[1]}} V_1(v^{[1]}) = \lambda_1 \nabla_{\bar{c}^{[1]}} I_1(v^{[1]}), \quad r \geq 1,$$

where V_1 is the cubic part of the potential energy, and $I_1(v^{[1]}) = \frac{1}{2} \int_D \sum_{i=1}^2 (\partial_{x_1} v_i^{[1]})^2$. This variational interpretation also holds for the Galerkin projections of (4.1), with V_1, I_1 replaced by their restrictions V_1^N, I_1^N to the subspaces spanned by N modes. The level sets of the I_1^N are ellipsoids in \mathbf{R}^{2N} , and this implies that the Galerkin projections of (4.1) have non-trivial solutions. The main question is therefore the limiting behavior of these approximate solutions as N increases.

By the homogeneity of (4.1) in $v_i^{[1]}$ and λ_1 , multiplying a Galerkin solution $v_N^{[1]}$, λ_1^N by any constant we obtain another solution. Given thus a sequence of solutions of Galerkin systems with larger and larger number of modes we can scale them arbitrarily. In this work we set a uniform scale, so that all Galerkin solutions lie on an ellipsoid of a fixed radius. Specifically, we set $\lambda_1 = 1$ and solve the Galerkin projections of (4.1) with $N_1 < N_2 < \dots$ modes numerically, using the hybrid Newton's method of [Po]. We then scale the numerical solutions $\tilde{v}_{N_i}^{[1]}$ by suitable factors α_{N_i} so that $v_{N_i}^{[1]} = \alpha_{N_i} \tilde{v}_{N_i}^{[1]}$ lie on $I_1^{N_i} = 1$. The result is a sequence of

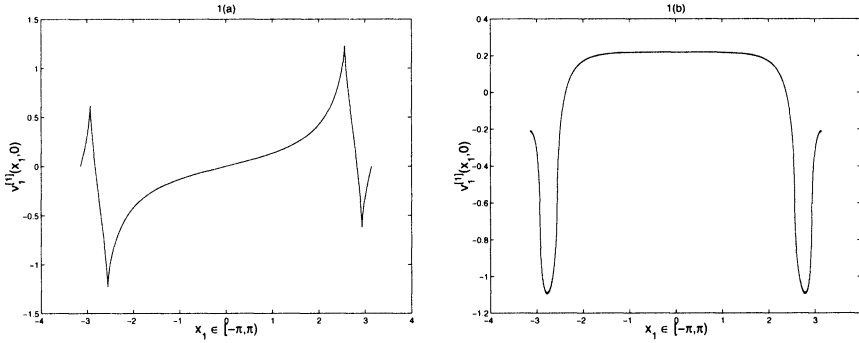


FIG.1. Horizontal (a) and vertical (b) surface elastic displacements for model NL1.

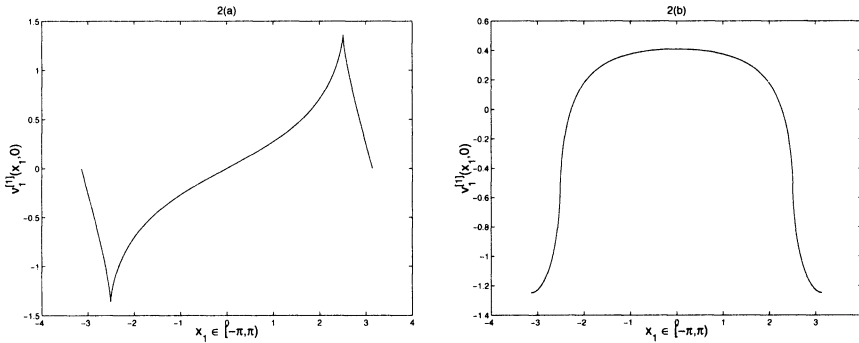


FIGURE 2. Horizontal (a) and vertical (b) surface elastic displacements for St.Venant-Kirchhoff material.

Galerkin solutions $v_{N_i}^{[1]}, \lambda_1^{N_i}$, with $\lambda_1^{N_1} = \alpha_{N_i}^{-1}$. Note that the sequence of $v_{N_i}^{[1]}$ yields a sequence of surface displacements that have weakly convergent subsequences in $L^2(S^1)$, although we can not rule out the possibility of solutions converging to the trivial surface displacement.

The first solvability condition was solved numerically for three hyperelastic materials. The first two are toy models with non-linearity given by the cubic potential energy densities

$$(4.4) \quad W_1^{NL} = \frac{1}{4}(\lambda + \mu)u_{1,1}u_{1,2}^2, \quad \text{and} \quad W_2^{NL} = \frac{1}{4}(\lambda + \mu)\left(u_{1,1}u_{1,2}^2 + u_{2,2}u_{2,1}^2\right).$$

We also considered the St.Venant-Kirchhoff material (see [C], ch. 4), where the potential energy density is

$$(4.5) \quad W = \frac{\lambda}{2}(\text{tr}E)^2 + \mu \text{tr}E^2, \quad \text{with} \quad E = \frac{1}{2}(\nabla u + (\nabla u)^T + (\nabla u)^T \nabla u).$$

The quadratic part in (4.5) is precisely given by (2.6). The Poisson ratio was set to $\frac{1}{4}$.

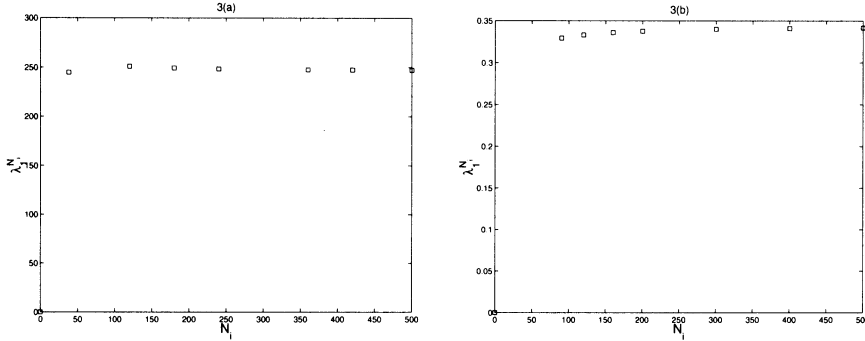


FIGURE 3. Speed corrections λ_1 for NL1 (a) and St.Venant-Kirchhoff (b) models.

Figures 1, 2 show the surface displacement $v^{[1]}(x_1, 0)$ for W_1^{NL} and the St.Venant-Kirchhoff material respectively, with (a) and (b) the horizontal and vertical components of $v^{[1]}(x_1, 0)$ for each material. Note that we have looked for solutions of prescribed parity. In all figures we show the results obtained with 500 modes. The shown shapes become well defined with truncations containing about 100 – 150 modes, and then we observe small change, mostly finer oscillations that decrease in amplitude. For instance, evaluating the surface displacements at 2500 uniformly distributed points in $[-\pi, \pi]$ we see that the difference between the respective components of surface displacements obtained using 400 and 500 modes is bounded by 2×10^{-2} for the solutions of Figures 1(a), (b) and by 2×10^{-3} for the solutions of Figures 2 (a), (b). The pointwise difference is in all cases oscillatory and its integral over $[-\pi, \pi]$ is in the range $10^{-6} - 10^{-5}$. The sequences of $\lambda_1^{N_i}$ corresponding to Figures 1, 2 are shown in Figures 3(a), (b) respectively. They appear to converge to non-zero values. Similar results are obtained for the model W_2^{NL} (see [Pa]).

An interesting feature of the numerical solutions shown is the appearance of well defined cusps in $v_1^{[1]}(x_1, 0)$ for all the non-linearities considered, while $v_2^{[1]}(x_1, 0)$ appears to be differentiable. The numerical results shown correspond to sequences of Galerkin solutions that appear to converge to non-trivial shapes, and suggest that non-trivial solutions to the first solvability condition may exist. Note that by (2.7), (2.8), $v_1^{[1]}(x_1, x_2)$ is smooth in the interior of D .

We also found a second type of numerical solutions that yield sequences of surface displacements that appear to converge (in $L^2(S^1)$) to the trivial displacement. Sequences of numerical solutions of this type were observed for all three non-linearities we considered (see [Pa]).

5. Discussion

The solutions of the first solvability conditions we presented are quite similar to the numerical solutions of [PT], although the higher spatial resolution used here allowed us to see well defined cusps in the horizontal surface displacement that were not observed before. [HIZ] on the other hand found only the Galerkin solutions that converge to the trivial displacement, and argued that no non-trivial solutions should exist. Here the variational formulation guaranteed the existence of Galerkin solutions and we were able to focus on the limits of the sequences $v_{N_i}^{[1]}, \lambda_1^{[N_i]}$. Also

the constraint gave us a natural common scale for the Galerkin solutions and we have identified two types of sequences of numerical solutions, namely sequences with apparently non-trivial limits, and sequences of solutions approaching the zero displacement. We thus consider that we have evidence for non-trivial solutions of the first solvability conditions and that the results of [PT] and [HIZ] can be reconciled. Clearly however, it would be desirable to have rigorous results on the question.

The formalism we described applies to other non-dispersive media. If the domain has no intrinsic length scale (examples are the half-plane, the wedge etc.), traveling linear waves that decay away from the boundary will have no dispersion and the investigation of the non-linear problem leads to infinite dimensional solvability conditions similar to the ones encountered here. The first solvability condition is also the equation for the traveling wave solutions of an asymptotic evolution equation describing $O(\epsilon)$ amplitude surface waves over an $O(\epsilon^{-1})$ time (see [H]). This model equation and the first solvability condition should thus be of intrinsic interest.

References

- [C] P.G. Ciarlet, *Mathematical Elasticity, Vol. I. Three dimensional Elasticity*, North-Holland, Amsterdam, 1988.
- [CPG] G. Carpiz, P. Podio Guidugli, *On Signorini's method in finite Elasticity*, Arch. Rat. Mech. Anal. **57** (1978), 1–30.
- [H] J.K. Hunter, *Nonlinear surface waves*, Contemp. Math. **100** (1989), 185–202.
- [HIZ] M.F. Hamilton, Y. A. Il'insky, E.A. Zabolotskaya, *On the existence of stationary nonlinear Rayleigh waves*, J. Acoust. Soc. Am. **93** (1993), 3089–3095.
- [La] R.W. Lardner, *Nonlinear surface waves on an elastic solid*, Int. J. Eng. Sci. **21** (1983), 1331–1342.
- [Lo] A.E.H. Love, *A treatise on the mathematical theory of Elasticity*, Dover, New York, 1944.
- [Pa] P. Panayotaros, *An expansion method for non-linear Rayleigh waves*, preprint (2000).
- [Po] M.J.D. Powell, *A hybrid method for nonlinear algebraic equations*, Numerical methods for nonlinear algebraic equations, ed. P. Rabinowitz, Gordon and Breach, New York, 1970.
- [PT] D.F. Parker, F.M. Talbot, *Analysis and computation for nonlinear elastic surface waves of permanent form*, J. Elasticity **15** (1985), 389–426.

DEPARTAMENTO DE MATEMÁTICAS Y MECÁNICA, I.I.M.A.S. - U.N.A.M., APARTADO POSTAL 20-726, 01000 MÉXICO D.F., MÉXICO

Current address: Department of Applied Mathematics, University at Colorado at Boulder, Campus Box 526, Boulder, Colorado 80309-0526, U.S.A.

E-mail address: panos@colorado.edu

Numerical Study of Two-Dimensional Stratified Turbulence

Leslie M. Smith

ABSTRACT. In an effort to gain further insight into phenomena associated with dispersive wave turbulence, numerical simulations are used to study homogeneously stratified, two-dimensional turbulence forced randomly at small scales. Consistent with what has been observed in simulations of rotating turbulence, the flow characteristics change dramatically when the Froude number passes through the value one, where the Froude number is defined in terms of the energy input rate and peak wavenumber of the force. For Froude numbers less than approximately one, the transfer of energy from small to large scales is anisotropic, leading to population of the slow manifold only, which in this case corresponds to vertically sheared, horizontal motions. There is evidence that resonant triads play an indirect but crucial role in the anisotropic transfer to the slow modes.

1. Introduction

Fundamental models for geophysical flows involve the complex interaction between waves and turbulence, *e.g.*, the β -plane model, the rotating shallow water equations, the Navier Stokes equations in a rotating frame, the Boussinesq equations, and the Boussinesq equations in a rotating frame. Numerical studies focusing on the anisotropic transfer to large scales for forced, weak turbulence have been performed for β -plane flow [1, 2] three-dimensional (3D) rotating flow [2] and two-dimensional (2D) flow on a sphere [3]. Strong transfer from small to large scales in 2D flows, including β -plane flow, is by now taken for granted, with well-established theoretical understanding [4]. The demonstration of such in fully 3D rotating flow was unexpected by many, and is lacking in mathematical foundation. Based on dimensional considerations, Rhines [5] predicted the large-scale β -plane spectrum $E(k) \propto k^{-5}$ instead of $E(k) \propto k^{-5/3}$ as in isotropic 2D turbulence [4]. Later, numerical simulations [1, 2] uncovered the anisotropic nature of the large-scale β -plane spectrum, *i.e.* the fact that $E(k) \approx E(k_x = 0, k_y) \propto k_y^{-5}$. For 3D rotating flow, the analogous large-scale spectrum $E(k) \approx E(k_h = 0, k_z) \propto k_z^{-3}$ with $k_h^2 = k_x^2 + k_y^2$ is also supported by numerical simulations [2]. However, a first principles analysis starting from the equations of motion has yet to be developed for the central feature of anisotropic transfer in any dispersive wave system.

The present study is a step towards a more complete understanding of dispersive wave flows in the regime of weak turbulence, defined here as the regime in which nonlinear inertial forces are essential, but smaller than dispersive wave effects. The

focus is on the transition from isotropic to anisotropic transfer of energy from small to large scales as the Froude number is decreased. Previous numerical studies of 2D stratified turbulence have focused on other phenomena, such as wave breaking [6, 7], flow over obstacles [8, 9], and stability [10]. Two-dimensional stratified turbulence may be a test case for theories of dispersive wave turbulence. Despite the limitation of zero potential vorticity, 2D stratified turbulence is not without merit as a model in its own right (see, *e.g.* [6, 7]). The Boussinesq equations for stratified flow are presented in Section 2. Section 3 gives parameter definitions and details of the numerical calculations. Section 4 describes the numerical results. Some of the many open questions are discussed in Section 5.

2. The governing equations and linear eigenmodes

The Boussinesq equations for vertically stratified flow are, in dimensional form, (*e.g.*, [11])

$$(1) \quad \frac{D\mathbf{v}}{Dt} + N\theta\hat{\mathbf{z}} + \nabla P = \nu_o \nabla^2 \mathbf{v} + \mathbf{f}_u,$$

$$(2) \quad \frac{D\theta}{Dt} - N(\mathbf{v} \cdot \hat{\mathbf{z}}) = \kappa \nabla^2 \theta,$$

$$(3) \quad \nabla \cdot \mathbf{v} = 0,$$

where $\mathbf{v} = u(x, z)\hat{\mathbf{x}} + w(x, z)\hat{\mathbf{z}}$ is the Eulerian velocity, P is the effective pressure, N the buoyancy frequency, $D/Dt = \partial/\partial t + \mathbf{v} \cdot \nabla$ is the material derivative, ν_o is the kinematic viscosity, κ is the diffusion coefficient and θ , which has units of velocity, is proportional to the density fluctuations. The total mass density ρ has been decomposed as

$$(4) \quad \rho = \rho_o - bz + \rho', \quad \rho' = \left(\frac{b\rho_o}{g}\right)^{1/2} \theta,$$

where ρ_o is a reference density, b is a positive constant (for uniform, stable stratification), z is the vertical coordinate and g is the gravitational acceleration. The buoyancy (Brunt-Väisälä) frequency N is

$$(5) \quad N = \left(\frac{gb}{\rho_o}\right)^{1/2}.$$

The term \mathbf{f}_u in (1) represents external forcing of the velocity; note that we do not consider external forcing of the density fluctuations θ . It is interesting to note that equations (1)-(3) are exactly the same as the equations for three-component (3C), two-dimensional flow rotating about the $\hat{\mathbf{x}}$ -direction at rate $N/2$, with velocity $\mathbf{v} = u(x, z)\hat{\mathbf{x}} + \theta(x, z)\hat{\mathbf{y}} + w(x, z)\hat{\mathbf{z}}$. In this equivalence, $\theta \propto \rho'$ plays the role of the velocity in the $\hat{\mathbf{y}}$ -direction. The analogy between stratified flow and rotating flow in the linear limit is well-known; this analogy holds also for the fully nonlinear equations in the 3C-2D case. Note also that since the vorticity $\boldsymbol{\omega}$ is in the $\hat{\mathbf{y}}$ direction and density $\rho = \rho(x, z)$, then the potential vorticity $\boldsymbol{\omega} \cdot \nabla \rho$ is identically zero.

For an unbounded or periodic domain, the linear eigenmodes of (1-3) are Fourier modes (internal gravity waves)

$$(6) \quad \begin{pmatrix} \mathbf{v} \\ \theta \end{pmatrix} (\mathbf{x}, t) = \phi(\mathbf{k}) e^{i(\mathbf{k} \cdot \mathbf{x} - \sigma(\mathbf{k})t)}$$

where $\phi = (\widehat{\mathbf{v}}, \widehat{\theta})$. There are only two modes per wavevector as a result of the continuity constraint (3). Substituting (6) into the linearized form of the equations (1)-(3) leads to the dispersion relation for the internal gravity waves

$$(7) \quad \sigma(\mathbf{k}) = \frac{\pm N k_x}{k}$$

where $k = |\mathbf{k}|$. The eigenfunction ϕ^+ corresponding to σ^+ in (7) is

$$(8) \quad \phi^+ = \frac{1}{\sqrt{2}} \begin{pmatrix} k_z \\ k \\ -k_x \\ k \\ -i \end{pmatrix}.$$

The eigenfunction ϕ^- corresponding to σ^- in (7) is the complex conjugate of ϕ^+ . For the case $k_x = 0$, when the wavevector is parallel to the stratification axis, (8) are vertically sheared horizontal flow modes, with no vertical velocity.

In the (numerical) solution and analysis procedure, we expand the Fourier transformed velocity and density fluctuations in terms of the orthonormal, solenoidal eigenmodes

$$(9) \quad \begin{pmatrix} \widehat{\mathbf{v}} \\ \widehat{\theta} \end{pmatrix} (\mathbf{k}, t) = a^+(\mathbf{k}, t) \phi^+(\mathbf{k}) + a^-(\mathbf{k}, t) \phi^-(\mathbf{k}),$$

$$(10) \quad a^{(\alpha)}(\mathbf{k}, t) = \overline{\phi^{(\alpha)}} \cdot \begin{pmatrix} \widehat{\mathbf{v}} \\ \widehat{\theta} \end{pmatrix}$$

where $\alpha = -, +$. In the inviscid, unforced case ($\nu_0 = \kappa = \mathbf{f}_u = 0$), the evolution of $a^\alpha e^{i\sigma^{(\alpha)}t}$ results from nonlinear interactions only

$$(11) \quad \frac{d}{dt} \left(a^\alpha e^{i\sigma^\alpha t} \right) = -e^{i\sigma^\alpha t} \overline{\phi^\alpha} \cdot \begin{pmatrix} \widehat{\mathbf{v} \cdot \nabla \mathbf{v}} \\ \widehat{\mathbf{v} \cdot \nabla \theta} \end{pmatrix},$$

where $\widehat{\mathbf{v} \cdot \nabla \mathbf{v}}$ and $\widehat{\mathbf{v} \cdot \nabla \theta}$ are the Fourier transforms of the nonlinear terms.

3. The numerical simulations

Equations (1)-(4) are solved using a pseudo-spectral code in a periodic square. The linear terms are treated using an integrating factor technique, in effect removing them from the time-integration (as in (11) above). The viscous terms are treated with an integrating factor as well [12]. At each step of the third-order Runge-Kutta time-stepping scheme, the Fourier transformed velocity and density fields are projected onto the gravity wave solutions of the linearized equations. Each wave is multiplied by the proper integration factor, and the time step is chosen to sufficiently resolve the waves (*i.e.*, $\sigma \Delta t < N \Delta t < 0.2$). The projection onto the gravity waves automatically satisfies incompressibility and eliminates pressure. The

nonlinear terms $\mathbf{v} \cdot \nabla \mathbf{v}$ and $\mathbf{v} \cdot \nabla \theta$ are calculated in physical space and Fast Fourier transforms are used to go back and forth between Fourier and physical space.

In the simulations, the forcing spectrum $F(k)$ is Gaussian with standard deviation $s = 1$, given by

$$(12) \quad F(k) = \epsilon_f \frac{\exp(-0.5(k - k_f)^2/s^2)}{(2\pi)^{1/2}s}.$$

Typically, the spectrum $F(k)$ is truncated to include only a small number of wavenumbers, for example, for resolution 512^2 Fourier modes and $k_f = 96$, we truncate the force for $k < 88$ and $k > 104$. Based on the energy input rate ϵ_f and the peak wavenumber k_f of the force, we define the Froude number as

$$(13) \quad Fr = \frac{2(\epsilon_f k_f^2)^{1/3}}{N}$$

To vary the Froude number, we fix $\epsilon_f = 1$, $k_f = 96$ and $s = 1$, and vary the value of the Brunt-Vaisala frequency N .

The small-scale dissipation is modeled by a hyperviscosity $(-1)^{p+1}\nu(\nabla^2)^p\mathbf{u}$ with $p = 8$ in place of the normal viscosity term $\nu\nabla^2\mathbf{u}$. Likewise the dissipation of the density fluctuations is modeled by $(-1)^{p+1}\kappa(\nabla^2)^p\theta$ with $p = 8$ and $\kappa = \nu$ such that the Prandtl number ν/κ is unity. The purpose of using hyperviscosity, which turns on much more abruptly than the gradual increase of normal viscosity at small scales, is to eliminate as much as possible the effects of viscosity at intermediate scales, thus extending the turbulence inertial ranges. In general, we do not dealias in order to preserve more distance between k_f and the dissipation wavenumber k_d ; this distance insures a region of constant enstrophy flux for $k > k_f$. The use of hyperviscosity precludes accurate simulation of the tails of the spectra in any case. By maintaining a constant-flux of enstrophy in a wider interval $k_f > k > k_d$, we diminish the possibility that the hyperviscosity affects the large-scale dynamics. We have performed simulations dealiased using the 2/3 rule (see, *e.g.*, [13]) to verify that the large-scale spectra are independent of the tails.

4. Results

The results are summarized in Fig. (1), showing kinetic energy vs time for a series of runs with varying Froude number. The data is nondimensionalized by the nonlinear time scale $(\epsilon_f k_f^2)^{-1/3}$ and nonlinear energy $(\epsilon_f/k_f)^{2/3}$. The resolution is fixed at $R = 512^2$ Fourier modes, the energy input rate is $\epsilon_f = 1$ and the forcing is between $88 \leq k \leq 104$ ($k_f = 96$). For $Fr \rightarrow \infty$ ($N = 0$), the flow approaches 2D isotropic turbulence with a forward cascade of enstrophy and an inverse cascade of energy. After an initial period of nonlinear adjustment, the energy grows linearly in time, $dE/dt \approx 0.78\epsilon_f t$. The linear growth of energy reflects a constant flux at 78% of the energy input rate ϵ_f . In this finite system, the energy and enstrophy inertial ranges are not isolated from each other, evidenced by the fact that 22% of the energy input is transferred to scales smaller than the force, and dissipated by viscosity.

Fig. (1) shows that as the Froude number is decreased, the growth of energy is reduced, until at a value $Fr \approx 1$, the growth is completely suppressed. Furthermore, the nonlinear behavior of the curves in Fig. (1) for $Fr < \infty$ reflect non-constant

flux of energy to large scales. Decreasing the Froude number from $Fr \rightarrow \infty$ to $Fr \approx 1$ reduces the importance of nonlinear effects as compared to stratification effects. The value $Fr = 1$ indicates that nonlinear and stratification effects are equally important. For the case $Fr \approx 1$, there is no nonlinear transfer of energy to wavenumbers $k < k_f$, and the energy input is balanced by the dissipation. In other words, for $Fr \approx 1$ there is no inverse cascade of energy. For values of the Froude number $Fr < 1$, when stratification effects are stronger than nonlinear effects, one sees that the energy again grows in time. However, as we shall explain, the transfer of energy to large scales is quite different for the two regimes $Fr > 1$ and $Fr < 1$. The fact that the crossover behavior occurs at $Fr \approx 1$ supports the definition (13) based on the forcing parameters ϵ_f and k_f as the appropriate measure of the ratio of nonlinear and stratification effects.

Next we compare energy spectra for two runs, with $Fr = 10.5$ (Fig. 2) and $Fr = 0.5$ (Fig. 4), on either side of the critical value $Fr \approx 1$. The essential difference between these two runs can be understood by comparing the full spectrum $E(k)$, given by the solid line in each plot, to the one-dimensional spectrum $E(k_x = 0, k_z)$, given by the short dashed line in each plot. The spectrum $E(k_x = 0, k_z)$ represents the energy in horizontal motions, independent of k_x , with vertical shear. In Fig. 2, one sees that the spectrum $E(k_x = 0, k_z)$ is much smaller in magnitude than the full spectrum $E(k)$. In this case there is no obvious statistical difference between $E(k_x = 0, k_z)$ and $E(k_x, k_z = 0)$ (long dash), indicating that the energy spectrum is not far from isotropic at the large value $Fr = 10.5$. The time in Fig. 2 is $t(\epsilon_f k_f^2)^{1/3} = 2568$ when the kinetic energy has reached the value $K(k_f/\epsilon_f)^{2/3} = 338$ (off the scale in Fig. 1). It is important to note that the energy of all wavenumbers in Fig. 2 continues to grow for times up to $t(\epsilon_f k_f^2)^{1/3} = 2568$, such that the energy spectrum is everywhere unsteady; there is no quasi-steady range of wavenumbers as is observed in isotropic 2D turbulence forced at small scales (see, *e.g.*, [14, 15]). Figure 3 shows energy spectra at several times to illustrate the spectral evolution. At the latest time of our simulation, the energy spectrum of wavenumbers larger than the forcing wavenumbers scales close to $E(k) \propto k^{-3}$ up to $k \approx 20$, rather than the isotropic scaling $E(k) \propto k^{-5/3}$ [4, 14, 15]. Dimensional considerations lead immediately to the scaling $E(k) = C(Fr)N^2 k^{-3}$ (see *e.g.*, [7]). A new scale appears corresponding to wavenumber $k \approx 20$, which is the same order of magnitude as the Lumley-Ozmidov scale $k_o = (N^3/\epsilon_f)^{1/2}$ with value $k_o = 8$ in this case with $N = 4$. [17, 18]. The Lumley-Ozmidov wavenumber is an estimate for the wavenumber above which overturning can occur; it is considered a boundary between waves and turbulence.

In contrast, Fig. 4 ($Fr = 0.5$) shows that $E(k_x = 0, k_z)$ contains all of the energy in wavenumbers smaller than $k \approx 50$. Fig. 4 is at time $t(\epsilon_f k_f^2)^{1/3} = 6367$ when the kinetic energy has reached the value $K(k_f/\epsilon_f)^{2/3} = 312$ (off the scale in Fig. 1). The total energies in Figs. 2 and 4 are about the same, but the time of Fig. 4 is about 2.5 times longer than the time of Fig. 2. The anisotropic transfer to large scales for $Fr < 1$ is a much slower process than the more isotropic transfer associated with pure 2D turbulence and weakly stratified 2D turbulence. This may be because only a subset of nonlinear interactions is responsible for the anisotropic transfer. In Section 5 we show that resonant interactions account for a large part of the energy transfer at early times in a simulation forced by a single mode. It appears that another new length scale which we denote $l_N = 2\pi/k_N$ different from

the Lumley-Ozmidov scale, has been introduced into the problem for $Fr < 1$. The value of k_N is $k_N \approx 40$ in Fig. 4. We have not attempted to fit a power law to the data for $10 < k < 40$ in Fig. 4 because the fluctuations are too large and the range $10 < k < 40$ is too short. Even for longer times when the low wavenumbers $k < 10$ are populated, we feel that attempting to fit the data to a power law is not meaningful because of the large fluctuations in a single realization of a one-dimensional spectrum. Averaging over time is not possible unless a statistically steady state is established by low-wavenumber damping, something we wished to avoid in this study, but may pursue at a later date. A possible scaling for the range $k < k_N$ is $E(k) = C(Fr)N^2k^{-3}$ (see *e.g.*, [7]), though the spectra in Fig. 4 appear steeper than k^{-3} . It is interesting to note that the structure of the large-scale spectrum $E(k)$ in Fig. 4 is reminiscent of the spectrum of wind velocities measured by aircraft (see, *e.g.*, [16]). These atmospheric spectra scale approximately as $E(k) \propto k^{-3}$ in the range 800 – 2500 kilometers, and approximately as $E(k) \propto k^{-5/3}$ in the range 10 – 500 kilometers [16]. In 2D isotropic turbulence, the scaling $E(k) \propto k^{-3}$ appears at wavenumbers *larger* than scales corresponding to the scaling $E(k) \propto k^{-5/3}$ [4]. Figure 5 shows energy spectra for the case $Fr = 0.7$ just below critical, for which anisotropy is evident but the growth of energy is weak compared to the case $Fr = 0.5$ (see Fig. 1).

Fig. 6 shows scalar energy spectra $E_\rho(k)$ for $Fr = 10.5$ (solid) and $Fr = 0.5$ (dash) for the same times, respectively, as in Figs. 2 and 4. The line k^{-1} is shown for comparison. For $Fr = 10.5$, one sees that the data scale close to $E_\rho(k) \propto k^{-1}$ for $k > 20$. The pile-up of energy at $k = 20$ is evident in both the scalar and kinetic energy spectra for $Fr = 10.5$; there is also a pile-up of energy at $k = 1$ in the scalar spectrum, suggesting non-local transfer to density fluctuations at the largest scale in the system. For $Fr = 0.5$, the new length scale $l_N = 2\pi/k_N$ with $k_N \approx 40$ appears again in the density spectrum, with transition to a steeper spectrum $E_\rho(k)$ for $k < k_N$.

Portions of the physical space fields corresponding to the velocity and density spectra for $Fr = 10.5$ are shown, respectively, in Figs. 7 and 8 at a relatively early time $t(\epsilon_f k_f^2)^{1/3} = 805$ corresponding to the bottom spectrum in Fig. 3. The velocity vectors in Fig. 7 show small-scale vortices. Contours of the density fluctuations (Fig. 8) show that mass tends to be concentrated in the centers of the small-scale vortices. At later times, a regular, grid-like pattern of vortices emerges corresponding to the accumulation of energy near $k = 20$, and this pattern is also evident in the density field. For these long times, the velocity vectors show a predominance of clockwise vorticity. It will be interesting to further investigate the long-time structure of the density and velocity fields for $Fr \gg 1$, especially the sense of rotation of the vortices and the large-scale structure associated with the pile-up of scalar energy at $k = 1$.

In contrast to Figs. 7 and 8, portions of the physical space velocity and density fields for $Fr = 0.5$ show a layered structure. The velocity vectors in Fig. 9 are nearly horizontal, with vertical shear, and the density contours in Fig. 10 also show that a layered structure is starting to form in the density field. As time progresses, the layers merge and thicken, and the velocity is higher within each layer.

5. Discussion

A surprising feature of 2D stratified turbulence is the lack of energy transfer to large scales when $Fr \approx 1$. This is in contrast to the case of β -plane turbulence, in which there is always transfer of energy from small to large scales, but the nature of this transfer changes from isotropic to anisotropic at a scale $k_\beta \propto (\beta^3/\epsilon_f)^{1/5}$ [1]. The analogous scale for stratified flow is $k_o = (N^3/\epsilon_f)^{1/2}$, called the Lumley-Ozmidov wavenumber (see, *e.g.*, [17, 18]). The Lumley-Ozmidov wavenumber is an estimate for the wavenumber above which overturning can occur; it is considered a boundary between waves and turbulence, and is much higher than the dissipation wavenumber in our simulation with $Fr = 2(k_f/k_o)^{2/3} \approx 0.5$; $N = 80$ and $\epsilon_f = 1$ lead to $k_o \approx 715$. The scale $k_N \approx 40$ in Fig. 4 and 6 marking the transition to steeper spectra for $Fr = 0.5$ is clearly distinct from the Lumley-Ozmidov scale, and needs further investigation.

It is well understood that gravity wave oscillations have the effect of reducing, on average, the energy transfer between modes, except for resonant triad interactions with

$$(14) \quad \mathbf{k} + \mathbf{p} + \mathbf{q} = 0, \quad \sigma(\mathbf{k}) + \sigma(\mathbf{p}) + \sigma(\mathbf{q}) = 0$$

where $\sigma(\mathbf{k})$ is the frequency of the gravity wave given by (7). It is also well known that resonant triad interactions cannot directly transfer energy between two modes with nonzero frequency and another mode with zero frequency [19, 20]. From (7), the zero-frequency modes have $k_x = 0$, and are the only modes populated at wavenumbers $k < k_N$ in our simulations with $Fr < 1$ (Fig. 4). This zero manifold corresponds to horizontal flow with vertical shear (Fig. 9). It remains to explain, then, precisely how energy is transferred from fast to slow modes in 2D stratified flow, and many other dispersive wave systems including β -plane flow and rotating flow. For β -plane flow where the slow manifold consists of zonal flow, Newell [21] showed that resonant quartets of Rossby waves can transfer energy to the zonal flow. These resonant quartets involve two resonant triads. In rotating flow where the slow modes correspond to cyclonic vortical columns, Smith and Waleffe [2] found analogous resonant quartets of inertial waves that can transfer energy to the vortical columns. Another possible mechanism for the transfer of energy from fast to slow modes, discussed in [2], is a two-step (or multi-step) process whereby the resonant triads transfer energy towards the zero modes, and then nearly zero modes with $\sigma(\mathbf{k}) = O(Fr)$ transfer energy into exactly zero modes with $\sigma(\mathbf{k}) = 0$. Smith and Waleffe [2] considered deterministic forcing of a single mode in a resonant triad, and showed that energy is indeed transferred towards the zero manifold. Their analysis for rotating flow applies directly to the present case of 2D stratified flow after a rotation of the coordinate axes. Majda, Timofeyev and Vanden Eijnden [22] showed that the same result holds for stochastic forcing.

Here we present numerical evidence for resonant triadic transfer from fast to nearly zero modes, and then from nearly zero to exactly zero modes. We consider a simulation forced randomly by a single mode with wavevector $\mathbf{k} = (80, 40)$ and other parameter values $R = 512^2$, $\epsilon_f = 1$ and $N = 80$ such that $Fr \approx 0.5$. The long-time results are similar to those for the run with forcing in the wavenumber shell $88 < k_f < 104$, shown in Figs. 4, 6, 9 and 10. However, for forcing of a single mode, it is easy to compute all modes resonant with the force using (14),

and then to compare those resonant traces to the energy density $E(\mathbf{k})$. Contours of $E(\mathbf{k})$ are compared to the resonant traces in Figs. 11 and 12 for an early and later time, respectively, in the simulation at $Fr = 0.5$ forced randomly by a single mode with $\mathbf{k} = (80, 40)$. Fig. 11 shows that most of the energy at early times is concentrated on or near some parts of the resonant traces. At later times, the energy has accumulated near the slow manifold with $k_x = 0$.

Of the many higher-order mechanisms for anisotropic transfer from fast to slow modes in dispersive wave turbulence, the challenge is to determine which one(s) are essential. This is an issue fundamental to the mathematical theory of dispersive wave turbulence and to the modeling of geophysical flows. It is one of the main reasons to pursue test cases such as 2D stratified turbulence, where it is easier to study subsets of interactions, and results of such studies will be the subject of future reports.

Acknowledgements

LMS gratefully acknowledges the support of NSF under grant DMS-0071937 and SCREMS award DMS-9977384. LMS is also grateful for computing resources provided by the National Center for Supercomputing Applications at the University of Illinois.

References

- [1] A. Chekhlov, S.A. Orszag, S. Sukoriansky, B. Galperin & I. Staroselsky, "The effect of small-scale forcing on large-scale structures in two-dimensional flows," *Physica D* **98**, 321-334 (1996).
- [2] L. Smith & F. Waleffe, "Transfer of energy to two-dimensional large scales in forced, rotating three-dimensional turbulence," *Phys. Fluids* **11**, 1608-1622 (1999).
- [3] H.-P. Huang, B. Galperin & S. Sukoriansky, "Anisotropic spectra in two-dimensional turbulence on the surface of a sphere," *Phys. Fluids* **13**, 225-240 (2000).
- [4] R.H. Kraichnan, "Inertial ranges in two-dimensional turbulence," *Phys. Fluids* **10**, 1417-1423 (1967).
- [5] P.B. Rhines, "Waves and turbulence on a beta-plane," *J. Fluid Mech.* **69**, 417-443 (1975).
- [6] P. Bouruet-Aubertot, J. Sommeria & C. Staquet, "Breaking of standing internal gravity waves through two-dimensional instabilities," *J. Fluid Mech.* **285**, 265-301 (1995).
- [7] P. Bouruet-Aubertot, J. Sommeria & C. Staquet, "Stratified turbulence produced by internal wave breaking: two-dimensional numerical studies," *Dyn. Atmos. Oceans* **23**, 357-369 (1996).
- [8] Y.L. Lin & T.A. Wang, "Flow regimes and transient dynamics of two-dimensional stratified flow over an isolated mountain ridge," *J. Atmos. Sci.* **53**, 139-158 (1996).
- [9] H. Hanazaki, "A numerical study of nonlinear waves excited by an obstacle in the flow of stratified fluid," *J. Wind Eng. Ind. Aerod.* **46**, 283-288 (1993).
- [10] C. Staquet, "2-dimensional secondary instabilities in a strongly stratified shear layer," *J. Fluid Mech.* **296**, 73-126 (1995).
- [11] R. Salmon, "Lectures on Geophysical Fluid Dynamics," Oxford University Press, New York (1998).
- [12] R.S. Rogallo, "Numerical experiments in homogeneous turbulence," NASA Tech. Mem. 81835 (1981).
- [13] C. Canuto, M.Y. Hussaini, A. Quarteroni & T.A. Zang, *Spectral Methods in Fluid Dynamics*, Springer-Verlag, New York (1988).
- [14] L. Smith and V. Yakhot, "Finite-size effects in forced two-dimensional turbulence," *J. Fluid Mech.* **274**, 115-138 (1994).
- [15] J. Paret & P. Tabeling, "Intermittency in the two-dimensional inverse cascade of energy: experimental observations," *Phys. Fluids* **10**, 3126-3136 (1998).
- [16] G.D. Nastrom, K.S. Gage & W.H. Jasperson, "Kinetic energy spectrum of large-scale and mesoscale atmospheric processes," (Letter) *Nature* **310**, 36-38 (1984).
- [17] J.L. Lumley, "The spectrum of nearly inertial turbulence in a stably stratified fluid," *J. Atmos. Sci.* **21**, 99-102 (1964).
- [18] R.V. Ozmidov, "On the turbulent exchange in a stably stratified ocean," *Atmos. Ocean. Phys.* **1**, 493-497 (1965).
- [19] O.M. Phillips "The interaction trapping of internal gravity waves," *J. Fluid Mech.* **34**, 407-416 (1968).
- [20] P. Lelong & J.J. Riley "Internal wave-vortical mode interactions in strongly stratified flows," *J. Fluid Mech.* **232**, 1-19 (1991).
- [21] A.C. Newell, "Rossby wave packet interactions," *J. Fluid Mech.* **35**, 255-271 (1969).
- [22] A.J. Majda, I. Timofeyev & E. Vanden Eijnden, "Models for stochastic climate prediction," *PNAS* **96**, 14687-14691 (1999).

DEPARTMENTS OF MATHEMATICS & MECHANICAL ENGINEERING, UNIVERSITY OF WISCONSIN-MADISON, MADISON WI 53706

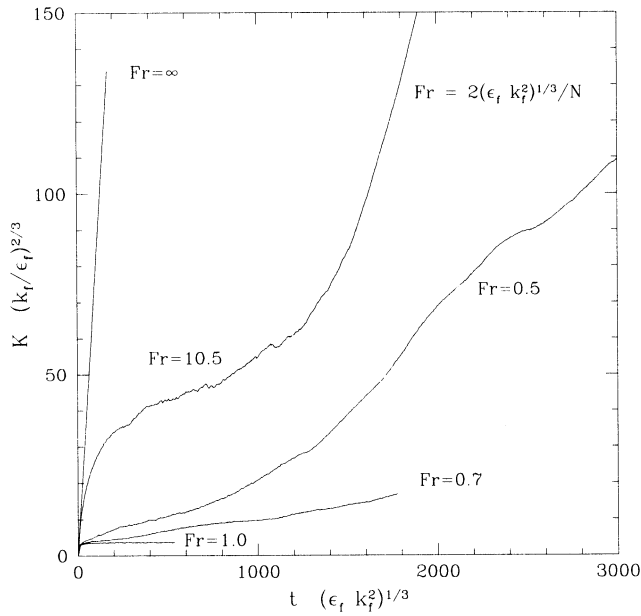


FIGURE 1. Energy vs time for varying Froude number: $R = 512^2$, $\epsilon_f = 1$, $k_f = 96$.

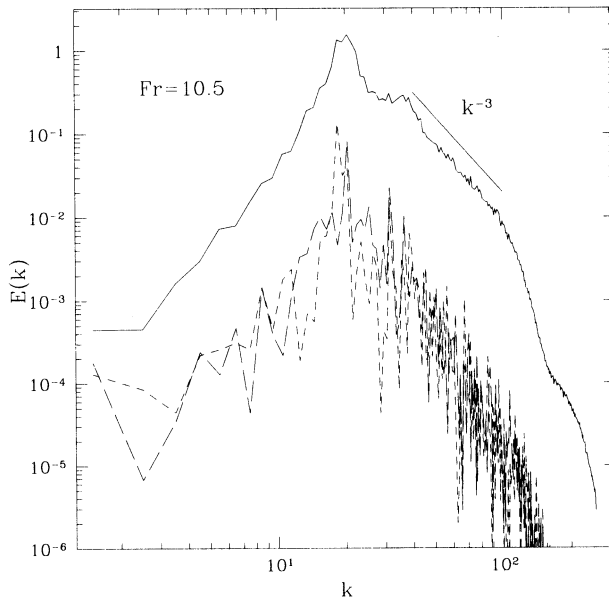


FIGURE 2. $E(k)$ vs k (solid), $E(k_z = 0, k_x)$ vs k_x (long dash), $E(k_x = 0, k_z)$ vs k_z (short dash): $Fr = 10.5$, $R = 512^2$, $\epsilon_f = 1$, $k_f = 96$, latest time $t(\epsilon_f k_f^2)^{1/3} = 2568$.

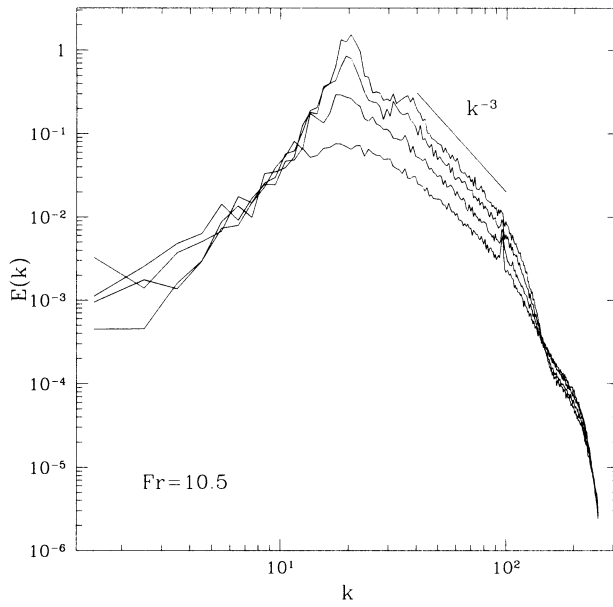


FIGURE 3. $E(k)$ vs k (top spectrum is at the latest time), $Fr = 10.5$, $R = 512^2$, $\epsilon_f = 1$, $k_f = 96$.

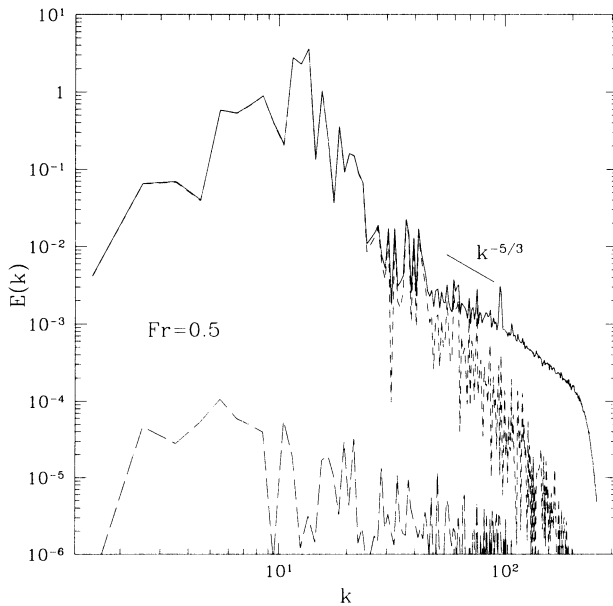


FIGURE 4. $E(k)$ vs k (solid), $E(k_z = 0, k_x)$ vs k_x (long dash), $E(k_x = 0, k_z)$ vs k_z (short dash): $Fr = 0.5$, $R = 512^2$, $\epsilon_f = 1$, $k_f = 96$, latest time $t(\epsilon_f k_f^2)^{1/3} = 6367$.

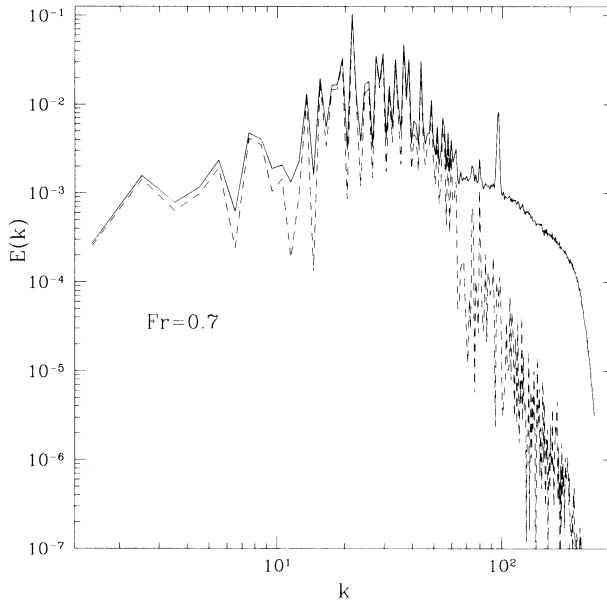


FIGURE 5. $E(k)$ vs k (solid), $E(k_x = 0, k_z)$ vs k_z (short dash): $Fr = 0.7$, $R = 512^2$, $\epsilon_f = 1$, $k_f = 96$, $t(\epsilon_f k_f^2)^{1/3} = 1782$.

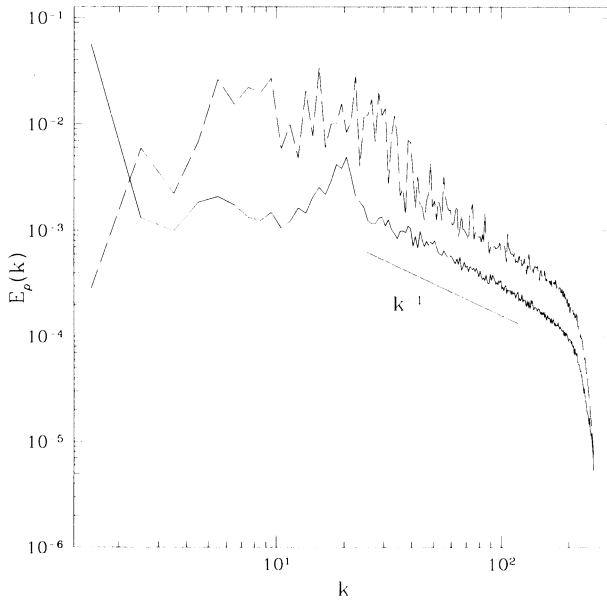


FIGURE 6. $E_\rho(k)$ vs k for $Fr = 10.5$ (solid, $t(\epsilon_f k_f^2)^{1/3} = 2568$) and $Fr = 0.5$ (dash, $t(\epsilon_f k_f^2)^{1/3} = 6367$): $R = 512^2$, $\epsilon_f = 1$, $k_f = 96$.

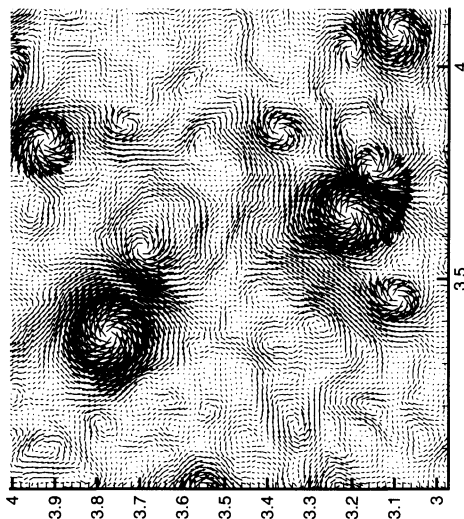


FIGURE 7. Velocity vectors in a portion of (x, z) physical space for $Fr = 10.5$ at time $t(\epsilon_f k_f^2)^{1/3} = 805$ corresponding to the bottom spectrum in Fig. 3.

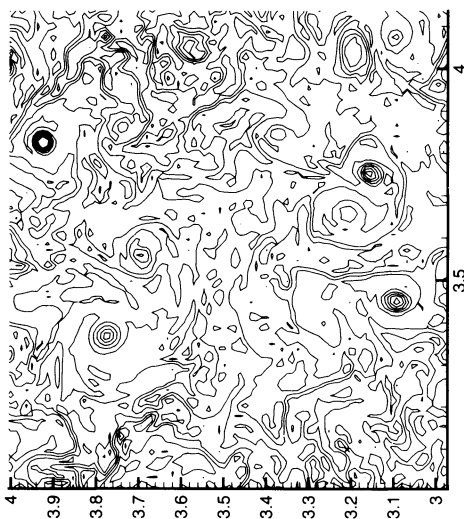


FIGURE 8. Contours of density in a portion of (x, z) physical space for $Fr = 10.5$ at time $t(\epsilon_f k_f^2)^{1/3} = 805$ corresponding to the bottom spectrum in Fig. 3.

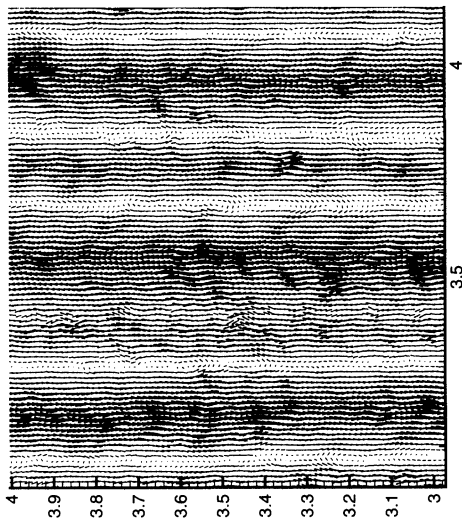


FIGURE 9. Velocity vectors in a portion of (x, z) physical space for $Fr = 0.5$ (same time as Fig. 4).

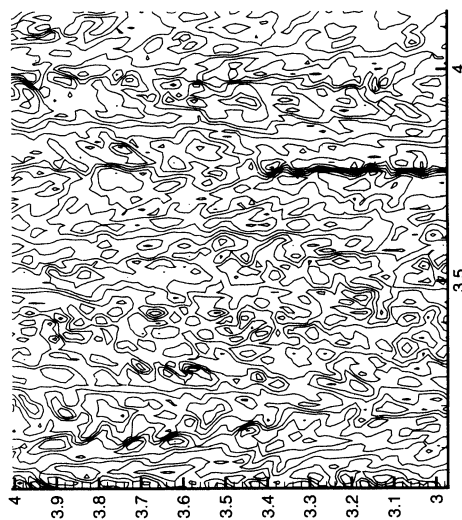


FIGURE 10. Contours of density in a portion of (x, z) physical space for $Fr = 0.5$ (same time as Fig. 4).

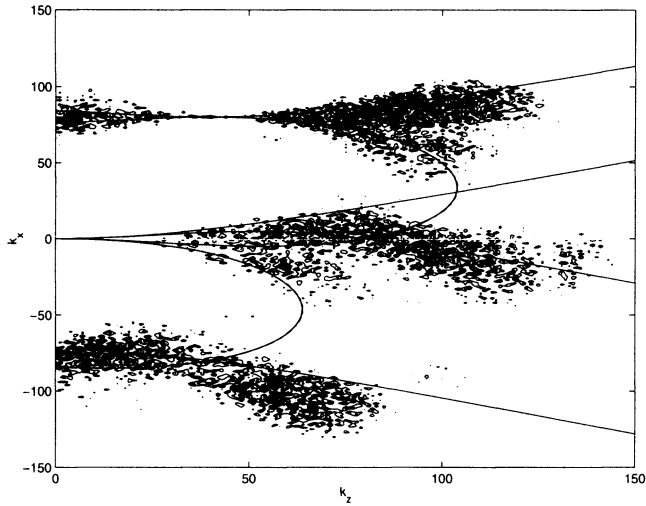


FIGURE 11. Contours of $E(\mathbf{k})$ and resonant traces at an early time [$t(\epsilon_f k_f^2)^{1/3} = 4.9$, $tN = 19.8$] for forcing of a single mode with $\mathbf{k} = (80, 40)$, $Fr = 0.5$.

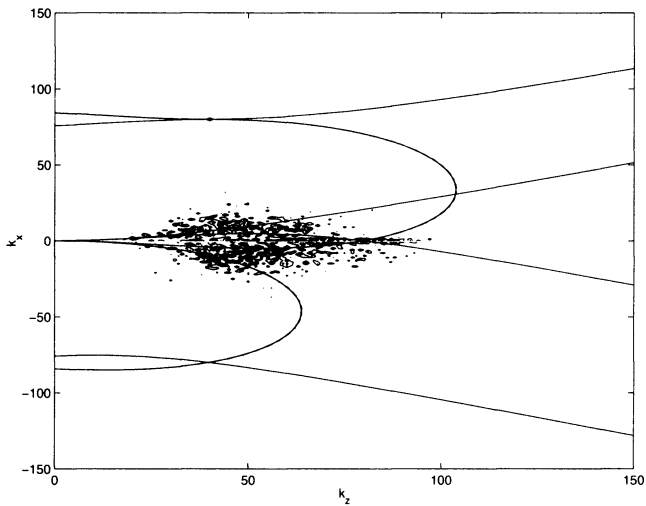


FIGURE 12. Contours of $E(\mathbf{k})$ and resonant traces at a later time [$t(\epsilon_f k_f^2)^{1/3} = 28.7$, $tN = 114.8$] for forcing of a single mode with $\mathbf{k} = (80, 40)$, $Fr = 0.5$.

This page intentionally left blank

Turbulence of one-dimensional weakly nonlinear dispersive waves

V. E. Zakharov, P. Guyenne, A. N. Pushkarev, and F. Dias

ABSTRACT. The turbulence of weakly nonlinear dispersive waves is studied by numerically integrating a three-parameter one-dimensional model equation. In particular the validity of weak turbulence theory is assessed. The predicted power-law solutions are explicitly determined and then compared with the numerical results. For both signs of nonlinearity, it is shown that the weakly turbulent regime is strongly influenced by the presence of coherent structures. These are wave collapses and quasisolitons.

1. Introduction

The weak turbulence theory developed by Zakharov [8] is a tool for obtaining the shape of frequency spectra in problems dealing with weakly nonlinear dispersive waves. The applications of this theory range from water waves in hydrodynamics to ion-acoustic waves in plasma physics. The weak turbulence theory is based on a hamiltonian formulation of the problem where only resonant interactions between weakly nonlinear waves are taken into account. It is then possible to derive approximate equations by performing perturbation expansions in terms of the nonlinearity parameter. Although the theory was developed more than thirty years ago, few proofs, either experimental or numerical, have been given to assess its validity (e.g. [7]). Recently, Majda et al. [5] proposed a one-dimensional model equation as a basis to check the validity of weak turbulence theory. Numerical computations on this model have been reported in [1], [3], [5] and [9]. In this paper we summarize the most important numerical results on this equation, which depends on three parameters, and show that the weakly turbulent regime is strongly influenced by the presence of coherent structures, namely wave collapses and quasisolitons.

1991 *Mathematics Subject Classification.* Primary 76F55; Secondary 60H15.

Key words and phrases. weak turbulence, Kolmogorov spectra, water waves, wave collapse, quasisoliton.

The first and the third authors were supported in part by US Army, under the grant DACA 39-99-C-0018, and by ONR, under the grant N00014-98-1-0439. The second and fourth authors were supported in part by DGA, under the contract ERS 981135. The four authors were supported as well by NATO, under the Linkage Grant OUTF.LG 970583.

2. One-dimensional model equation

The following three-parameter nonlinear dispersive equation was proposed by Majda et al. [5]:

$$(2.1) \quad i \frac{\partial \hat{\psi}_k}{\partial t} = \omega_k \hat{\psi}_k + \int T_{123k} \hat{\psi}_1 \hat{\psi}_2 \hat{\psi}_3^* \delta(k_1 + k_2 - k_3 - k) dk_1 dk_2 dk_3.$$

In equation (2.1), which has been written in Fourier space, $\hat{\psi}_k$ denotes the k -th component in the Fourier decomposition of the complex wave field $\psi(x, t)$ and $(*)$ stands for complex conjugation. Equation (2.1) depends on three parameters. The first parameter, α , is related to the linear frequency $\omega_k = |k|^\alpha$. The second parameter, β , is related to the interaction coefficient

$$(2.2) \quad T_{123k} = \lambda |k_1 k_2 k_3 k|^{\beta/4}.$$

The third parameter, λ , which also appears in the interaction coefficient (2.2) and is equal to ± 1 , governs the balance between dispersive and nonlinear effects. One can use the terminology *focusing* for $\lambda = -1$ and *defocusing* for $\lambda = +1$. The system possesses two important first integrals, the Hamiltonian

$$H = \int \omega_k |\hat{\psi}_k|^2 dk + \frac{1}{2} \int T_{123k} \hat{\psi}_1 \hat{\psi}_2 \hat{\psi}_3^* \hat{\psi}_k^* \delta(k_1 + k_2 - k_3 - k) dk_1 dk_2 dk_3 dk$$

and the wave action (or number of particles)

$$N = \int |\hat{\psi}_k|^2 dk.$$

Equation (2.1) describes four-wave resonant interactions satisfying

$$(2.3) \quad k_1 + k_2 = k_3 + k$$

$$(2.4) \quad \omega_1 + \omega_2 = \omega_3 + \omega_k.$$

It can be shown that when $\alpha < 1$ the system (2.3)-(2.4) has nontrivial solutions and that dominant interactions occur between four waves. In all computations the parameter α has been set equal to $1/2$. This case mimics gravity waves in deep water, whose dispersion relation is given by $\omega_k = (gk)^{1/2}$, where g is the acceleration due to gravity. Computations for $\lambda = +1$ were performed by Majda et al. [5]. Computations for $\lambda = \pm 1$ were recently performed by Cai et al. [1] and by Zakharov et al. [9].

3. Kolmogorov-type spectra

For a weak nonlinearity, Zakharov's theory [10] leads to a kinetic equation for the two-point correlation function $n_k = \langle |\hat{\psi}_k|^2 \rangle$:

$$\begin{aligned} \frac{\partial n_k}{\partial t} &= 4\pi \int |T_{123k}|^2 (n_1 n_2 n_3 + n_1 n_2 n_k - n_1 n_3 n_k - n_2 n_3 n_k) \\ &\quad \times \delta(\omega_1 + \omega_2 - \omega_3 - \omega_k) \delta(k_1 + k_2 - k_3 - k) dk_1 dk_2 dk_3. \end{aligned}$$

The two main hypotheses for deriving the kinetic equation are the assumptions of gaussianity and of random phases. The stationary Kolmogorov-type solutions are given by

$$(3.1) \quad n_k = a_1 |Q|^{1/3} k^{-2\beta/3-1+\alpha/3}$$

$$(3.2) \quad n_k = a_2 |P|^{1/3} k^{-2\beta/3-1}$$

TABLE 1. Slope and flux sign for the Kolmogorov-type solutions (3.1)-(3.2). The dispersion parameter α is equal to $1/2$.

β	-1	-3/4	-1/2	-1/4	0	+3
power of k in (3.1)	-1/6	-1/3	-1/2	-2/3	-5/6	-17/6
sign of Q	+	+	0	-	-	-
power of k in (3.2)	-1/3	-1/2	-2/3	-5/6	-1	-3
sign of P	-	0	+	+	+	+

and are associated respectively with a particle flux Q and an energy flux P . The coefficients a_1 and a_2 denote the dimensionless Kolmogorov constants. It is important to emphasize that these solutions do not depend on the sign of nonlinearity λ . Such solutions can be written for all values of β and $\alpha < 1$. But there is a physical argument which plays a crucial role in deciding the realizability of the Kolmogorov-type spectra. Suppose that pumping is performed at some frequencies ω_k around ω_f and that damping operates at frequencies ω_k near zero as well as at frequencies ω_k much larger than ω_f . Weak turbulence theory then states that the energy is expected to flow from ω_f to higher ω_k 's (direct cascade with $P > 0$) while the particles mainly head for lower ω_k 's (inverse cascade with $Q < 0$). Accordingly, we need to evaluate the fluxes in order to select, among the rich family of power laws (3.1) and (3.2), those which are likely to result from numerical simulations of equation (2.1) with damping and forcing. Only the cases

$$\beta < -3/2 \quad \text{and} \quad \beta > 2\alpha - 3/2$$

i.e.:

$$\beta < -3/2 \quad \text{and} \quad \beta > -1/2 \quad \text{if} \quad \alpha = 1/2$$

are relevant because they correspond to a particle flux towards large scales ($Q < 0$) and to an energy flux towards small scales ($P > 0$). The signs of the fluxes are shown in Table 1 for $\alpha = 1/2$ [9]. Computations are performed in the range $\beta > -1/2$, which includes the case of simple cubic nonlinearity ($\beta = 0$) and the case of gravity waves ($\beta = 3$).

4. Solitons, collapses and quasisolitons

The numerical results presented below show that the weakly turbulent regime is strongly influenced by the presence of coherent structures. These are solitons, quasisolitons or collapses. The existence of solitons depends on the parameter λ . Looking for soliton solutions of (2.1) of the form

$$\hat{\psi}_k(t) = e^{i(\Omega - kV)t} \hat{\phi}_k$$

with Ω and V constant leads to

$$(4.1) \quad \hat{\phi}_k = -\frac{1}{\Omega - kV + \omega_k} \int T_{123k} \hat{\phi}_1 \hat{\phi}_2 \hat{\phi}_3^* \delta(k_1 + k_2 - k_3 - k) dk_1 dk_2 dk_3.$$

For $\alpha < 1$, the condition $\Omega - kV + |k|^\alpha \neq 0, \forall k \in \mathbb{R}$, implies that the propagating speed V is zero. Rewriting equation (4.1) in variational form:

$$\delta(H + \Omega N) = 0$$

one can conclude that ‘stationary’ solitons can exist only if $\lambda = -1$. In that case an equilibrium between nonlinear and dispersive effects is possible. As for nonlinear Schrödinger-type equations, the linear stability criterion for solitons is given by $\partial N/\partial \Omega > 0$ [4]. In our case this gives

$$\beta < \alpha - 1$$

i.e.

$$\beta < -1/2 \quad \text{if} \quad \alpha = 1/2.$$

Therefore the solitons are unstable in the regime of interest.

In view of this result, it is natural to look at the formation of collapses. They are typically described by self-similar solutions of the form

$$\hat{\psi}_k(t) = (t_0 - t)^{p+i\epsilon} \chi(\xi)$$

where

$$\xi = k(t_0 - t)^{1/\alpha}, \quad p = \frac{\beta - \alpha + 2}{2\alpha}, \quad \epsilon = \text{arbitrary constant}.$$

An analysis of the convergence of the Hamiltonian and of the wave action integral as $t \rightarrow t_0$ shows that necessary conditions for collapses to exist when $\alpha = 1/2$ are $\beta > -1/2$ for $\lambda = -1$, which coincides with the soliton instability criterion, and $\beta > 0$ for $\lambda = +1$. In spectral space, the self-similar solution behaves at $t = t_0$ like

$$(4.2) \quad n_k \simeq k^{-\beta+\alpha-2}$$

which is analogous to Phillips spectrum for deep water gravity waves [6].

In the case $\lambda = +1$, quasisolitons can exist. These are approximate solutions of equation (4.1) which look like envelope solitons. In the limit of a narrow spectrum centered at $k = k_m$, such as $\Omega - k_m V + k_m^\alpha \neq 0$, these quasisolitons are given by

$$(4.3) \quad \psi(x, t) \simeq \phi(x - Vt) e^{i\Omega t + ik_m(x - Vt)}$$

with ϕ , Ω and V given by

$$\phi(\xi) = \sqrt{\frac{\alpha(1 - \alpha)}{k_m^{\beta-\alpha+2}} \frac{\kappa}{\cosh(\kappa \xi)}}, \quad \kappa = |k - k_m| \ll k_m$$

$$\Omega = -(1 - \alpha) k_m^\alpha - \frac{1}{2} \alpha (1 - \alpha) k_m^{\alpha-2} \kappa^2, \quad V = \alpha k_m^{\alpha-1}.$$

When κ/k_m is small, the quasisolitons look almost like true solitons and can persist for a long time. They can play an important role in weak turbulence. When κ/k_m is large, the quasisolitons can become unstable and develop into wave collapse.

5. Numerical results

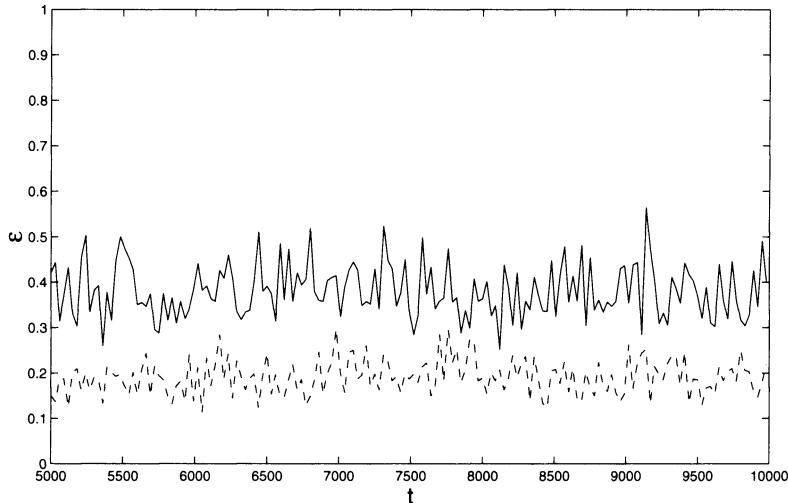
The numerical computations are performed by adding to equation (2.1) a source term in a narrow spectral band as well as a damping term containing a wave action sink at large scales and an energy sink at small scales:

$$(5.1) \quad i \frac{\partial \hat{\psi}_k}{\partial t} = \omega_k \hat{\psi}_k + \int T_{123k} \hat{\psi}_1 \hat{\psi}_2 \hat{\psi}_3^* \delta(k_1 + k_2 - k_3 - k) dk_1 dk_2 dk_3 + i (F_k + D_k) \hat{\psi}_k$$

with

$$F_k = \sum_j f_j \delta(k - k_j) \quad \text{and} \quad D_k = -\nu^- |k|^{-d^-} - \nu^+ |k|^{d^+}.$$

FIGURE 1. Level of nonlinearity as a function of time. The parameters are $\alpha = 1/2$, $\beta = 0$ and $\lambda = +1$ (solid line); $\lambda = -1$ (dashed line).



A pseudospectral code with 2048 modes is used to integrate equation (5.1). Details can be found in [9].

5.1. Numerical results for $\beta = 0$, $\lambda = \pm 1$. The study is restricted to the direct cascade. Typical initial conditions are given by random noise. Simulations are run until a quasi-steady regime is established which is characterized by small fluctuations of the energy and the number of particles around some mean value. Then time averaging begins and continues for a length of time which significantly exceeds the characteristic time scale of the slowest harmonic from the inertial range (free of the source and the sink). In turn, the time-step of the integration has to provide, at least, accurate enough resolution of the fastest harmonic in the system. As our experiments show, one has to use an even smaller time-step than defined by the last condition: the presence of fast nonlinear events in the system requires the use of a time-step $\Delta t = 0.005$, which is 40 times smaller than the smallest linear frequency period. Time averaging with such a small time step leads to a computationally time-consuming procedure despite the one-dimensionality of the problem. Figure 1 shows the time evolution of the average nonlinearity ϵ , which is defined as the ratio of the nonlinear part to the linear part of the Hamiltonian, each part being calculated over the whole field. Of course, this definition does not really make sense when external forces are applied but it provides a relatively good estimation of the level of nonlinearity once the system reaches the steady state. The mean values of ϵ are 0.4 when $\lambda = +1$ and 0.2 when $\lambda = -1$. They are relatively small. Thus, the condition of small nonlinearity required by the theory holds for both systems. However the theory cannot explain the difference in the values of ϵ , since the same forcing is imposed in both systems.

The difference between the focusing and the defocusing cases is even more obvious when one looks at the dissipation rates of particles and quadratic energy

TABLE 2. $\alpha = 1/2, \beta = 0$. Time-averaged values of the wave action, quadratic energy and corresponding fluxes in the stationary state.

λ	N	E	Q^-	Q^+	P^-	P^+
+1	3	19	0.1957	0.0090	0.276	0.258
-1	1	9	0.0098	0.0478	0.014	1.430

for small wavenumbers:

$$Q^- = 2 \int_{k < k_f} \nu^- |k|^{-d^-} |\hat{\psi}_k|^2 dk, \quad P^- = 2 \int_{k < k_f} \nu^- |k|^{-d^-} \omega_k |\hat{\psi}_k|^2 dk$$

and for large wavenumbers

$$Q^+ = 2 \int_{k > k_f} \nu^+ |k|^{d^+} |\hat{\psi}_k|^2 dk, \quad P^+ = 2 \int_{k > k_f} \nu^+ |k|^{d^+} \omega_k |\hat{\psi}_k|^2 dk$$

where k_f is the characteristic wavenumber of forcing. Their time-averaged values in the stationary state are collected in Table 2.

The stationary isotropic spectra of turbulence are displayed in Figures 2 and 3. Again the results depend on the value of λ . For both cases the theoretical spectrum provides a higher level of turbulence than the observed one. In the focusing case ($\lambda = -1$) this difference is almost of one order of magnitude but the slope fits the predicted value -1 well. For $\lambda = +1$, the observed spectrum almost coincides with the weak turbulence one at low frequencies and then decays faster at higher wavenumbers. In this range, the slope is close to $-5/4$ as found in [5]. Note that a new derivation of the Majda et al.'s spectrum is proposed in [9].

Comparison of the turbulence levels and fluxes of particles Q^\pm for both signs of nonlinearity leads to a paradoxal result. At $\lambda = -1$ the total number of particles is three times less than at $\lambda = +1$, while the dissipation rate of particles is higher by one order of magnitude. It can be explained only by the presence in this case of a much more powerful mechanism of nonlinear interactions, which provides very fast wave particles transport to high frequencies. In our opinion, this mechanism is wave collapse. Sporadic collapsing events developing on top of the weak turbulence background could send most of particles to high wavenumbers without violation of energy conservation, because in each self-similar collapse structure the amount of total energy is zero. Such a collapsing event is shown in Figure 4. Note that the contribution of collapses to the high-frequency spectrum is weak because they produce a Phillips-type spectrum which decays very fast as $k \rightarrow +\infty$. In our case, equation (4.2) becomes

$$n_k \simeq k^{-3/2}.$$

Hence, only the weakly turbulent component k^{-1} survives at large wavenumbers. The coexistence of wave collapse and weak turbulence was also observed in [2] for the nonlinear Schrödinger equation.

At $\lambda = +1$ the picture of turbulence matches the weak turbulence prediction both quantitatively and qualitatively. Meanwhile, the spectrum at high k 's is steeper than the theoretical one. So far we cannot give a consistent explanation of this fact. We can just guess that it is somehow connected with quasisolitons.

FIGURE 2. $\beta = 0, \lambda = -1$. Stationary and isotropic spectra n_k vs. wavenumber. We compare the computed spectrum with the predicted one of Kolmogorov-type $n_k = c k^{-1}$ with $c = a_2 P^{1/3}$ (straight line).

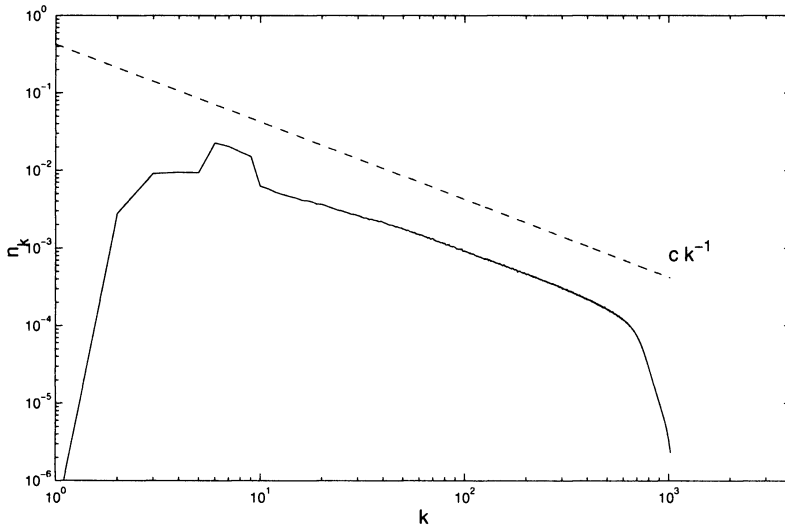


FIGURE 3. $\beta = 0, \lambda = +1$. Stationary and isotropic spectra n_k vs. wavenumber. We compare the computed spectrum with the predicted one of Kolmogorov-type $n_k = c k^{-1}$ with $c = a_2 P^{1/3}$ (straight line).

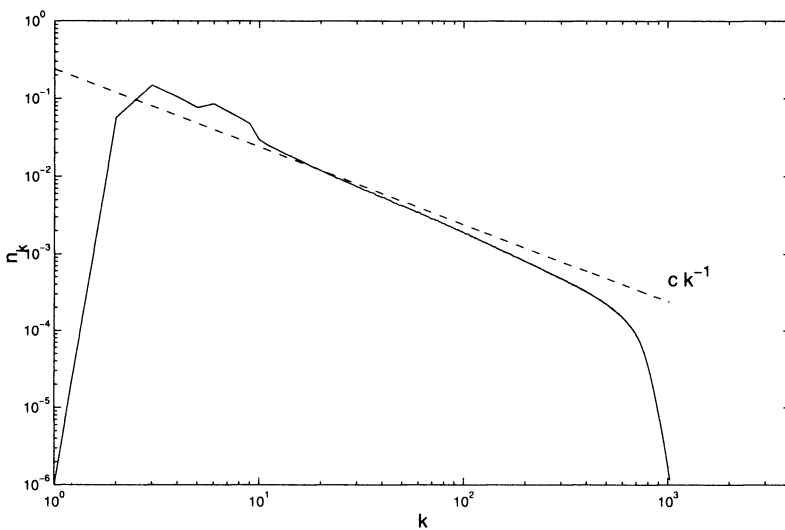
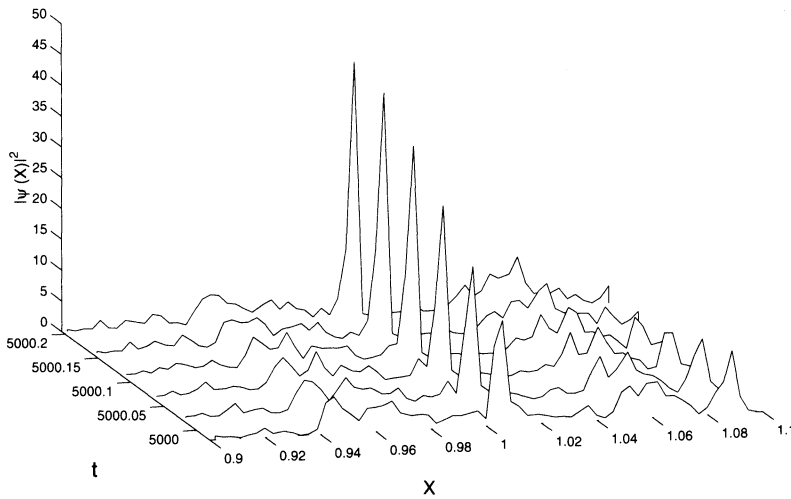


FIGURE 4. $\beta = 0, \lambda = -1$. Evolution towards collapse at $x \simeq 1$ between $t = 4999.980$ and $t = 5000.205$.



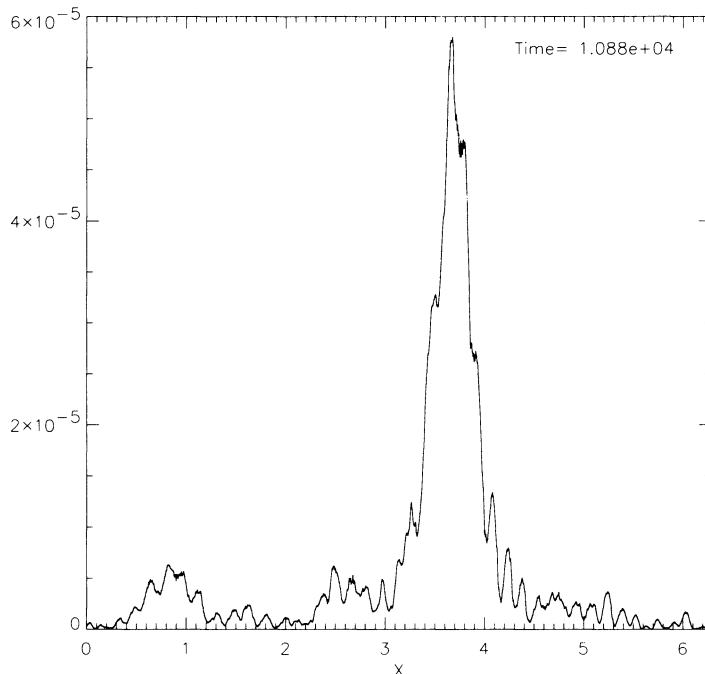
5.2. Numerical results for $\beta = 3, \lambda = +1$. Computations were performed with $\beta = 3$ because this case is analogous to gravity water waves. Moreover the strength of the interactions is larger than in the case $\beta = 0$.

Equation (5.1) was again integrated numerically over long times. The system is first separated into several soliton-like structures and low-amplitude quasi-linear waves. Processes of mutual interactions slowly redistribute the number of waves in a way leading to the growth of initially bigger quasisolitons and the decay of initially smaller quasisolitons. The final state then consists of one big quasisoliton moving in a sea of small quasilinear waves as shown in Figure 5. The shape of the quasisoliton is well described by the formula (4.3). The reader is referred to our paper [9] for more detail on quasisolitons. This phenomenon is similar to the ‘droplet’ effect observed in the non-integrable nonlinear Schrödinger equation [11]. The soliton solution turns out to be a statistical attractor for the system: long time evolution leads to the condensation of the number of particles into a single soliton which minimizes the Hamiltonian.

6. Conclusions

In conclusion, the numerical results show a discrepancy with the theory, which is mainly due to the presence of localised coherent structures, collapses in the focusing case ($\lambda = -1$) and quasisolitons in the defocusing case ($\lambda = +1$). In other words, both mechanisms, weak turbulence and coherent structures, are present and lead to a complex mixed picture. The discrepancy between numerics and theory may also be due to the sparsity of resonances in one dimension and the numerical discretization. Four-wave interactions are not as efficient and localised structures become dominant. Therefore equation (2.1) is not such a good model to assess the validity of weak turbulence theory.

FIGURE 5. $\beta = 3, \lambda = +1$. Snapshot of a quasisoliton at $x \simeq 3.7$ and $t = 10880$.



References

- [1] D. Cai, A. J. Majda, D. W. McLaughlin, E. G. Tabak, *Spectral bifurcations in dispersive wave turbulence*, Proc. Nat. Acad. Sci. **96** (1999), 14216–14221.
- [2] S. Dyachenko, A. C. Newell, A. Pushkarev, V. E. Zakharov, *Optical turbulence: weak turbulence, condensates and collapsing filaments in the nonlinear Schrödinger equation*, Physica D **57** (1992), 96–160.
- [3] P. Guyenne, V. E. Zakharov, A. Pushkarev, F. Dias, *Turbulence d'ondes dans des modèles unidimensionnels*, C. R. Acad. Sci. Paris, Série IIb **328** (10) (2000), 757–762.
- [4] E. A. Kuznetsov, A. M. Rubenchik, V. E. Zakharov, *Soliton stability in plasmas and hydrodynamics*, Phys. Rep. **142** (1986), 103–165.
- [5] A. J. Majda, D. W. McLaughlin, E. G. Tabak, *A one-dimensional model for dispersive wave turbulence*, J. Nonlinear Sci. **6** (1997), 9–44.
- [6] O. M. Phillips, *The dynamics of the upper ocean*, Cambridge Univ. Press, 1977.
- [7] A. N. Pushkarev, V. E. Zakharov, *Turbulence of capillary waves*, Phys. Rev. Lett. **76** (1996), 3320–3323.
- [8] V. E. Zakharov, *Stability of periodic waves of finite amplitude on the surface of deep fluid*, J. Appl. Mech. Tech. Phys. **2** (1968), 190–194.
- [9] V. E. Zakharov, P. Guyenne, A. Pushkarev, F. Dias, *Wave turbulence in one-dimensional models*, Physica D **152–153** (2001), 573–619.
- [10] V. E. Zakharov, V. S. L'vov, G. Falkovich, *Kolmogorov Spectra of Turbulence I*, Springer-Verlag, 1992.
- [11] V. E. Zakharov, A. N. Pushkarev, V. F. Shvets, V. V. Yankov, *Soliton turbulence*, JETP Lett. **48** (2) (1988), 83–87.

LANDAU INSTITUTE FOR THEORETICAL PHYSICS, MOSCOW, RUSSIA AND DEPARTMENT OF
MATHEMATICS, UNIVERSITY OF ARIZONA, USA

E-mail address: zakharov@itp.ac.ru

INSTITUT NON LINÉAIRE DE NICE, 1361 ROUTE DES LUCIOLES, 06560 SOPHIA ANTIPOLIS,
FRANCE

E-mail address: guyenne@cmla.ens-cachan.fr

LANDAU INSTITUTE FOR THEORETICAL PHYSICS, MOSCOW, RUSSIA AND DEPARTMENT OF
MATHEMATICS, UNIVERSITY OF ARIZONA, USA

E-mail address: andrei@imap3.asu.edu

CENTRE DE MATHÉMATIQUES ET DE LEURS APPLICATIONS, FRANCE

E-mail address: dias@cmla.ens-cachan.fr

Selected Titles in This Series

(Continued from the front of this publication)

- 258 **Karsten Grove, Ib Henning Madsen, and Erik Kjær Pedersen, Editors**, Geometry and topology: Aarhus, 2000
- 257 **Peter A. Cholak, Steffen Lempp, Manuel Lerman, and Richard A. Shore, Editors**, Computability theory and its applications: Current trends and open problems, 2000
- 256 **Irwin Kra and Bernard Maskit, Editors**, In the tradition of Ahlfors and Bers: Proceedings of the first Ahlfors-Bers colloquium, 2000
- 255 **Jerry Bona, Katarzyna Saxton, and Ralph Saxton, Editors**, Nonlinear PDE's, dynamics and continuum physics, 2000
- 254 **Mourad E. H. Ismail and Dennis W. Stanton, Editors**, q -series from a contemporary perspective, 2000
- 253 **Charles N. Delzell and James J. Madden, Editors**, Real algebraic geometry and ordered structures, 2000
- 252 **Nathaniel Dean, Cassandra M. McZeal, and Pamela J. Williams, Editors**, African Americans in Mathematics II, 1999
- 251 **Eric L. Grinberg, Shiferaw Berhanu, Marvin I. Knopp, Gerardo A. Mendoza, and Eric Todd Quinto, Editors**, Analysis, geometry, number theory: The Mathematics of Leon Ehrenpreis, 2000
- 250 **Robert H. Gilman, Editor**, Groups, languages and geometry, 1999
- 249 **Myung-Hwan Kim, John S. Hsia, Yoshiyuki Kitaoka, and Rainer Schulze-Pillot, Editors**, Integral quadratic forms and lattices, 1999
- 248 **Naihuan Jing and Kailash C. Misra, Editors**, Recent developments in quantum affine algebras and related topics, 1999
- 247 **Lawrence Wasson Baggett and David Royal Larson, Editors**, The functional and harmonic analysis of wavelets and frames, 1999
- 246 **Marcy Barge and Krystyna Kuperberg, Editors**, Geometry and topology in dynamics, 1999
- 245 **Michael D. Fried, Editor**, Applications of curves over finite fields, 1999
- 244 **Leovigildo Alonso Tarrío, Ana Jeremías López, and Joseph Lipman**, Studies in duality on noetherian formal schemes and non-noetherian ordinary schemes, 1999
- 243 **Tsit Yuan Lam and Andy R. Magid, Editors**, Algebra, K -theory, groups, and education, 1999
- 242 **Bernhelm Booss-Bavnbek and Krzysztof Wojciechowski, Editors**, Geometric aspects of partial differential equations, 1999
- 241 **Piotr Pragacz, Michał Szurek, and Jarosław Wiśniewski, Editors**, Algebraic geometry: Hirzebruch 70, 1999
- 240 **Angel Carocca, Víctor González-Aguilera, and Rubí E. Rodríguez, Editors**, Complex geometry of groups, 1999
- 239 **Jean-Pierre Meyer, Jack Morava, and W. Stephen Wilson, Editors**, Homotopy invariant algebraic structures, 1999
- 238 **Gui-Qiang Chen and Emmanuele DiBenedetto, Editors**, Nonlinear partial differential equations, 1999
- 237 **Thomas Branson, Editor**, Spectral problems in geometry and arithmetic, 1999
- 236 **Bruce C. Berndt and Fritz Gesztesy, Editors**, Continued fractions: From analytic number theory to constructive approximation, 1999
- 235 **Walter A. Carnielli and Itala M. L. D'Ottaviano, Editors**, Advances in contemporary logic and computer science, 1999

For a complete list of titles in this series, visit the
AMS Bookstore at www.ams.org/bookstore/.

This page intentionally left blank

Advances in Wave Interaction and Turbulence

Paul A. Milewski, Leslie M. Smith, Fabian Waleffe, and Esteban G. Tabak, Editors

We often think of our natural environment as being composed of very many interacting particles, undergoing individual chaotic motions, of which only very coarse averages are perceptible at scales natural to us. However, we could as well think of the world as being made out of individual waves. This is so not just because the distinction between waves and particles becomes rather blurred at the atomic level, but also because even phenomena at much larger scales are better described in terms of waves rather than of particles: It is rare in both fluids and solids to observe energy being carried from one region of space to another by a given set of material particles; much more often, this transfer occurs through chains of particles, neither of them moving much, but each communicating with the next, and hence creating these immaterial objects we call waves.

Waves occur at many spatial and temporal scales. Many of these waves have small enough amplitude that they can be approximately described by linear theory. However, the joint effect of large sets of waves is governed by nonlinear interactions which are responsible for huge cascades of energy among very disparate scales. Understanding these energy transfers is crucial in order to determine the response of large systems, such as the atmosphere and the ocean, to external forcings and dissipation mechanisms which act on scales decades apart.

The field of wave turbulence attempts to understand the average behavior of large ensembles of waves, subjected to forcing and dissipation at opposite ends of their spectrum. It does so by studying individual mechanisms for energy transfer, such as resonant triads and quartets, and attempting to draw from them effects that should not survive averaging.

This book presents the proceedings of the AMS-IMS-SIAM Joint Summer Research Conference on Dispersive Wave Turbulence held at Mt. Holyoke College (MA). It drew together a group of researchers from many corners of the world, in the context of a perceived renaissance of the field, driven by heated debate about the fundamental mechanism of energy transfer among large sets of waves, as well as by novel applications—and old ones revisited—to the understanding of the natural world. These proceedings reflect the spirit that permeated the conference, that of friendly scientific disagreement and genuine wonder at the rich phenomenology of waves.

ISBN 0-8218-2714-6



9 780821 827147

CONM/283

AMS on the Web
www.ams.org